GUILHERME MIRANDA TAVARES

β-LACTOGLOBULIN AND LACTOFERRIN COMPLEX COACERVATES: CHARACTERIZATION AND PUTATIVE APPLICATIONS AS ENCAPSULATION DEVICE

Dissertation thesis presented to the Universidade Federal de Viçosa as part of the requirements of the PostGraduate Progam in Food Science and Technology, to obtain the title of Doctor Scientiae.

RENNES
FRANÇA
2015

Ficha catalográfica preparada pela Seção de Catalogação e Classificação da Biblioteca Central da UFV

T

T231b
2015

Tavares, Guilherme Miranda, 1988-
β-lactoglobulin and lactoferrin complex coacervates : characterization and putative applications as encapsulation device / Guilherme Miranda Tavares. - Rennes, FR, 2015.
xxviii,176f. : il. (algumas color.) ; 29 cm.

Orientador: Antônio Fernandes de Carvalho.
Tese (doutorado) – Universidade Federal de Viçosa.
Referências bibliográficas: f.161-176.

1. Leite - Proteínas. 2. Beta-lactoglobulina. 3. Lactoferrina. 4. Biomoléculas. 5. Encapsulação. I. Universidade Federal de Viçosa. Departamento de Tecnologia de Alimentos. Programa de Pós-graduação em Ciência e Tecnologia de Alimentos. II. Título.

CDD 22. ed. 664

GUILHERME MIRANDA TAVARES

β-LACTOGLOBULIN AND LACTOFERRIN COMPLEX COACERVATES: CHARACTERIZATION AND PUTATIVE APPLICATIONS AS ENCAPSULATION DEVICE

Dissertation thesis presented to the Universidade Federal de Viçosa as part of the requirements of the PostGraduate Progam in Food Science and Technology, to obtain the title of Doctor Scientiae.

APROVED: October 8th, 2015

André Matagne

Christian Sanchez

Francis Canon

Michel Desmadril

Saïd Bouhallab

Thomas Croguennec

Antonio Fernandes de Carvalho

“The only source of knowledge is experience”

A. Einstein

REMERCIEMENTS

Ce n'est vraiment pas facile pour moi d'écrire ces remerciements, c'est probablement la partie de la thèse la plus compliquée à rédiger. Ces trois années de thèse ont été définitivement intenses. Quotidiennement, je me suis rendu compte de mon évolution personnelle et scientifique grâce à tous les moments partagés avec les gens extraordinaires que j'ai eu la chance d'avoir à mes côtés.

La réalisation de ce projet de thèse n'aurait pas pu être possible sans le support financier du Ministère Brésilien de Science et Technologie (au travers du programme Science sans Frontières du *Conselho Nacional do Desenvolvimento Científico e Tecnológico* – CNPq), de l'INRA, de l'Université Européenne de Bretagne (Collège Doctoral International), du Conseil Régional de Bretagne et de l'Université Fédérale de Viçosa. Merci beaucoup. Je remercie également Joëlle Léonil de m'avoir accueilli au sein de son laboratoire, le STLO.

Tout au long de mon parcours académique j'ai eu de la chance d'être encadré par des personnes que j'admire, pour la thèse ce n'était pas différent. Dans l'ordre dans lequel ils sont « rentrés » dans ma vie : Antônio, Thomas et Saïd, MERCI.

Professor Antônio, merci beaucoup pour toute ton aide, tes encouragements et pour avoir cru dans mon potentiel depuis 2006 quand j'ai rejoint ton équipe. Je n'aurais pas pu arriver où je suis aujourd'hui sans toi.

Thomas, merci pour ta présence et pour ta patience, même quand j'arrivais avec mes manuscrits pleins de fautes d'anglais et mes énormes phrases. Ce serait impossible de ne pas vouloir travailler sur les protéines laitières après avoir suivi tes cours passionnés/passionnants sur la physico-chimie du lait.

Saïd, j'ai beaucoup appris avec toi pendant ces trois années. Même si tu n'as pas eu l'occasion de m'apprendre à jouer au babyfoot, tu m'as appris plein d'autres choses qui seront

déterminantes pour mon avenir professionnel. Merci également d'avoir toujours priorisé ma formation en tant que chercheur par rapport à l'obtention des résultats.

J'espère sincèrement que vous avez apprécié autant que moi ces trois ans de travail.

Un grand merci également à Ken Mok de m'avoir accueilli et encadré pendant les trois mois au sein de son labo à Dublin. Merci pour toutes nos discussions et ta curiosité sur mon travail. J'espère que l'on se recroisera dans un futur proche.

Je ne peux pas continuer mes remerciements sans remercier Pascaline. C'est facile de mener un projet de thèse lorsque l'on sait que l'on peut compter sur quelqu'un d'aussi compétent que toi. Merci pour tous les moments partagés devant l'HPLC et l'ITC ou à purifier des protéines. Merci pour tout ce que tu m'as appris et pour tout ce qu'on a pu apprendre ensemble.

Je remercie aussi Olivia Lerideau pour son engagement lors de son stage au sein de l'équipe et Anne-Laure pour toutes nos discussions scientifiques. Anne-Laure, je te souhaite bonne continuation pour la suite de ta thèse.

Merci à André Matagne, Christian Sanchez, Francis Canon et Michel Desmadril d'avoir accepté de faire partie de mon jury de thèse.

Merci à Taco Nicolai, Denis Poncelet et à Sylvain Guyot pour tous leurs précieux conseils lors de mes comités de thèse. Merci à tous les membres de l'équipe ISF-PL Power (Coralie, j'essaie aussi d'éterniser le nom) pour votre grande sympathie et pour toutes nos discussions lors des réunions d'équipe. Un merci spécial à Stéphane, Marie-Hélène et Fanny.

Pendant ma thèse, plusieurs collaborations internes et externes ont été établies. Merci beaucoup à Sébastien Lê, Claire Roiland, Paulo Peixoto, Aurélie Nicolas, Chantal Cauty, Nadine Leconte, Marie No Madec, Gwenaële Henry, Julien Jardin, Valérie Briard, Florence Rousseau et Stéphane Pezennec. Au travers du partage de votre expertise vous avez rendu possible la réalisation de mon projet de thèse, merci encore...

Egalement, cette thèse n'aurait jamais pu être la même sans l'aide des personnes responsables de tâches parallèles à la recherche qui sont tellement importantes. Un grand merci à Paulette, Jessica, Laurence, Danielle, Nathalie, Anne Giboulot, Marie-Claude, Dominique, Michel, Laurent, Christophe et Rachel.

Même si à priori ces remerciements sont pour la thèse, pour moi c'est impossible de dissocier la thèse du temps que j'ai passé en master. Pour moi, la thèse représente l'aboutissement de ces quatre ans passés à Rennes. La fin d'une très belle partie de ma vie.

Je remercie donc le team poudre du STLO (Romain, Pierre et Anne Dolivet) pour tout que j'ai pu apprendre avec eux pendant mon master. Merci à tous mes collègues et voisins de bureau : Marielle, Samira, Kéra, Solène, Céline, Melanie, Claire, Christelle, Naaman... pour la bonne humeur et pour avoir su me supporter pendant tout ce temps (pas facile, j'en suis conscient).

Merci encore à Naaman pour les longues discussions du vendredi après-midi, même pour celles dont la conclusion était : il faut refaire le monde. Ce sera toujours un grand plaisir pour moi de parler de science (pas que) avec toi.

Merci à tous les doctorants de l'unité pour les moments de détente lors des repas du midi et pauses chez Paulette. D'ailleurs, merci encore Paulette de nous offrir tous les jours des bons moments pendant les pauses…

Je remercie également tous ceux qui ont activement participé à ma vie pendant mon séjour en Irlande. Merci à Anna, Ji Yoon, Nadia, Nadine, Sara, Marcelo, Vanessa, Moacir et tous les membres de l'IFSC Force, mon séjour était aussi agréable grâce à vous.

Une grande partie de mon temps « libre » pendant ces quatre ans de Rennes a été consacré aux activités du Jeong Tong Taekwondo dojang. Merci à tous les membres du club, avec vous j'ai pu apprendre que vivre ensemble c'est mourir ensemble. Un merci spécial à Sébastien,

Tibo, Etienne, Vincent, Gaëtan, Lydie, Didier, Blandine, Judith, Mathilde, Kévin, Emilien, Nathalie, Kévin, Phuc-loi...PATCHOOO !

Après le travail et le sport, le troisième point clé de ma vie à Rennes : Merci énormément à tous les membres (et ex-membres) de la Goutte Pendante, du Square de la Rance et de l'Alcoolocation pour tous les moments de détente. Merci à Samira pour la *meta 10*. Merci aux *Carinhosos* pour avoir renforcé ma certitude sur l'effet papillon. Merci à Gaëtan pour ton grand cœur. Merci à tous les grands amis que j'ai pu avoir pendant ce séjour à Rennes : Samira, Arlan, Marilia, Lélia, Juliana, Gaëtan, Anne-C, Xaxa, Féfé, Carlos, Clarisse, Elise, Flavia, Guillaume, Livia, Rachid, Song, Andreza (*meu monstro*), Perrine, Andreas, Adèle, Priscilla, Naaman, Rosangela, Renam, Rozenn....

Finalement je tiens à remercier ma famille (*pai, mãe, mã et Iago*). Même loin vous avez essayé d'être proches. *Eu dedico a vocês esse diploma, sem vocês eu não teria chegado aqui.*

C'est une très belle étape de ma vie qui finit. Je rentre au Brésil, prêt pour de nouvelles aventures, tout en emportant un petit bout de chaque personne qui a fait partie de ma vie pendant ces quatre ans à Rennes, telle une grande mosaïque. MERCI !

Table of Contents

TABLE OF FIGURES

TABLE OF TABLES

LIST OF ABBREVIATIONS

AA: amino acid

α-CN: α-casein

AFM: atomic force microscopy

Ala: alanine

α-LA: α-lactalbumin

ANS: 8-anilinonaphthalene-1-sulfonic acid

Apo-α-LA: apo α-lactalbumin

Asp: aspartic acid

β-CN: β-casein

β-LG: β-lactoglobulin native

β-LG A: β-lactoglobulin isoform A

β-LG B: β-lactoglobulin isoform B

β-LG (A+B): β-lactoglobulin equimolar mixture of isoforms A and B

BSA: bovine serum albumin

Ceq: concentration of bound fluorescent molecule

CNPq: *Conselho Nacional de Desenvolvimento Científico e Tecnológico*

CP: cross polarization

Cys: cysteine

D_{eff}: effective diffusion

D_f: pure diffusion

ΔG: Gibbs free energy

ΔH: change in enthalpy

Dh: hydrodynamic diameter

DLS: dynamic light scattering

DMSO: dimethyl sulfoxide

ΔS: change in entropy

DSC: differential scanning calorimetry

EGCG: epigallocathechin-3-gallate

FA: folic acid

F_{eq}: concentration of unbound fluorescent molecule

FITC: Fluorescein isothiocyanate

frap(t): fluorescence intensity at time t

FRAP: fluorescence recovery after photo bleaching

FRET: Fluorescence resonance energy transfer

Gly: glycine

HAMLET/BAMLET: human/bovine α-lactalbumin made lethal to tumor cells

Holo-α-LA: apo α-lactalbumin

HPLC: high pressure liquid chromatography

HSA: human serum albumin

INRA: *Institut National de la Recherche Agronomique*

ITC: isotherm titration calorimetry

K_a: association constant / binding constant

K_b: Boltzmann constant

κ-CN: κ-casein

K_d: dissociation constant

k_{off}: dissociation rate

k_{on}: association rate

l: light path length

LF: lactoferrin

LYS: lysozyme

MAS: magic angle spinning

MES: 4-Morpholineethanesulfonic acid

Mw: molecular weight

η: solvent viscosity

n: stoichiometry

NMR: Nuclear Magnetic Resonance

PDADMAC: poly-dimethyldiallyammonium chloride

RBITC: Rhodamine B isothiocyanate

Rh: hydrodynamic radius

RP-HPLC: reverse phase –HPLC

SA: serum albumin

SANS: Small-angle neutron scattering

SAXS: Small-angle X-ray scattering

SDS: sodium dodecyl sulfate

T: temperature

τ: turbidity

T1 and T2: spin relaxation times

τc: correlation time

TEM: transmission electronic microscopy

T_{max}: denaturation temperature

TTMA: cationic gold nanoparticle coupled to 3,6,9,12-tetraoxatricosan-1-aminium, 23-mercapto-N,N,N-trimethyl

Val: valine

w: radius of the bleach spot

WPC: whey protein concentrate

WPI: whey protein isolate

[FA bound]: bound folic acid concentration

[FA free]: unbound folic acid concentration

[FA]: initial folic acid concentration

[LF saturated]: concentration of lactoferrin saturated with folic acid

[LF]: lactoferrin concentration

RESUMO

TAVARES, Guilherme Miranda, D.Sc., Universidade Federal de Viçosa, outubro de 2015. **Coacervados complexos de β-lactoglobulina e lactoferrina: caracterização e aplicação potencial para a encapsulação de bioativos.** Orientador: Antônio Fernandes de Carvalho; Coorientadores: Saïd Bouhallab, Thomas Croguennec, Eduardo Basílio e Ítalo Tuler Perrone.

A encapsulação de moléculas bioativas é utilizada há décadas pelas industrias de alimentos e representa uma real oportunidade de desenvolvimento de produtos inovadores. Dada a sua versatilidade funcional, as proteínas do leite, em particular as proteínas do soro de leite, tem sido utilizadas para fins de encapsulação por meio de diferentes técnicas. Complementarmente, estudos recentes mostraram a habilidade de proteínas alimentares de carga oposta de se co-associar formando micro-esferas através da coacervação complexa. Compreender as forças que governam o processo de coacervação de hetero-proteínas e o efeito da presença de pequenos ligantes (bioativos) são pré-requisitos para o uso de coacervados complexos de hetero-proteínas como agentes de encapsulação. Neste contexto, o objetivo do meu projeto de tese foi entender o mecanismo de coacervação complexa entre β-lactoglobulina (β-LG) e lactoferrina (LF) na ausência ou na presença de pequenos ligantes. As condições ótimas para a coacervação entre β-LG e LF foram identificadas como sendo entre os pH 5.4 – 6.0 e em presença de um excesso molar de β-LG. Interessantemente, LF demonstrou uma seletividade de coacervação com a β-LG A, a isoforma ligeiramente mais eletronegativa. A nivel molecular, a presença de dois sítios de interação da β-LG com a LF foram evidenciados. Em complemento, hetero-complexos como o pentâmero LF$(\beta\text{-LG}_2)_2$ e outros complexos maiores (LF$\beta\text{-LG}_2)_n$ foram identificados como constituintes da fase coacervada. Para avaliar o efeito da presença de pequenos ligantes na coacervação complexa entre β-LG e LF, foram usados modelos de moléculas hidrofóbica (ANS) e hidrofílica (ácido fólico). Embora nas condições experimentais os pequenos ligantes não tenham interagido com a β-LG, ambos interagiram com a LF induzindo sua auto-associação em nano-partículas. Concentrações relativamente elevadas de pequenos ligantes afetaram a interação entre as duas proteínas levando a uma transição entre os regimes de coacervação e agregação.

RESUME

TAVARES, Guilherme Miranda, D.Sc., Universidade Federal de Viçosa, Octobre 2015. **Coacervats de β-lactoglobuline et de lactoferrine : caractérisation et application potentielle pour l'encapsulation de bioactifs.** Encadrant: Antônio Fernandes de Carvalho; Co-encadrants: Saïd Bouhallab, Thomas Croguennec, Eduardo Basílio e Ítalo Tuler Perrone.

Le bénéfice de l'encapsulation des molécules bioactives a séduit les industries agroalimentaires depuis plusieurs décennies et constitue toujours un levier de développement pour des produits innovants. Plus récemment des études ont montré la capacité de protéines alimentaires de charge opposée à s'assembler en microsphères par coacervation complexe. La compréhension des forces gouvernant le processus de coacervation complexe entre protéines et l'influence exercée par la présence de petits ligands (bioactifs) demeurent des prérequis pour l'utilisation des coacervats complexes de protéines comme agent d'encapsulation. Dans ce contexte, l'objectif de mon projet de thèse a été de comprendre le mécanisme de coacervation complexe entre une protéine chargée négativement, la β-lactoglobuline (β-LG), et une protéine chargée positivement, la lactoferrine (LF), issues du lactosérum en absence et en présence de petits ligands. Les conditions optimales de coacervation entre la β-LG et la LF ont été définies entre pH 5.4 et 6.0 ainsi qu'en présence d'un excès de β-LG. La LF a présenté une coacervation préférentielle avec le variant A de la β-LG qui se distingue du variant B par la substitution de 2 acides aminés. Au niveau moléculaire, deux sites de fixation de la β-LG sur la LF ont été identifiés. En outre, par la mesure d'une part des coefficients de diffusion rotationnel et d'autre part de la cinétique de diffusion des entités moléculaires constituant les coacervats, il est suggéré que ces derniers sont formés à partir de β-LG libre, de pentamère, LF(β-$LG_2)_2$, ainsi que des entités plus larges, (LFβ-$LG_2)_n$. Afin d'évaluer l'effet de la présence de petits ligands sur la coacervation complexe entre la β-LG et la LF, des ligands modèles, l'un hydrophobe (ANS), l'autre hydrophile (acide folique) ont été utilisés. Dans les conditions expérimentales testées ces deux ligands n'ont pas d'affinité pour la β-LG, mais après interaction avec la LF ils sont capables d'induire son auto-association en nanoparticules. En concentrations élevées de ligands, la coacervation complexe entre la β-LG et la LF est perturbée et une transition vers un régime d'agrégation est observée.

ABSTRACT

TAVARES, Guilherme Miranda, D.Sc., Universidade Federal de Viçosa, October, 2015. **β-lactoglobulin and lactoferrin complex coacervates: Characterization and putative applications as encapsulation device.** Advisor: Antônio Fernandes de Carvalho; Co-advisor: Saïd Bouhallab, Thomas Croguennec, Eduardo Basílio e Ítalo Tuler Perrone.

Encapsulation of bioactives has been used by the food industries for decades and represents a great potential for the development of innovative products. Given their versatile functional properties, milk proteins in particular from whey have been used for encapsulation purposes using several encapsulation techniques. In parallel, recent studies showed the ability of oppositely charged food proteins to co-assemble into microspheres through complex coacervation. Understanding the driving forces governing heteroprotein coacervation process and how it is affected by the presence of ligands (bioactives) is a prerequisite to use heteroprotein coacervates as encapsulation device. In this context, the objective of my thesis work was to understand the mechanism of complex coacervation between β-lactoglobulin (β-LG) and lactoferrin (LF) in the absence and presence of small ligands. The conditions of optimal β-LG - LF coacervation were found at pH range 5.4-6 with a molar excess of β-LG. Remarkably, LF showed selective coacervation with β-LG A, the slightly more negative isoform. At molecular level, the presence of two binding sites on LF for β-LG was evidenced. Moreover, the heterocomplexes such as pentamers LF$(\beta\text{-LG}_2)_2$ and quite large complexes (LFβ-LG_2)n were identified as the constituent molecular species of the coacervate phase. To evaluate the β-LG - LF complex coacervation in the presence of small ligands, models of hydrophobic (ANS) and hydrophilic molecules (folic acid) were used. Although under the experimental conditions tested the small ligands did not interact with β-LG, both interacted with LF inducing its self-association into nanoparticles. High relative concentrations of small ligands affected the interaction between the two proteins leading to a transition from coacervation to aggregation regime.

THESIS OUTPUTS

Review

Tavares, G.M., Croguennec, T., Carvalho, A.F., Bouhallab, S. (2014). Milk proteins as encapsulation devices and delivery vehicles: Applications and trends. Trends in Food Science and Technology, 37(1), 5 – 20.

Published or Submitted papers

Tavares, G.M., Croguennec, T., Hamon, P., Carvalho, A.F., Bouhallab, S. (2015). Selective coacervation between lactoferrin and the two isoforms of beta-lactoglobulin. Food Hydrocolloids, 48, 238 – 247.

Tavares, G.M., Croguennec, T., Lê, S., Lerideau, O., Hamon, P., Carvalho, A.F., Bouhallab, S. Binding of folic acid induces specific self-association of lactoferrin into nanoparticles: thermodynamic characterization. Submitted to Langmuir.

Papers in preparation

Peixoto, P., Tavares, G.M., Croguennec, T., Nicolas, A., Hamon, P., Roiland, C., Bouhallab, S. Molecular mechanism of proteins complex coacervation: Case of β-lactoglobulin and lactoferrin. In preparation for submission to Soft Matter.

Tavares, G.M., Croguennec, T., Lerideau, O., Hamon, P., Carvalho, A.F., Bouhallab, S. How the presence of a small molecule affects the complex coacervation between lactoferrin and β-lactoglobulin. In preparation for submission to Food Chemistry.

Oral presentations

Tavares, G.M., Croguennec, T., Hamon, P., Carvalho, A.F., Bouhallab, S. *Biopolymers 2013: Biopolymer assemblies for material design* (December 2013). Specificity of beta-lactoglobulin variants for spontaneous assembly with lactoferrin. Nantes, France.

Bouhallab, S., Tavares, G.M., Hamon, P., Croguennec, T. *Minerals & Dairy Products Symposium* (February 2014). Specific binding of Minerals affects spontaneous co-assembly of globular proteins. Auckland, New Zealand.

Tavares, G.M., Croguennec, T., Hamon, P., Carvalho, A.F., Bouhallab, S. *Food Structure and Functionality forum Symposium: From molecules to functionality* (April 2014). Particular spontaneous assembly of lactoferrin with the two variants A and B of beta-lactoglobulin. Amsterdam, Netherlands.

Tavares, G.M., Croguennec, T., Hamon, P., Carvalho, A.F., Bouhallab, S. *6es Rencontres Biologie-Physique du Grand Ouest* (June 2014). Co-assemblage de la beta-lactoglobuline et de la Lactoferrine en microsphères. Le Mans, France.

Tavares, G.M., Croguennec, T., Carvalho, A.F., Bouhallab, S. *VII Workshop de laticinios* (October 2014). Proteinas Lácteas como dispositivos de encapsulação: aplicações e tendências. Viçosa, Brazil.

Tavares, G.M., Croguennec, T., Hamon, P., Peixoto, P., Carvalho, A.F., Bouhallab, S. *6th International Symposium on Delivery of Functionality in Complex Food-Systems* (July 2015). Protein co-assembly for the encapsulation of bioactives. Paris, France.

Poster presentations

Tavares, G.M., Croguennec, T., Peixoto, P., Hamon, P., Carvalho, A.F., Bouhallab, S. *6th International Symposium on Delivery of Functionality in Complex Food-Systems* (July 2015). Amino acid substitution on β-lactoglobulin changes its coacervation properties with lactoferrin. Paris, France.

Supervision

Co-supervision of undergraduate student (*Biologie-Environnement/Université Bretagne Sud*) from April to June 2014.

1 GENERAL INTRODUCTION

Milk is a product secreted by the females of all mammals whose objective is to provide to the newborns all necessary elements for their survival and development during the first stages of life [1]. After the domestication of animals, milk became an important part of the human diet, even for adults. Nowadays, it is estimated that in USA, several European countries, Canada, Australia and New Zealand, 30% of the protein diet is supplied by the consumption of dairy products [2]. Thanks to the domestication of animals and the better control of milk production, different milk products could be developed aiming milk conservation or the diversification of sensory aspects. However, for centuries the knowledge associated with milk was empirical. A great example of how the development of scientific knowledge changed the dairy market and industry is the whey.

Smithers [3] well described in his review "Whey and whey proteins - From gutter-to-gold" how a set of factors (e.g. environmental, scientific and technological advances...) contributed to change the image and perception of whey by the consumers and industries. The whey which was considered as an industrial by-product is now recognized for its high biological value and the technical and functional properties of its proteins.

Nevertheless the knowledge accumulation and the scientific development are continuous and point to a new trend now; whey proteins are no longer considered only as functional ingredients; they are also valuable and versatile raw materials for the development of several innovative objects. From gold nugget to gold jewelry. In the last 10 years, many scientific papers have been published describing the formation of supramolecular structures from whey proteins. The formation of fibers, nanotubes and coacervates (microspheres) using whey proteins as elementary bricks has gained attention from several scientific communities because of their intriguing structures and their high potential applications. Encapsulation and controlled release of bioactives is one of these potential applications [4].

Several different encapsulation techniques using whey proteins, such as spray drying, has been applied at industrial scale for decades. It is estimated that the encapsulation applied to food represented in 2014 a market of around 3 billion of dollars and a turnover of more than 5 billion of dollars is expected in 2020 [5]. The use of new and innovative whey proteins based supramolecular structures as encapsulation devices is expected to be more interesting compared to the traditional encapsulation techniques. These supramolecular structures allows a better control of the assembly and disassembly process, essential for the delivery and control of release of bioactives. Special attention is given to coacervates (microspheres) which require very low energy to be formed, being durable potential encapsulation devices. All these factors match with the consumer demands for healthy and sustainable food systems.

In this context, two main objectives were assigned to the work of this thesis: (i) to understand the mechanism of coacervation process between two oppositely charged whey proteins: β-lactoglobulin (β−LG) and Lactoferrin (LF); (ii) to determine how the presence of small ligands (bioactive) affects the process of coacervation between these two proteins and therefore to extract some important parameters conditioning the use the heteroprotein coacervates as encapsulation devices.

This document is divided into 3 distinct sections:

- **Review of Literature** section presents a compilation of the use of whey proteins as encapsulating devices pointing out the gap in the literature about the use of heteroproteins complex coacervates for encapsulation; principles governing the complex coacervation especially between globular proteins are also described. Part of this section was extracted from the much larger review "Milk proteins as encapsulation devices and delivery vehicles: Applications and Trends" written during this thesis and published in 2014 [4].

- **Results and Discussion** section is divided into two chapters, each divided into two parts.

The first chapter presents the study of the complex coacervation between β-LG and LF. Different scales were explored; the first part focuses on the macro/mesoscopic study, identifying the optimal conditions for coacervation. This part was published in 2015 in Food Hydrocolloids [6]. The second part explores the interaction between these two proteins at molecular level, a mechanism leading to β–LG - LF coacervation is proposed. These results will be submitted soon to Soft Matter.

The second chapter explores the interaction of small ligands (models for bioactive molecules) with the proteins and how they affect the coacervation process between the two proteins. The first part focuses on the impact of ANS (chosen as model molecule to mimic a hydrophobic bioactive molecule) on the complex coacervation between β-LG and LF. This first part is in preparation for submission to Food Chemistry. The second part describes how a hydrophilic charged bioactive, i.e. folic acid, interacts and affects the properties of the two proteins. The obtained results were submitted for publication in Langmuir.

- Finally, the third section presents a **General Discussion** of the messages of the present work**, Conclusions** and open **Perspectives**.

2 REVIEW OF LITERATURE

Encapsulation technologies that have been used for a long time in the pharmaceutical industry for drug delivery applications offer a real opportunity for the food industry. Encapsulation represents a means to develop innovative products to satisfy the growing demand of the consumer for foods with health and well-being benefits. For some food applications, encapsulation can be performed using relatively simple operations, such as emulsions, suspensions, gels and solid matrices. Due to their high abundance, nutritional value and high acceptance by consumers, whey proteins have largely been tested to design encapsulation devices, owing to their versatility and excellent functional properties. Special attention is given to the novel potential of heteroprotein complex coacervates, reversibly co-assembled protein supramolecular structures.

2.1 Whey Proteins

Proteins in milk are divided into two main groups: caseins and whey proteins (Table 2.1). Caseins are the fraction of proteins that precipitate at pH 4.6 and are often considered as intrinsically unstructured proteins associated as micelles with calcium phosphate in milk [7]. The caseins are synthesized exclusively in the mammary glands, suggesting that one of their functions is to provide amino acids (AA) and soluble calcium required for the development of the neonate [1]. Besides this function, caseins allow milk to be supersaturated in calcium phosphate, due to their capacity to bind divalent and multivalent ions [1, 8].

Whey proteins are typically globular proteins that exhibit various biological functions including source of essential amino acids, transport of molecules, co-factors for enzymes. β-lactoglobulin (β-LG) and α-lactalbumin (α-LA), are exclusively synthesized in the mammary gland [9]. In contrast, minor whey proteins (serum albumin (SA), lactoferrin (LF)) are transferred from blood plasma to milk through the lactating cell. The properties of the main whey proteins are described below.

Table 2.1. Physical-chemical properties of bovine milk proteins

Origin	Proteins		Concentration in milk (g/kg)	Molecular Weight (kDa)	Isoelectric point
Synthesized in the mammary gland	Casein micelle		26	$\approx 10^5$ (100-500nm)	4.6
	Caseins Fractions	α_{S1}	10.7	23.6	4.9
		α_{S2}	2.8	25.2	5.2
		β	8.6	24	5.4
		κ	3.1	19	5.6
	Whey Proteins	β-LG	3.2	18.3	5.1-5.2
		α-LA	1.2	14.2	4.3-4.7
From blood		BSA	0.4	66.3	5.0
		LF	0.1	83	8.5

2.1.1 β-lactoglobulin (β-LG)

β-LG, although absent in human milk, is the major whey protein in cow milk (~ 3.2 g/kg). It belongs to the lipocalin family of proteins because of its ability to bind small hydrophobic molecules into its internal cavity [1]. It has 162 amino acids (AA), a molecular weight of 18.3 kDa and presents more than ten known genetic variants, although isoforms A and B are the most common [10]. β-LG A and β-LG B differ only by the substitution of two amino acids: AA64 corresponds to an aspartic acid in β-LG A and to a glycine β-LG B, in addition, AA118 corresponds to a valine in β-LG A and to an alanine β-LG B. Thus, β-LG A is slightly more hydrophobic and slightly more electronegative than the β-LG B, even though the tertiary structure of these two isoforms remain unchanged. The AA64 is already in a disordered region of the protein and the AA118 is buried into the protein calyx [11].

β-LG is an acidic protein presenting an isoelectric point of 5.1/5.2 (respectively for isoforms A and B) [12]. It has five cysteine (Cys) residues, four involved on two disulfide bridges and the other thiol group is free but hidden in the center of the β-LG structure [13]. The denaturation temperature (T_{max}) of this protein is around 75 °C and the Cys residues presented in the structure are essential to insure the protein thermo-stability [14].

The structure of β-LG is similar to that of retinol-binding proteins, even though little milk endogenous retinol is linked to β-lactoglobulin. Although β-LG has several binding sites for hydrophobic ligands such as fatty acids and vitamins, the biological function of this protein is still not well defined despite numerous studies conducted over many years [1].

β-LG is mainly in a monomeric state below pH 3.5 and above pH 7.5, and is able to form stable noncovalent dimer in equilibrium with the monomeric form between the two pH values [15]. The residues 145 to 153 are implicated in the dimer interface [16], as illustrated in Figure 2.1. In the dimeric state of the protein, the residue 64 is near the dimer interface, resulting in high electronegative zone close to the dimer interface for the β-LG A homodimers compared to β-LG B homodimers or β-LG A/β-LG B heterodimers [12]. The dimer/monomer equilibrium depends on the physical-chemical characteristics of the solution, this equilibrium being shifted towards the formation of dimers by increasing the protein concentration, increasing the pH or reducing the temperature [17].

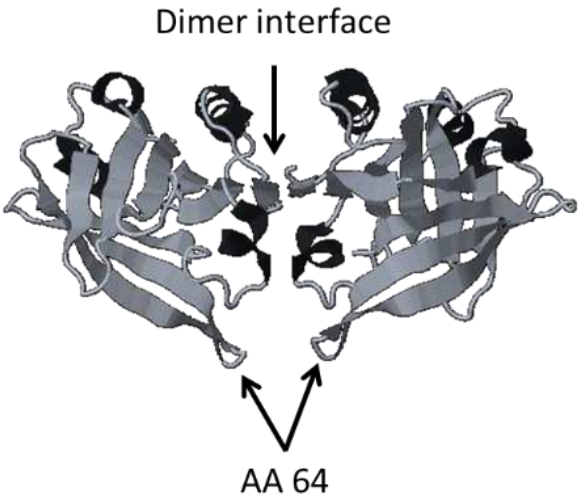

Figure 2.1. β-LG dimer (RCSB PDB code: 2Q2M). The arrows show the dimer interface and the position of the AA64, an important substitution between isoforms A and B.

2.1.2 α-lactalbumin (α-LA)

α-LA is the second most quantitatively important whey protein of cow milk (~1.2 g/kg). Contrarily to β-LG, α-LA is present in the milk of all species of mammals [1]. It has 123 AA, a molecular weight of 14.2 kDa and a pI between 4.3 and 4.7. This protein has a high similarity to the hen egg white lysozyme (LYS), these two homologous proteins have 54 identical AA and 23 others are structurally similar [18]. α-LA tertiary structure is shown in Figure 2.2 A.

No free thiol group is present in α-LA, all the eight Cys residues are involved in disulfide bounds conferring certain rigidity to the protein. α-LA also presents a very specific calcium binding site ($Ka = 10^8\ M^{-1}$) formed by the residues 79 to 88 [1]. The holo form has a denaturation temperature of about 60 °C and is most abundant in milk, while apo form is much more flexible and has a denaturation temperature around 30 °C [19, 20].

2.1.3 Bovine Serum Albumin (BSA)

Although its concentration in milk is relatively low (~0.4 g/kg), BSA is an important protein in blood for the transport of molecules. It has 582 AA and a molecular weight of 66.4 kDa [15]. BSA is a monomeric protein presenting 17 disulfide bridges and only one free cysteine (Figure 2.2 B). This protein and human serum albumin (HSA) share 75% sequence identity [1].

BSA is also an acidic protein, with a pI around 4.9 [21]. Its denaturation temperature is around 60 °C, although its thermo-stability can be increased by binding of hydrophobic ligands [1, 22].

2.1.4 Lactoferrin (LF)

LF is an iron-binding glycoprotein composed by 689 AA distributed in two homologous lobes (around 40% of similarity) (Figure 2.2 C). Its molecular weight is around 83 kDa and it is the major basic protein in cow milk having a pI around 8.6 - 8.9 [15]. Its charges are distributed on its surface and important positive patches are located on the N lobe and on the inter-lobe region [23].

Lactoferrin tends to polymerize especially at high concentrations. It can exist in different polymeric forms ranging from monomers to tetramers. Usually lactoferrin is presented in a monomeric state at low ionic strengths, however increasing the ionic strength dimers/aggregates can be formed [24, 25].

Each lobe of the protein presents an iron binding site, which requires the fixation of bicarbonate as synergist ion for iron binding [1, 26]. According to the level of iron saturation, three different forms of LF exist. The apo form with less than 5% of iron saturation, the holo form is fully saturated while the native form presents approximately 15-20% of iron saturation [27]. Similarly to several metalloproteins, LF iron saturation affects its flexibility. At neutral

pH, apo LF denaturation temperature is around 71 °C whereas holo LF has a denaturation temperature of 91 °C [27]. The native-LF presents two denaturation peaks, the major one corresponds to the apo form presenting a denaturation temperature around 62 °C while the small one corresponding to the holo form population, presents a denaturation temperature around 90 °C [27].

Behind its role as iron transporter, LF has several biological activities such as antimicrobial, immunomodulatory and anticarcinogenic [28]. In addition, LF is a protein with very high industrial interest, especially for enrichment and formulation of infant formula, a market in full growth [29].

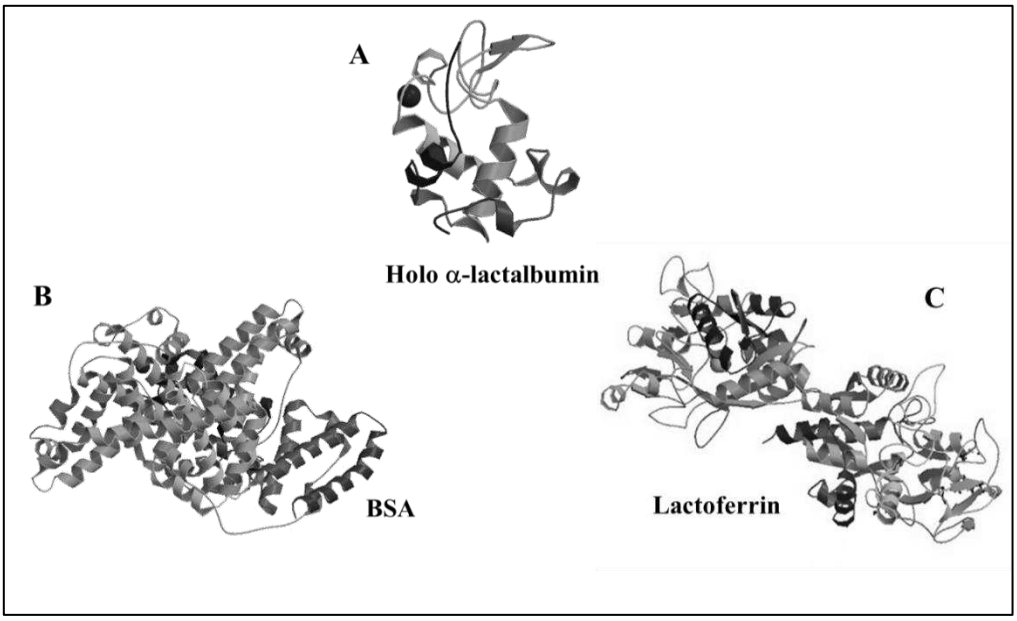

Figure 2.2. Tertiary structure of (A) α–lactalbumin (RCSB PDB code: 1ALC), (B) BSA (RCSB PDB code: 3V03) and (C) Lactoferrin (RCSB PDB code: 1BLF).

2.2 Whey proteins as encapsulation devices

Several recent reviews have dealt with the combination of whey proteins and polysaccharides for encapsulating various bioactives [30-33]. Here, the focus will be on the use of whey proteins as unique encapsulation agents. Whey proteins are interesting encapsulation agents

because of their ability to bind different bioactives or to entrap them through the formation of supramolecular structures, emulsions or hydrogels. The main strategies applied for encapsulation that involve whey proteins are summarized in Figure 2.3. The different studies were classified according to the applied encapsulation strategy.

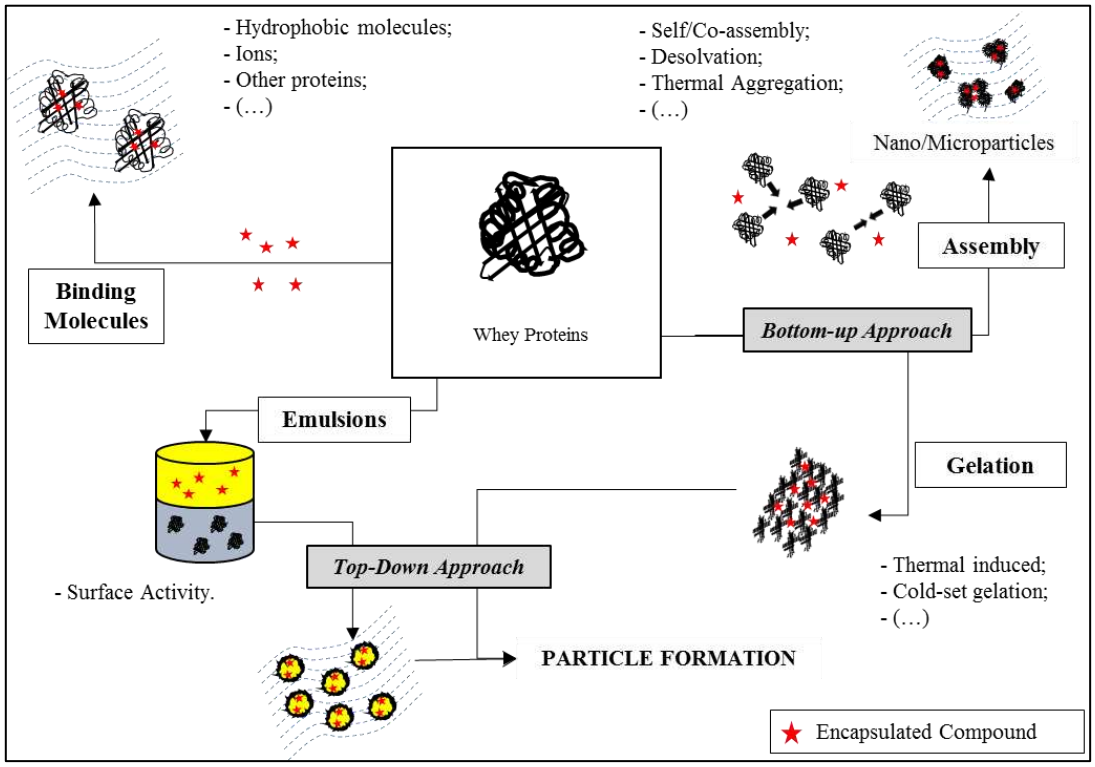

Figure 2.3. Illustration of encapsulation strategies applied to whey proteins (adapted from Tavares et al. [4]).

Many encapsulation techniques have been developed, but none is applicable to all bioactives [34]. The selection of a particular encapsulation technique depends on the nature of the bioactive and the coating material, as well as the properties of the particle to be designed, such as its size and morphology. In addition, inherent aspects relating to the encapsulation technique must be considered, such as the cost and encapsulation efficiency [35]. Several food components can interfere with the properties of bioactives at different stages of the product life cycle, therefore, it is essential that the selected encapsulation technique preserves the bioactives throughout the whole processing chain including engineering, formulation and

storage of the products [36]. In addition, it is also important to ensure the production of encapsulation devices that can be easily incorporated into food products without altering texture and flavor [34].

The most widely used encapsulation techniques and some related applications are summarized in Table 2.2. Furthermore, some procedures have been specifically developed to optimize the potential of biopolymers such as whey proteins as encapsulating agents. Several articles have summarized the potential of whey proteins to transport and protect bioactives such as ions, fatty acids and vitamins [8, 37-39]. Additionally, two distinct and complementary approaches i.e. "top-down" and "bottom-up", have been explored to widen the use of whey proteins as encapsulating biomaterials.

Table 2.2. Main conventional techniques used for the encapsulation of bioactive and food ingredients. Please refer to the following papers for more details: [34, 35, 40, 41].

Technique	Concept	Examples of applications
Spray Drying	Drying of the encapsulated material dispersed in the shell material. Encapsulation by starch, polysaccharides, maltodextrins and/or proteins. This technique produces particles between 10 and 100 µm.	Encapsulation of flavor compounds, polyphenols and vitamins
Spray Cooling/Chilling	Incorporation of the core material in the warm and liquefied shell material (often vegetable oils). Relatively low cost encapsulation technique. Through product atomization, and consequently cooling, micro-capsules are formed.	Encapsulation of flavor compounds, minerals, vitamins and probiotics
Freeze Drying	Co-lyophilization of the core and the shell materials after a homogenization process. Normally this technique produces non-uniform particles.	Encapsulation of flavor compounds, fatty acids and probiotics
Extrusion	Formation of core material droplets that became microparticles after immersion in a hardening bath with the shell material. Normally the shell material is a glassy carbohydrate matrix. The core material may be released in a high temperature medium. The encapsulation efficiency is small, moreover the produced particles shows high stability and an extended shelf life.	Encapsulation of flavor compounds, vitamins and food ingredients (lactic acid)
Spinning Disk	Passage through a spinning disk of a suspension of the core material	Encapsulation of Cells

	in the shell material. During processing, the shell material forms a thin film around the core material particles. Production of particles from20 µm to few millimeters of diameter.	(yeast)
Supercritical Fluid Extraction	This technique similar to spray drying, except that the shell material and the core material are solubilized/dispersed in a supercritical fluid.	Encapsulation of Heat-sensible cores as vitamins and polyphenols
Fludized bed	This technique is applied for solid particle encapsulation (100µm to few mm). The shell material is atomized onto core material fluidized by an upward stream of air.	Encapsulation of acidulates, vitamins and cells
Cocrystallization	Spontaneous crystallization of a supersaturated solution of sucrose simultaneously with the addition of the core material, forming a crystalline irregular network, allowing the encapsulation into the pores of the network.	Encapsulation of acids, flavor compounds, anti-oxidants and minerals
Coacervation	Phase separation of one or many polyelectrolytes from a solution and deposition of the colloidal particles around the active ingredient suspended or emulsified in the same reaction media. When hydrocolloids are used, they can be cross-linked using appropriate chemical or enzymatic agent.	Encapsulation of fatty acids and flavonoids
Liposomes	Spherical particles consisting of a membranous system formed by one or more concentric bi-layers of lipids (often phospholipids). They can be used in the entrapment, delivery and released of water-soluble, lipid-soluble and amphiphilic materials.	Encapsulation of vitamins, enzymes and peptides
Inclusion	This technique refers to the supra-molecular association through non-covalent interactions of a ligand (“encapsulated” compound) into a cavity formed by a “shell” material (e.g. cyclodextrins).	Encapsulation of vitamins, flavor compounds and essential oils

The "top-down" approach consists of the fragmentation of a large structure into smaller particles through external energy input, especially mechanical energy [37, 38]. The formed particles have the same composition as the initial structure [37]. The initial structure can be a preformed protein hydrogel and particles of definite size are obtained using the "top-down" approach. The formed particles have the ability to entrap and transport micronutrients and bioactive compounds. Several gelling strategies are available for encapsulating the bioactives in the preformed protein hydrogel: Enzymatic-induced gelation [42, 43], heat-induced gelation [44] and cold-set gelation [45, 46]. Protein cold-set gelation is particularly useful for

encapsulating heat-sensitive bioactives, including probiotics [38] and occurs in two steps; the first step involves an unfolding of the globular proteins (by a thermal treatment), resulting in the exposure of some reactive groups. After cooling and the addition of the heat-sensitive molecules of interest, the second step consists of a cold aggregation of the denatured proteins through a reduction in electrostatic repulsions, by decreasing pH or/and adding salts [45, 47]. Another advantage of this method is that reactive groups exposed during the heat treatment of the proteins might establish interactions with the bioactives [38].

In contrast, the “bottom-up” approach is based on the association of molecules or small particles into larger and more complex supra-structures [38, 48]. This approach allows a better kinetic and thermodynamic control of the supramolecular structure formation, but it is often more complex to implement. In addition, the ”bottom-up" approach usually requires less energy input than the “top-down” approach [37]. The assembly of proteins into supramolecular structures might be induced differently according to the applied chemical or physical treatments and energy input. For instance, different structures have been generated from whey proteins, depending on the intensity of the heat treatment applied [49], the combination of heat treatment and variations of ionic strength and/or pH conditions [50]. Another possibility consists of the spontaneous protein interactions that are driven and stabilized by weak reversible interactions, including electrostatic, hydrophobic and hydrogen interactions, or salt bridges [51-53]. A large variety of supra-structures can be obtained by changing the nature and concentration of the proteins, the concentration and type of salts, in the presence or absence of specific enzymes or by modulating the temperature. This variety of supra-structures represents a great potential regarding the encapsulation of bioactives. Protein assembly can also be triggered through protein desolvation in the presence of organic solvents [54-57]. Thus, heat-denatured proteins in aqueous solution form nanoparticles of about 100–200 nm subsequent to modification of the solvent properties following the addition of organic

solvents such as acetone or ethanol. The change in solvent properties strengthens hydrogen bonds and reduces hydrophobic associations between heat-denatured proteins [54, 56]. These nanoparticles, which can be further stabilized using a cross-linking reagent, are suitable for the encapsulation and transport of micronutrients [57] and bioactives [55]. Recently, milk proteins have been used to form nano- and microcapsules by electrospraying [58, 59]. Electrospraying is a versatile and low-cost technique that is easy to implement and allows the production of capsules or fibers (in this case the technique is called electrospinning) from polymer solutions [60]. Charges are induced on the surface of the liquid jet or droplet through the application of an electric field, which generates a repulsive force opposite to that of surface tension; while the jet or the droplet is exposed to the electric field, the solvent evaporates, generating fibers or capsules [61]. Usually, organic solvents are used for the dissolution of the polymers (polyethylene glycol, polyvinylchloride, polystyrene). The advantage of using biopolymers such as proteins, is that the electrospraying technique can be applied in aqueous solution [58]. This technique was used for the production of nano-, sub-micro- and microcapsules from solutions of whey protein concentrate (WPC) at different pH values, to encapsulate β-carotene in the presence of glycerol [58]. The authors reported an encapsulation rate of about 90%, with a good stability of β-carotene against photo-oxidation after resolubilization of the capsules and exposure of the solution to UV radiation for 50 h.

2.2.1 Binding properties of whey proteins

β-LG has been widely studied for its ability to bind hydrophobic and amphiphilic compounds such as flavor compounds, vitamins, fatty acids and polyphenols. Globally, the interactions between β-lactoglobulin and bioactives are mainly driven by hydrophobic bonds, although hydrogen bonds are also involved in the binding of polyphenols [62] and fatty acids [63]. It has been proposed that β-lactoglobulin binds hydrophobic compounds preferentially in its

internal calyx, but additional binding sites in the cavity near to the alpha-helix and the external surface of the β-barrel have also been described [64].

The parameters of the interaction (localization and number of binding sites on the protein and affinity) depend on the chemical nature of the ligand, the physico-chemical conditions of the medium and the conformation of the protein. The binding affinity constant of curcumin with native β-lactoglobulin was higher than that with heat-denatured protein [65]. This change was attributed to a conformational change of the internal calyx of β-LG, resulting in a non-specific binding of curcumin molecules. In contrast, Tavel et al. [66] showed that β-ionone and guaiacol aroma exhibited a higher binding affinity for partially denatured β-LG molecules (molten globule state) than for the native protein. This higher affinity was hypothesized to be due to the exposure of some internal hydrophobic regions on the surface of the partially denatured protein and an increased accessibility of the calyx [66]. In some cases, the ligand binding might induce changes in the β-LG structure as reported by Le Maux et al. [67]. These authors showed that linoleate binding to β-LG favored denaturation of the protein, with subsequent formation of protein covalent dimers and trimers [67].

Whey proteins other than β-LG have also been studied for their ability to bind specific ligands. Kuhn et al. [68] showed that BSA has two binding sites and has a higher affinity for 2-nonanone, a flavor compound, than β-LG or α-LA, which only possess one binding site. After binding to whey proteins, some ligand properties were improved, including, in a non-exhaustive manner: i) a reduction of UV radiation induced the photo-degradation of folic acid from 40% to 6% after 60 minutes of treatment [69]; ii) an increase in the photo-stability and solubility of resveratrol [70] and α-tocopherol [71]; iii) an increase in the solubility and half-life of curcumin [65]. In contrast, a decrease in the antioxidant activity of tea catechins was observed when they formed complexes with β-LG [62] and BSA [72]. In some cases, the complexes exhibited unexpected new functionalities that were not predictable from those of

isolated molecules. This was the case for the complex formed between apo α-LA (calcium-free form) and oleic acid, known as HAMLET/BAMLET (human/bovine α-lactalbumin made lethal to tumor cells), which induces apoptosis of tumor cells [73]. Heat-denatured α-LA was also able to form a complex with oleic acid that induced apoptosis in cancer cells [74]. In addition, a complex formed by β-LG and oleate was shown to induce apoptosis in cancer cells comparable to the activity of BAMLET [75]. The improvement in fatty acid solubility through its binding to these proteins is probably a driving mechanism behind the observed apoptotic effect.

2.2.2 Encapsulation devices obtained through the "bottom-up" approach

The ability of whey proteins, particularly β-LG, to form nanoparticles used as encapsulating agents has also been extensively studied. Thermal aggregation and desolvation are the main strategies used for the production of these nanoparticles.

Li et al. [76] evaluated the encapsulation efficiency of β-LG nanoparticles for epigallocatechin-3-gallate (EGCG) in a wide range of pH (2.5–7.0), thermal treatment intensity (30–85°C/20 min), β-LG concentration (1–10 mg/mL) and protein:EGCG molar ratio (1:2 to 1:32). Nanoparticles were formed on heating, concomitantly with the encapsulation of EGCG. The four studied factors affect the nanoparticle characteristics: particle size, zeta-potential and entrapment efficiency. The highest protection of EGCG was observed for heat treatment at 85°C and a protein:EGCG molar ratio of 1:2 [76]. Nanoparticles protect encapsulated EGCG via steric hindrance and exhibit antioxidative properties due to the free thiols of the heat-denatured proteins [77]. Similarly, heat-induced β-LG nanoparticles with a diameter less than 50 nm and a zeta potential of about -40 mV were produced from 1.0% w/w protein solutions [78]. These nanoparticles showed an encapsulation efficiency of over 60 to 70% for EGCG and according to sensory tests, the bitterness and

astringency of EGCG were significantly reduced. The release of EGCG was limited during simulated gastric digestion, which suggests that the nanoparticles could be used to protect EGCG in the stomach, allowing a possible release of the bioactive into the gut [78].

High-pressure homogenization was used to produce nanoparticles from heat-induced aggregates of whey proteins for α-tocopherol encapsulation [79]. The formed particles exhibited a diameter between 212 and 293 nm, depending on the pressures employed. Compared to homogenization at 300 bar, a pressure at 1,200 bar induced some protein structural changes that modified the zeta potential of the produced particles and improved the stability of encapsulated α-tocopherol during storage [79]. Alternatively, whey protein nanoparticles with a controlled size were also produced by pH-cycling treatment (acidification and neutralization). Particles with a diameter ranging from 100 to 300 nm were produced through the acidification of a low-concentrated solution of heat-denatured whey proteins [50]. The whey proteins were linked by covalent bonds in the nanoparticles after the neutralization step. The particle size varied depending on the pH of acidification (5.0–6.0), aggregation time (0–75 h) and calcium concentration (0–5.0 mM). Calcium concentration also influenced the voluminosity of the particles: increasing the concentration of calcium decreased the voluminosity of the particles [50]. This technique was used to produce particles for entrapping hydrophobic aroma [80]. The retention efficiency was maximum when the aroma molecules were added to the protein dispersion before the formation of the particles at pH 5.0 or 5.5 and without added calcium [80].

Nanoparticles of BSA were produced in the presence of the flavonoid quercetin by a desolvation process induced by the addition of 10% dimethyl sulfoxide (DMSO) [81]. These nanoparticles showed a ζ-potential of -12.5 mV and a diameter close to 10 nm, surprisingly smaller than the diameter measured for native BSA and for the nanoparticles produced in the absence of the flavonoid [81, 82]. Based on transmission electron microscopy observations,

the authors explained their results by the highest compaction of the nanoparticles in complexes with the flavonoid [81]. The antioxidant activity of encapsulated flavonoid was not substantially changed, but its stability under intestinal conditions appeared to increase. The latter observation was attributed to the formation of both hydrophobic interactions and hydrogen bonds between quercetin and BSA during the encapsulation process [82]. Desolvation was also used to produce nanoparticles of β-LG for curcumin encapsulation at alkaline pH using acetone [65]. The formed nanoparticles were stabilized using glutaraldehyde as a cross-linking agent [55]. Spherical particles with a diameter of 140 nm were obtained, which showed a curcumin encapsulation efficiency of about 96%, with a simultaneous increase in curcumin solubility in aqueous solution from 0.03 to ≈620 μM. However, the encapsulated curcumin was slowly released from protein nanoparticles at neutral pH, which limits the use of these nanoparticles as a vehicle for such substances [65].

To develop nanoparticles designed for food applications, i.e., without the use of non-food grade solvents and chemical cross-linking agents, Gulseren et al. [56] tailored nanoparticles of whey protein isolate (WPI) by desolvation using ethanol. These particles were used for the encapsulation of zinc and demonstrated an entrapment efficiency between 80 and 100%, with a maximum incorporation of zinc of about 8 mg/g WPI. These particles remained stable for 30 days at 22°C at pH 3.0 [57]. Another food-grade technology for the encapsulation of bioactives based on the supercritical drying of pre-formed hydrogels to form aerogels was applied with success to WPI [83]. Aerogels formed by controlled drying with supercritical carbon dioxide of WPI hydrogels exhibit a mesoporous structure with a high encapsulation capacity of ketoprofen, a hydrophobic molecule, compared to the macroporous structure found for cryogels formed by conventional freeze-drying techniques. Hence, similar to polysaccharides, protein aerogels with a high encapsulating efficiency offer new possibilities as an alternative to aerogels from synthetic polymers.

2.2.3 Encapsulation devices obtained from a “top-down” approach

Top-down approaches for the encapsulation of bioactives using whey proteins are basically restricted to strategies of protein cold gelation, the formation of emulsions or a combination of these two strategies using extrusion techniques. Remondetto et al. [84] reported that cold-set gels of β-LG induced by the addition of iron show different morphologies, depending on the iron/protein ratio. For the lower ratios tested, filamentous gels were formed, whereas particulate gels were obtained at high ratios [84]. Particulate gels are mainly stabilized by van der Waals interactions; the large concentration of iron causes a rapid decrease in the repulsive forces, which generates random aggregation and leads to particulate gels. Moreover, low concentrations of iron mainly drive the formation of gels via hydrophobic interactions; the low iron concentration causes a decrease in the surface charge of the molecules and/or aggregates, facilitating interaction between exposed hydrophobic regions, which orients the growth of the assembly in only one direction, leading to filaments [85]. The microstructure of the gels affects the iron release properties. At acidic pH, iron was released more efficiently from particulate gels than from filamentous gels. In contrast, iron release was more efficient with filamentous gels at neutral pH, providing greater iron absorption under intestinal conditions, according to *in vitro* tests. This suggests that filamentous matrices are more efficient in the protection and transport of iron for nutritional purposes [86].

Although the fragmentation of protein hydrogels into particles characterizes the top-down approach, some authors limit their research to the ability of gels to entrap and release bioactives, without the stage of gel fragmentation into particles. Nevertheless, some papers describe the production of particles from hydrogels, which characterizes a real application of the top-down approach. Therefore, Martin and de Jong [45] investigated the effect of pH and pre-heating conditions on iron-induced cold-set gels of WPI. After gelation, gels were refined

into particles; both the stability of the particles and the iron-release kinetic were evaluated. The structural characteristics and the stability of the particles changed according to the severity of the pre-heating treatment. In this study, the iron:protein molar ratio in the particles was controlled by the duration of pre-heating at 80°C, reaching 5.3:1, 8.8:1 and about 17:1 after 0.5, 3 h, 10 h of pre-heating, respectively. However, irrespective of the conditions of pre-heating, the same iron-release kinetic was observed at acidic pH [45]. The preparation of protein particles for the simultaneous encapsulation of ferrous iron and ascorbate that protects iron against oxidation was also reported [46]. The particles had a mean diameter of 850 and 75 μm before and after lyophilization, respectively. The iron/protein molar ratio in the particles was approximately 5.7:1.0. The *In vitro* bio-accessibility of Fe^{2+} doubled following its encapsulation into protein particles and even increased from 10% to 80% in the presence of ascorbate [46]. These authors proposed that whey protein particles combined with ascorbate can be adequately used to fortify food products with iron. Cold-set gelation was also used to encapsulate microorganisms of interest. Reid et al. [87], and Hebrard et al. [88] used calcium-induced cold-set gelation to encapsulate probiotic bacteria and recombinant yeast, respectively. The protocol used is basically summarized by the dispersion of the selected cell cultures in a heat-treated WPI solution, followed by extrusion of the mixture in a solution of calcium chloride. The contact with the calcium solution induced the gelation of the proteins and consequently, the formation of capsules entrapping the probiotics [87, 88]. A SEM image of *Lactobacillus rhamnosus* cells homogeneously entrapped in the network of WPI capsules is shown in Figure 2.4. The formed capsules possessed a diameter of about 3.0 mm and were an effective protective barrier for the encapsulated cells against gastric digestion conditions [87, 88]. Similarly, Doherty et al. [89] produced capsules of about 200 μm in diameter from heat-treated WPI that were dropped in an acetate buffer solution at pH 4.6 for gelation. These capsules were used for the encapsulation of *L. rhamnosus*. In these studies, the encapsulation

efficiency of the bacteria reached 96%. Indeed, the encapsulation device increased the viability of the cells during storage and their resistance against gastric digestion. Hence, whey proteins constitute an ideal biopolymer for the encapsulation and protection of probiotics and their challenging delivery to intestinal absorption sites [89].

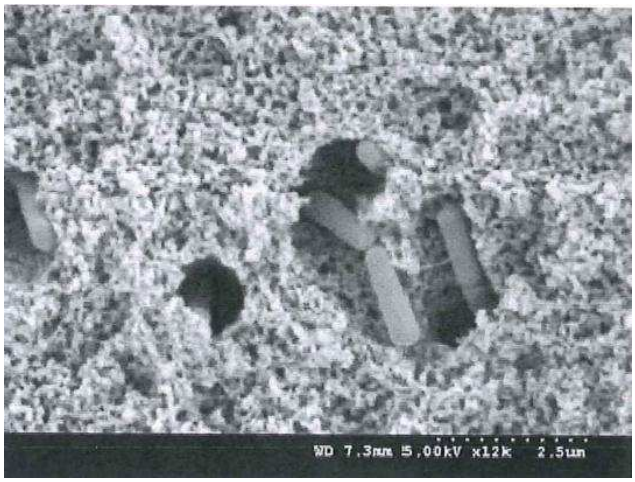

Figure 2.4. SEM cross-section image (12,000 x magnification) of a whey protein-isolate gel with encapsulated *Lactobacillus rhamnosus* (adapted from Reid et al. [87])

Betz and Kulozik [44] used WPI heat-set gels for the encapsulation of anthocyanins. The gels were formed by heating an acidified WPI solution (pH 3.0 and 1.5) containing the bioactive. They were evaluated for their stability and the kinetics of release of the encapsulated compound in simulated gastric fluid. The authors showed that the pH of the WPI solution affected the interaction between anthocyanins and the proteins. Gels formed at pH 1.5 were more stable than those formed at pH 3.0, representing a very favorable microenvironment for the encapsulation of anthocyanins [44]. The adsorption ability of heat-denatured proteins at an oil/water interface and their subsequent gelation has been explored, to stabilize emulsions with the aim of forming delivery systems. Hence, the interfacial properties of whey proteins are a key element explored for the encapsulation of various compounds. Immediately after the formation of the emulsion by mixing heat-denatured WPI solution and soybean oil containing

retinol, the lipid droplets were extruded into a calcium chloride solution to induce gelation of interfacial proteins [90]. The thus-formed encapsulating devices were about 2.0 mm in diameter and were stabilized by intermolecular β-sheet structures between protein molecules [90]. With the same objective, Liang et al. [91] produced an emulsion containing α-tocopherol stabilized by an interfacial layer formed by the calcium-induced cold-set gelation of pre-denatured β-LG. After *in vitro* enzymatic digestion of the encapsulating devices, the authors showed that the release of the bioactive is mainly controlled by the kinetics of protein hydrolysis. In addition, α-tocopherol released during the digestion process is degraded more slowly than free α-tocopherol, probably due to the protection effect provided by its interaction with the pre-denatured proteins and/or produced peptides [91]. Cornacchia and Roos [92] used whey proteins to stabilize oil in water emulsions to produce delivery systems capable of protecting and transporting β-carotene. Similarly, Tippetts et al. [93] produced emulsions stabilized with whey proteins to generate stable delivery systems for vitamin D_3-enriched cheeses.

2.2.4 Supra-molecular structures with putative encapsulation properties

In addition to the production of the encapsulation devices presented above, whey proteins can spontaneously form a large variety of supramolecular structures under specific physico-chemical conditions. The supramolecular structures differ in geometry, size and porosity. The main factors that drive the final structure are: protein conformation and concentration, pH, temperature, ionic strength and the presence of small solutes [15]. The supramolecular structures described in the literature are mainly fibrils [94], ribbons [95], spherulites [96], nanotubes [97] and microspheres (obtained by heteroprotein complex coacervation) [98, 99] (Figure 2.5).

Amyloid-type fibrils are linear polymers that are between 3 and 10 nm in width, and can reach several microns in length [94]. The formation of fibers involves two steps: nucleation and subsequent unidirectional growth [100]. The ability to form fibers has been described for β-LG [94] and α-LA [101]. Specific physico-chemical conditions are generally required to initiate fibrillation; the proteins have to contain exposed hydrophobic regions and to conserve some surface charges [15]. In addition, the fibrillation process is favored by the cleavage of some peptide bonds [102]. These fibers can further self-associate into more complex structures, e.g., ribbons and spherulites. Ribbons are the result of the lateral stacking of these fibers and are usually obtained after the prolonged heating of globular proteins under acidic conditions [95]. Alternatively, spherulites are formed by the radial association of the fibers, a structure that can reach hundreds of micrometers in diameter [96].

The formation of nanotubes from whey proteins is less widespread than the formation of fibers or aggregates. To date, whey protein nanotubes have only been obtained by the self-assembly of α-LA fragments formed by limited hydrolysis of the protein backbone by a serine protease [97]. Regular nanotubes with a length up to several microns, an external diameter of 20 nm and an internal diameter of about 8 nm can be obtained by adjusting the protein concentration, the concentration of added specific divalent cations and hydrolysis conditions [97]. It was suggested that the reversible association of α-LA into nanotubes could be explored as vehicles for delivering bioactives and for encapsulation and release purposes [103].

The spontaneous formation of nano- and microspheres was reported by complex cocervation between oppositely charged proteins [15]. The formation of coacervates (microspheres) betweeen positively charged lysozyme (LYS) and negatively charged α-LA and the underlying mechanisms are now well described [98, 99]. More details will be given below.

Although several authors have indicated that these supra-structures could be of potential interest as encapsulation agents, there are almost no publications dealing with the effectiveness of such applications [4]. This new research area of controlled assembly, involving heteroprotein complex coacervation, offers new opportunities to develop innovative, reversible and versatile vehicles to encapsulate bioactive or sensitive ingredients.

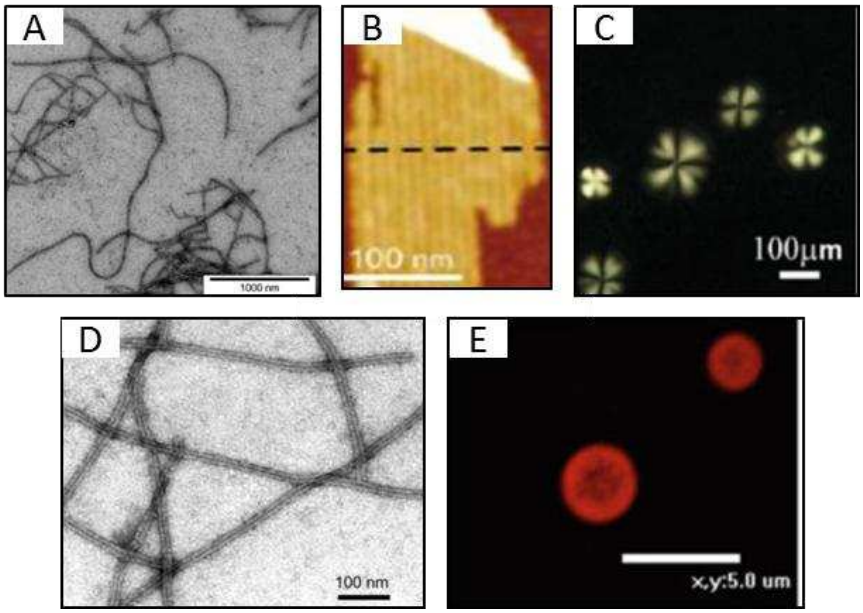

Figure 2.5. Different supramolecular structures obtained from whey proteins. (A) TEM micrograph of whey protein isolate (WPI) obtained from 2 % of WPI at pH 2 solution heated at 80 °C for 16h (adapted from Loveday et al. [104]). (B) AFM micrograph of β-LG ribbons obtained after heating β-LG (2 %wt.) at 90 °C and pH 2 (adapted from Lara et al. [95]). (C) Polarised light microscopy micrograph of β-LG spherulites (adapted from Krebs et al. [105]). (D) TEM micrograph of hydrolysed a-LA nanotubes (adapted from Graveland-Bikker et al. [106]). (E) Confocal scanning laser micrograph of heteroprotein complex coacervates obtained from apo a-LA (0.2 mM) and LYS (0.2 mM) mixture (adapted from Nigen et al. [107]).

2.3 Complex coacervation of whey protein

2.3.1 Complex coacervation: principle

The coacervation is an equilibrium phenomenon of a colloidal system characterized by the formation of two liquid phases, one having a higher concentration of the colloid, called coacervate phase, and the other poorly concentrated called equilibrium solution [108]. When the phase separation is induced by the interaction of two oppositely charged colloids, the equilibrium phenomenon is called complex coacervation. Usually the two phases separation process starts with the formation of coacervates droplets dispersed in the equilibrium phase that coalesce over time into a continuous phase [108].

The complex coacervation has been studied since several decades. The first study describing the complex coacervation between macromolecules dates back to 1929 when Bungenberg de Jong & Kruyt published the interaction between arabic gum and gelatin [109]. Since this pioneering work, the complex coacervation has aroused interest in many fields of science. The Russian biochemist Oparin suggested that complex coacervation was the first living organism [110]. He supported his assumption on the relative solubility of complex coacervates, their ability to dissolve, to increase in size and to disintegrate under slight environmental changes [111]. Although nowadays, after the discovery of DNA, we know that description of complex coacervates is not plausible.

More recently, the occurrence of complex coacervation in nature has been advanced in the case of the construction of the mineral protection tubes by Sandcastle worm and Caddisfly larvae [112]. To build up their protection tubes, these two invertebrates are able to produce an adhesive material by complex coacervation of proteins allowing the fixation of particles (rocks, sand...) (Figure 2.6A) [112]. The elegant artistic ability of Caddisfly larvae have even been explored to jewelry design (Figure 2.6B).

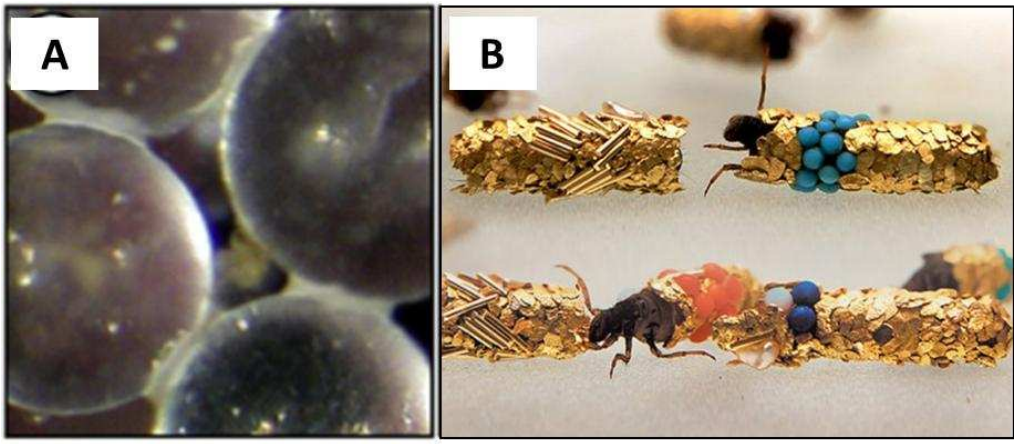

Figure 2.6. (A) Glass beads glued together using proteins complex coacervates produced by sandcastle worm (adapted from Stewart et al. [112]); and (B) Gold and gemstones jewelry built by Caddisfly Larvae (adapted from Matus [113])

Several theoretical models have been developed to describe the complex coacervation between oppositely charged macromolecules; nevertheless none of these models is able to perfectly predict the phenomenon [114, 115]. First Voorn [116] explained the spontaneous coacervation between macromolecules as a competition between the attractive electrostatic component and the unfavourable entropic component [116, 117]. This model was adapted by Sato and Nakajima [118] to take into account the effect of the solute/solvent interaction initially neglected in the parent model.

Chronologically, the second model proposed was the "Symmetrical Aggregate Model" by Veis et al. [119]. These authors described the complex coacervation between oppositely charged macromolecules in two steps: (i) spontaneous formation of heterocomplexes by electrostatic interactions presenting small conformational entropy and (ii) Rearrangement of the heterocomplexes by the conformational entropy gain, leading to the formation of the coacervates. Afterwards, this model was adapted by Tainaka [120] to take into account the presence of counterions and their important entropic contribution, effects that were initially

neglected [120, 121]. These last authors also extended the model, applying it to the complex coacervation of unsymmetrical heterocomplexes (i.e. formed by polyions presenting different sizes and charges). It is assumed today that the model proposed by Tainaka, although still not perfect, better relates the complex coacervation of polyions [114].

More recently Veis [122] revisited and completed his initial model to take into account a possible excess of charge or a disequilibrium of molecular size between the two polyions. The author proposed that the heterocomplexes forming the coacervates could be symmetrical or random and the polyion presenting the excess of charge would always remain in the equilibrium phase.

Various applications of the coacervation has been reported in literature: (i) immobilization of enzymes, (ii) antigen delivery, (iii) design and production of new biomaterials, (iv) protein purification and (v) stabilization of food products [123]. Anyway the knowledge about different coacervation systems is not uniform. While the complex coacervation between polyelectrolytes, polyelectrolytes-proteins, polysaccharides and polysaccharide-protein is well described [15, 115, 123], the coacervation of heteroproteins is much less described and more difficult to be predicted mainly due to heterogeneous distribution of electric charges and their anisotropy on protein surfaces [15, 123].

2.3.2 Complex coacervation of globular proteins

The first publications describing the interaction between two oppositely charged globular proteins date back to the end of 80s early 90s. Matsudomi et al. [124] and Lampreave et al. [125] described respectively the ability of LYS to form complexes with heat-denatured ovalbumin and LF to form complexes with β-LG and BSA via electrostatic interactions. Howell et al. [126], on their side, described the ability of lysozyme to electrostatically interact with α-LA and β-LG to form insoluble precipitates. These authors described an increase of

turbidity of solutions resulting from the mixture of LYS and α-LA or β-LG throughout the formation of co-precipitates. However, the first clear description of the complex coacervation between two oppositely charged globular proteins was the interaction between apo α-LA (calcium-depleted form) and LYS reported fifteen years later by Nigen et al. [98]. The complex coacervation between these two proteins is today without doubts the most studied coacervation system between two globular proteins.

Egg white LYS has a high sequence similarity with α-LA. It does not present specific metal binding sites, it has a molecular weight of 14.3 kDa and 129 AA. From its 129 AA, 54 are identical and 23 are structurally similar to α-LA, but LYS is a basic protein with a pI of 10.7 [1, 15].

Nigen et al. [98] described the ability of LYS to interact with apo α-LA and form different supramolecular structures. Interestingly, these authors pointed out the inability of LYS to form supramolecular structures when mixed in the same experimental conditions with native-LA (holo form). Indeed, the shape of the apo α-LA/LYS formed molecular assemblies depended on the working temperature, below 30 °C the formation of amorphous aggregates was observed while coacervates were formed at temperatures higher than 30 °C. Despite the different shapes, the elementary bricks forming the coacervates and the amorphous aggregates seemed to be the same [127].

As shown on Figure 2.7, regardless the temperature, mixing these two proteins at low ionic strength, different LYS/apo α-LA molar ratio and neutral pH (pH 7.5), turbid solutions that separated into two distinct phases over time were obtained. When amorphous aggregates were formed, a very compact and opaque dense phase was observed while a more translucent and liquid/gelatinous dense phase was observed when coacervates were formed. The coacervates presented an equimolar proportion of the two proteins. Interestingly, the increase of the

solutions temperature resulted in structural reorganisation from amorphous aggregates to coacervates [98, 127].

Apo α-LA presents a denaturation temperature of about 30°C, above this temperature the protein adopts a more flexible unfolded state. The key role of the temperature on the coacervates formation was attributed to the necessity of a higher flexibility and the exposition of some hydrophobic domains of apo α-LA to allow structuration of the complexes into coacervates [98].

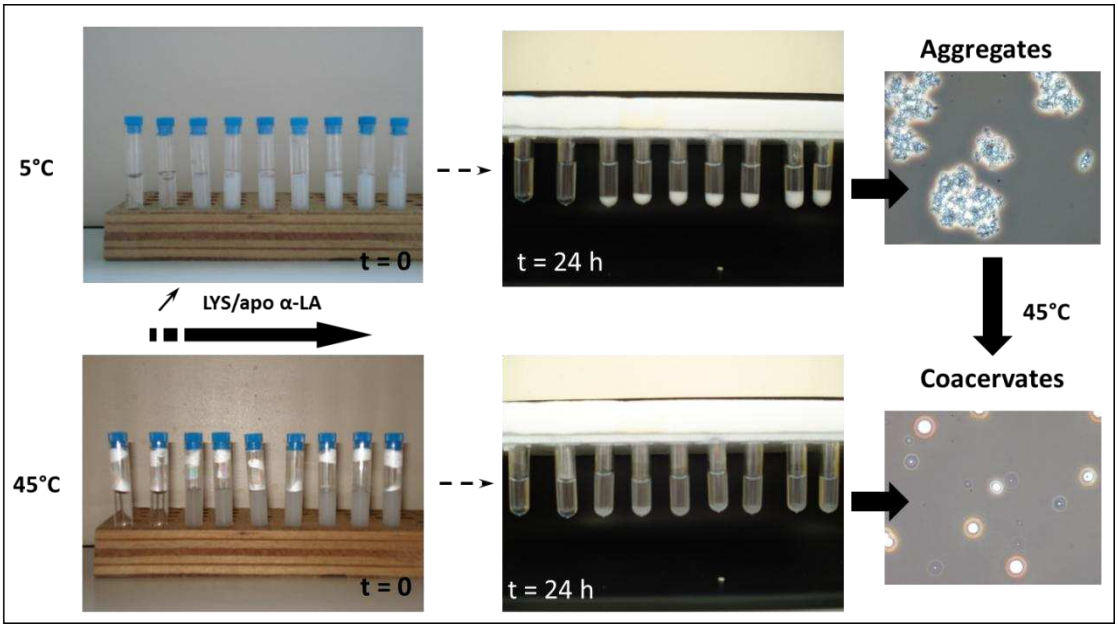

Figure 2.7. Summary of the interactions, supramolecular structure formation and phase separation of apo α-LA-LYS mixture at 5 and 45 °C ranging from 0.05 to 2 LYS/α-LA molar ratio at fixed α-LA concentration (0.266 mM) (adapted from Nigen et al. [98]).

Using labelled apo α-LA and LYS some information on the dynamics and organization of each protein into the coacervates (microspheres) dispersed in the equilibrium solution could be obtained. From confocal microscopy images and FRET experiments, perfect co-localization of the two proteins in the formed coacervates was demonstrated. [128].

Also, using confocal microscopy, the dynamic exchange between the proteins in coacervates and those remaining in dilute phase was evaluated (Figure 2.8). The coacervates were first formed between unlabelled apo α-LA and LYS-FITC (green fluorescent probe), then LYS-RBITC (red fluorescent probe) was added and the protein exchange was monitored throughout the evolution of the fluorescence over time (green to orange). The observation of completely orange coacervates (after 75 min) indicates the continuous equilibrium between the proteins forming the coacervates and those remaining in dilute phase [107].

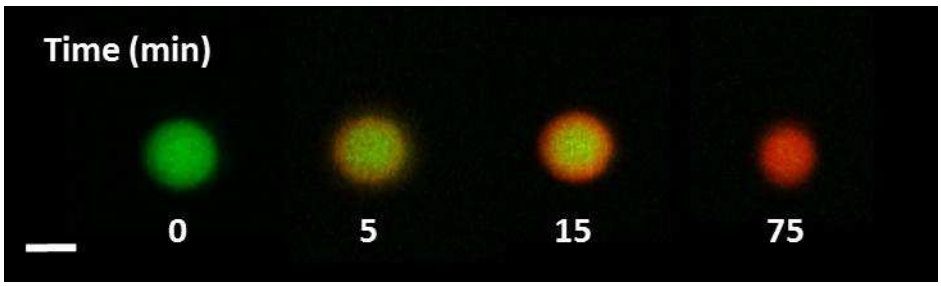

Figure 2.8. Internal dynamic of apo α-LA-LYS coacervates and time-dependent protein exchange between coacervates and dilute phase (adapted from Nigen et al. [107]).

Similarly to others coacervation systems, the heteroprotein complex coacervation is also directed by electrostatic interactions, thus the process is significantly affected by the increase in ionic strength [99]. Reaching a critical ionic strength, the contribution of the entropy gain on the coacervation linked to the release of counterions disappears because the concentration of counterions on the polyions neighbourhood and in solvent becomes almost the same [129]. In addition, non-electrostatic forces are also involved on the stabilization of protein coacervates as clearly pointed for example in the case of apo α-LA-LYS system [99].

Nigen et al. [130] showed that although holo α-LA were not able to form supramolecular structures with LYS, at molecular level similar association constant was found for the interactions of holo α-LA - LYS and apo α-LA - LYS. The mechanisms of the interaction between LYS and the two forms α-LA were further elucidated through selective identification

of amino-acids involved of the interacting surfaces. These experiments were performed by titration of one ^{15}N-labelled protein with its unlabelled partner using NMR chemical shift perturbation technic [131]. As summarized by Figure 2.9, α-LA presents a narrow interaction site to form heterodimers, while LYS displays sites spread across its surface. The formation of tetramers by interaction of heterodimers requires additional interaction sites between α-LA and LYS. Unlike holo α-LA, calcium depleted apo α-LA exposes another electronegative domain on the protein surface that corresponds to required second interaction site making possible the formation of tetramers, the building blocks for coacervation [131]. Most of the electrostatic charge patches on of the protein surfaces are masked on the tetramers. As a consequence, the increase of hydrophobic interactions was proposed as driving force allowing the self-assembly of tetramers into coacervates. Performed Monte Carlo simulations that show preferential alignment between proteins according to their dipole moments support experimental findings [131].

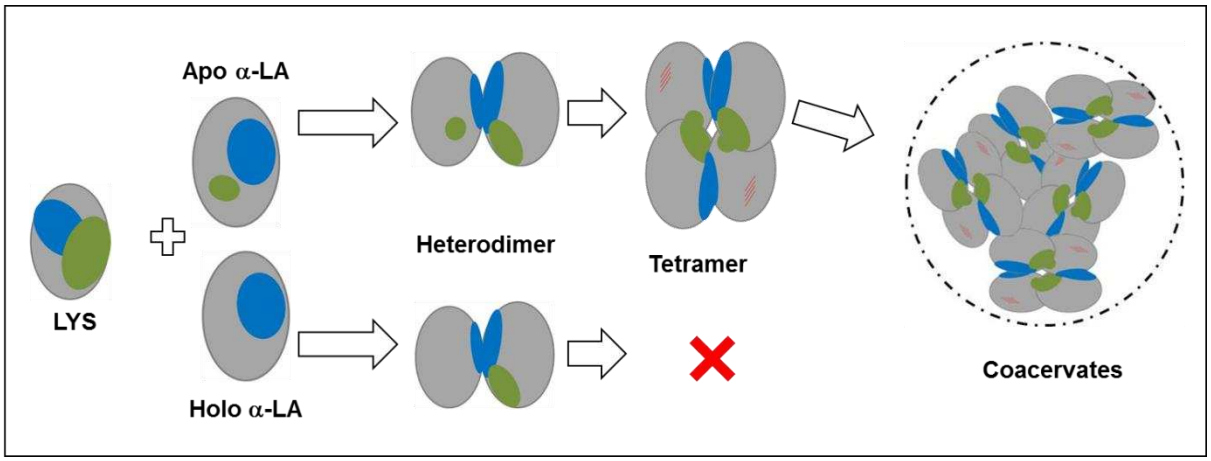

Figure 2.9. Proposed mechanism explaining selective formation of coacervates following the interaction of lysozyme with calcium depleted α-LA (apo α-LA - LYS) but not with holo α-LA (adapted from Salvatore et al. [131]). Blue zones indicate the binding sites leading to the heterodimer formation, green zones indicate the binding site required to the formation of tetramer.

Complex coacervation involving others food globular proteins was also reported [53]. Table 2.3 summarizes the main studies concerning the spontaneous co-assembly of oppositely charged food proteins. From these different studies, it was concluded that it is possible to form coacervates in various binary protein mixtures, providing adapted experimental conditions. Whatever the binary system, protein surface charge compensation, consistent with the complexation theory between biopolymers, seems to prevail in the mechanism that governs heteroprotein coacervation. Interestingly, as the stoichiometry found in coacervates depends, among other considerations, on the extent of the relative size difference between mixed proteins, charge compensation is necessary but not sufficient. Consequently, size compensation is also a key parameter that guides protein assembly and their stoichiometry in coacervates of heteroproteins. Hence, the experimental conditions for protein coacervation are specific for each system because of the required charge and size compensation.

Anema and co-workers were also interested on the complex coacervation of food proteins, however their publications generally refer to the complex coacervation between basic globular proteins (LF or LYS) and unstructured acidic proteins (α, β, or κ-casein; α-CN, β-CN, κ-CN) [132-135]. They described the formation of a precipitate by non-covalent aggregation (electrostatic interaction) between the proteins [132, 133] or the liquid-liquid phase separation by complex coacervation [135]. In the case of the co-precipitation (LYS - β-CN) the formed aggregates presented an "infinite" growth [133]. On the other hand, in the case of the liquid-liquid phase separation kinetics of nucleation and coalescence (LF-β-CN and LF-κ-CN) or nucleation, growth and coalescence (LF-α-CN) were evidenced [135].

So far, the only studies on heteroprotein complex coacervation involving two whey proteins concerns the case of β-LG and LF.

Table 2.3. Main studies concerning the spontaneous co-assembly of oppositely charged food

proteins (adapted from Bouhallab and Croguennec [15]).

Acidic protein	Basic protein	Formed structures	Reference
Denatured ovalbumin	LYS	undetermined	[124]
β-LG	LF	undetermined	[125]
BSA	LF	undetermined	[125]
Holo α-LA	LYS	undetermined	[126]
β-LG	LYS	undetermined	[126]
Succinylated LYS	LYS	undetermined	[136]
Caseins	LF	coacervates	[132, 135]
Gelatin B	Gelatin A	coacervates	[137]
Apo α-LA	LYS	aggregates / coacervates	[98, 107, 127, 131]
Ovalbumin	LYS	coacervates	[53]
Ovalbumin	Avidin	coacervates	[53]
BSA	LYS	coacervates	[53]
β-LG	LYS	coacervates	[138]
β-LG	LF	aggregates / coacervates	[6, 139, 140]

2.3.3 Specific case of complex coacervation between β-LG and LF

β-LG is the major whey protein in cow milk, its industrial purification process is known and well controlled thus it is an available protein. LF, the major basic protein in cow milk, is also produced at industrial scale. In addition LF presents a high industrial value mainly because of its biological properties. Hence, these two proteins are the obvious choice for the generation of encapsulation devices compatible with dairy matrices by heteroproteins complex coacervation.

During the execution of this thesis two others research teams published on the coacervation process between β-LG and LF. First Dubin, Schmitt & co-workers [139] published some general aspects about the conditions of coacervation between these two proteins. A few months later Anema & De Kruif [140] published a very similar study confronting in some points and corroborating in others the previously published results.

Two other papers about the structure of β-LG - LF coacervates were published by Dubin, Schmitt & co-workers. The first focused on the validation of the model previously proposed for the structure of the building block of the coacervates using small angle neutron scattering [141]. The second one concerned the equilibrium between β-LG - LF structures forming the coacervates and those remaining in the equilibrium solution as a function of the β-LG/LF molar ratio [142].

These results will not be presented in this review of literature section. As the publications appeared during the realization of this thesis they influenced the strategy adopted during the execution of this project. Anyway, these results will be widely discussed and compared to ours in the results and discussion section.

RESULTS AND DISCUSSION

3 CHAPTER 1: Multiscale characterization of Lactoferrin and β-lactoglobulin complex coacervation

PART 1: SELECTIVE COACERVATION BETWEEN LACTOFERRIN AND THE TWO ISOFORMS OF β-LACTOGLOBULIN

PREAMBLE

The complex coacervation between globular proteins is a universal process depending on specific reactional conditions. The results from the binary protein systems already studied, in particular by our group, evidenced the sensitivity to structural and conformational modifications of the proteins involved. In the present work, we focused on the complex coacervation between β-LG and LF, respectively the major acidic and basic protein from whey of cow milk. The aim of the first part of the Chapter 1 was to determine the optimal conditions of complex coacervation between β-LG and LF, the thermodynamic of the initial interaction, and the sensitivity of this process to subtle protein surface charge and hydrophobicity changes comparing the two major isoforms of β-LG.

Our questions:

- What are the optimal reactional conditions for β-LG - LF complex coacervation?
- What are the interactions and thermodynamic parameters governing the initial steps?
- How the subtle amino acid substitution of the β-LG main isoforms affects the coacervation process at defined optimal physico-chemical conditions?

The domain of formation of coacervates after mixing β-LG A + LF, β-LG B + LF and β-LG (A+B) + LF were determined at different pH and in a large range of protein concentrations and protein molar ratios. The proteins recovered in the coacervate phases were quantified, as well as the proportion of each β-LG isoform for the mixtures containing β-LG (A+B) + LF.

In addition, the molecular interaction of β-LG A and β-LG B with LF was studied by Isothermal titration calorimetry (ITC).

Our main results:

- We determined the conditions (pH, protein concentration and protein molar ratio) allowing the complex coacervation between β-LG and LF to occur.
- The transition between coacervation and aggregation regimes depends on the initial β-LG/LF molar ratio.
- Variable β-LG/LF molar ratios in the coacervate phase were observed (4 – 8).
- LF showed a preference for β-LG A isoform. Compared to β-LG B, β-LG A presented a larger coacervation domain with LF and was able to shift the coacervation equilibrium towards the formation of coacervates.
- β-LG binds to LF at two different binding sites.
- The interaction of LF with the dimeric form of β-LG seems to be a prerequisite for the complex coacervation.

Selective coacervation between lactoferrin and the two isoforms of β-lactoglobulin

The content of this first part of the chapter has been published in:

Food Hydrocolloids, 2015. 48(0): p. 238-247.

Guilherme M. Tavares, Thomas Croguennec, Pascaline Hamon,

Antônio F. Carvalho, Saïd Bouhallab

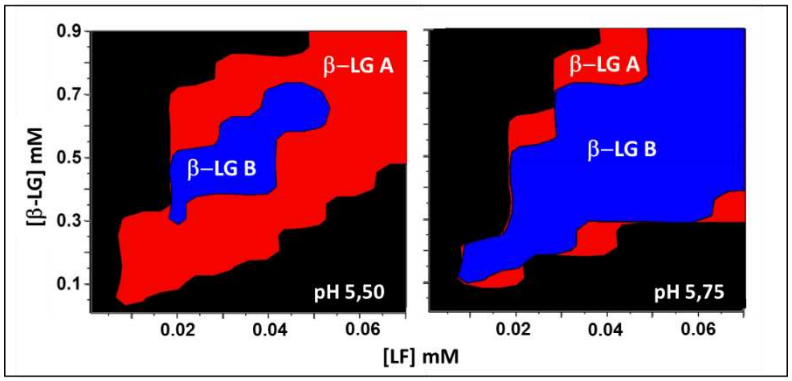

Graphical Abstract: Superposition of the coacervation domains obtained by mixing LF and β–LG A (red) or β–LG B (blue) at pH 5.50 and pH 5.75.

ABSTRACT

This work reports on the impact of subtle change of protein charge on coacervation and subsequent liquid-liquid phase separation between two oppositely charged globular proteins. For this purpose, a comparative study was conducted on the coacervation of lactoferrin (LF) with the two β-lactoglobulin (β-LG) isoforms. Upon mixing LF with an excess of β-LG, microspheres were formed throughout coacervation under narrow pH range (5.4-6.0). At the optimal pH of coacervation, LF being the limiting partner under tested concentration ranges. The β-LG/LF molar ratio recovered in the formed coacervates varied from 4 to 8 depending

on the total protein concentration. Remarkably, LF showed a selective coacervation with isoform A of β-LG as judged by a larger concentration domain for coacervation and a high yield of LF recovered once mixed with β-LG A i.e. 80% against a maximum of 42% with β-LG B. At thermodynamic level, the interaction of LF with both β-LG isoforms exhibited complex exothermic binding isotherms with both enthalpic and entropic contributions.

Keywords: β-lactoglobulin isoforms, lactoferrin, co-assembly, microspheres, coacervates

3.1 Introduction

Protein assembly is the focus of research teams from various fields (medical, pharmaceutical, cosmetic, food) with the aim to understand the underlying mechanisms that trigger protein interactions and the factors affecting the growth of the assemblies. This constitutes a prerequisite to control the protein assembly process and to consider industrial applications. Protein assembly may be divided into two classes depending on a preliminary protein unfolding step: induced assembly or spontaneous assembly [15]. Compared to induced assembly that requires energy input and large changes of the protein structure, spontaneous assembly involves native proteins. In the latter case, the driving forces for protein assembly are intermolecular attractive interactions between protein's surface residues and the indirect entropy effect associated to the release of counter ions and/or water molecules during protein assembly. Interactions between proteins involve weak interactions making the assembly reversible when changing ionic strength and other factors that modify protein surface charge properties [12, 99, 133, 143]. Spontaneous assembly is obtained with systems containing one protein (self-assembly), usually close to the protein pI [12] or in systems containing oppositely charged proteins (co-assembly) at intermediate pH between the pI of the involved proteins [53, 126, 132, 133, 139]. Co-assembly is maximum for pH conditions where molar

charge equivalent ratio (charge neutralization) is reached [99, 132]. Under these conditions, liquid/liquid phase separation occurs which was described as, random aggregates [98, 133], complex coacervation [139] or well-defined microspheres [127, 128]. Behind the physic-chemical parameters of the medium, protein size, protein conformation, protein concentration and protein molar ratio are important parameters for co-assembly into coacervates [15]. Compared to other macromolecular systems, available studies on spontaneous co-assembly of proteins into coacervates are rare. Desfougeres et al. [53] pointed out the key role of both charge neutralization and protein size compensation for liquid-liquid phase separation i.e. formation of coacervates in binary protein systems. Mechanisms behind this type of co-assembly were explored in the case of Lysozyme (LYS) and apo-α-lactalbumin (apo-α-La). After mixing LYS and apo-α-La, random aggregates were formed that reorganized progressively in a temperature-dependent manner into microsphere [107, 127]. The relative rates of protein co-assembly into random aggregates and their subsequent reorganization into coacervates could explain the shape of formed supramolecular structures according to time laps after mixing the proteins.

Interestingly, it was observed that LYS formed coacervates leading to a liquid-liquid phase separation with apo-α-La but not with holo-α-La even if at molecular level LYS interacts equally with holo (with calcium) and apo (without calcium) α-La to form heterodimers [130]. The specific behavior of the apo-α-LA - LYS heterodimer rely on the higher flexibility of the apo-α-La compared to holo-α-La and the exposition of an additional negatively charged region on the apo-α-La surface giving another site for the interaction with LYS to form tetramers as demonstrated by nuclear magnetic resonance [131]. In the tetramers all charged patches on the protein's surface are shielded allowing their association into large supra-molecular structures through preponderant hydrophobic interactions [131].

Recently, liquid-liquid phase separation described either as microspheres [15] or coacervates [139, 140] was reported after mixing beta-lactoglobulin (β-LG), an acid protein, and lactoferrin (LF), a basic protein (pI 8.6-8.9) under appropriate conditions. For homogeneity between these studies, the term coacervates is used instead of microspheres in the rest of the manuscript. In the above studies β-LG was a mixture of the two main genetic isoforms, β–LG A and β–LG B [15, 139] or only β–LG B [140], but the specific contribution of β-LG isoforms to coacervation was not investigated yet. β–LG A and β–LG B has 162 amino acids with a molecular weight (Mw) of 18362 Da and 18277 Da respectively. They differ one from another by only two amino acids (Asp64 and Val118 in β–LG A are changed to Gly and Ala in β–LG B, respectively [11]), without affecting β–LG secondary and tertiary structure. These substitutions modify some physical and chemical properties of β–LG: β–LG A with a pI of ≈ 5.1 is more hydrophobic and more negatively charged than β–LG B with a pI ≈ 5.2 [12]. At neutral pH and room temperature β–LG exists as a stable non-covalent dimer but its stability depends on β–LG isoforms [144]. The two isoforms also exhibit different pH-dependent aggregation rate [12], thermal denaturation temperature [145], susceptibility to chemicals [146, 147] and affinity to hydrophobic molecules such as fatty acids [148]. In the present paper we investigated the impact of these two isoforms of β-lactoglobulin molecule on its ability to co-assemble into coacervates once mixed with LF. Selective behavior of LF toward the two isoforms was evidenced with a higher preference for β–LG A, the more negative isoform. The relative concentration domain for coacervation was larger for β–LG A - LF compared to β–LG B - LF mixture. Under optimal conditions, until 8 β–LG molecules were bond per LF molecule in formed coacervates.

3.2 Materials and Methods

3.2.1 Reagents and stock solutions

Bovine lactoferrin (LF) (purity of 90% and iron saturation of 10 - 20 % according to technical specification) was purchased from Fonterra Cooperative Group, New Zealand. Bovine beta-lactoglobulin isoforms A (β–LG A) and B (β–LG B) were purified by anion exchange chromatography from a confidential industrial source of β-lactoglobulin. Basically, the protein was dispersed in deionized water (45 g/L), adjusted to pH 4.6 with 1M HCl and kept at 30°C for 5 min in order to precipitate non-native forms of β-lactoglobulin. The dispersion was centrifuged at 20 000*g* at room temperature for 10 min (Heraeus Biofuge Primo, Thermo Scientific, Waltham, MA, USA). The supernatant containing a mix of native β-lactoglobulin isoforms was diluted twice with Tris-HCl buffer (40 mM, pH 7.0). Ion-exchange purification was performed on a Q-Sepharose Fast Flow resin (GE Healthcare, Velizy-Villacoublay, France) packed in a LRC 50/80 – 200 column (Pall Corporation, Ann Arbor, MI, USA) connected to the VARIAN preparative chromatography system (PrepStar 218/ProStar 210, Varian Inc., Mulgrave, Australia) equipped with a 280 nm UV detector. Elution was performed at 20 mL min^{-1} using a NaCl gradient in a 20 mM Tris-HCl buffer, pH 7.0. Collected β–LG A and β–LG B fractions were concentrated and then diafiltrated with deionized water on a 5.0 kDa ultrafiltration membrane. The protein solutions were then freeze-dried and stored at – 20 °C until use. The purity of prepared protein powders was higher than 95% as assessed by reverse phase liquid chromatography.

LF, β–LG A and β–LG B solutions were prepared by solubilizing the protein powders in 10 mM MES buffer adjusted at various pH from 5.0 to 6.0. The solutions were filtered through a 0.2 µm membrane (cat. no. 4612, Pall Corporation, Ann Arbor, MI, USA). The exact protein concentration was determined by absorbance at 280 nm (SAFAS UV MC2, Safas, Monaco) using 0.96 L g^{-1} cm^{-1} and 1.47 L g^{-1} cm^{-1} as extinction coefficients for β–LG and LF

respectively. Then stock solutions of β–LG A and β–LG B at 1.5 mM and LF of 0.3 mM were prepared by dilution with 10 mM MES buffer. In addition, a stock solution containing an equimolar ratio of β–LG A and β–LG B, β–LG A+B, was prepared by mixing equal volume of β–LG A and β–LG B stock solutions. No sign of self-aggregation was detected in the stock solutions that were translucent in the whole range of pH tested.

3.2.2 Turbidity measurements

Turbidity measurements were performed at 600 nm (A_{600nm}) with the spectrometer FLX-Xenius (Safas, Monaco) to monitor co-assembly between the two proteins. Absorbance measurements were converted to turbidity using the following relationship: $\tau = (2.303A_{600nm})/l$, where τ is the turbidity (cm^{-1}) and l is the light path length (0.26 cm) corresponding to the height of the liquid column (100 µL) into the microplate well.

For all experiments, protein mixing was performed directly into the microplate wells in the following order: buffer + β–LG + LF. Absorbance measurements were made immediately after the protein mixing.

3.2.3 Phase boundaries of coacervation

Phase boundaries were built-up to identify the zones of formation of coacervation after mixing β–LG (β–LG A, β–LG B or β–LG A+B) and LF in 10 mM MES buffer at pH 5.50 or pH 5.75. The ionic strength was chosen in order to reach good coacervation yield under buffered conditions, coacervation being suppressed above a total ionic strength of 25 mM. Each phase boundary was constructed from 96 points corresponding to protein mixtures containing final β–LG concentration ranging from 10 to 900 µM and final LF concentration ranging from 1 to 70 µM. Preliminary experiments have shown that coacervation is favored by an excess of

β–LG explaining the disproportionality in concentrations chosen for the present phase boundaries.

For all 96 points of the phase boundary, the presence of coacervates, amorphous aggregates or the absence of suprastructures was determined at room temperature using a phase contrast optical microscope (Olympus BX51TF, Olympus, Hamburg, Germany) set at the magnification 100x. Proteins were quantified in the coacervation domains to determine the coacervation yield and protein stoichiometry. For this purpose, a volume of 300 µL of β–LG + LF mixtures was prepared. Supernatant and dense phase were separated by centrifugation (Heraeus Biofuge Primo, Thermo Scientific, Waltham, MA, USA) at 28000*g* for 30 min. Proteins in both phases were quantified using a PLRPS column (S/N 1006329-5, Varian Inc., Shropshire, UK) connected to a Waters 26 95 HPLC. Milli-Q water containing 1.06 ‰ (v/v) of trifluoroacetic acid and a 80/20 acetonitrile/milli-Q water (v/v) mixture containing 1.0 ‰ (v/v) of trifluoroacetic acid were used for elution. The absorbance at 280 nm was measured during the elution using a Waters 2487 detector. Control samples containing only β–LG (A, B or A+B) or LF were prepared at the highest protein concentration tested. Less than 1 % of protein was recovered in the dense phase of the control samples. The phase boudaries and the contours plots were made using the software Origin 7.0. The Renka-cline gridding method was used to convert the random XYZ data to matrices and then to graphics.

3.2.4 Isothermal titration calorimetry (ITC)

The interaction of LF with the two isoforms of β–LG was quantified at 25°C using ITC. ITC experiments were performed on a VP-ITC microcalorimeter (Microcal, Northampton MA). Solutions of β–LG A (2.0 mM), β–LG B (2.0 mM) and LF (0.1 mM) were prepared in 10 mM MES buffer at two pH values 5.50 and 5.75. All solutions were degassed under vacuum before titration experiments. The reference cell was filled with 10 mM MES buffer and the

sample cell (1.425 mL) was filled with LF solution. LF was titrated with 58 successive 5 µL-injections of β–LG A or β–LG B. The injection time was 10 s and the lag time between two successive injections was set to 200 s to allow thermodynamic equilibrium. During the titration, the solution in sample cell was stirred at 310 rpm to ensure complete homogeneity of the solution. ITC data were analyzed using the software Origin 7.0. For each ITC experiment, the area under each peak was plotted versus the β–LG/LF molar ratio. For all experiments, the interaction signal at the end of the titration (plateau) was moved to 0.0 kcal mol^{-1} before ITC data fitting. The dissociation profiles of β–LG A or β–LG B dimers in the same experimental conditions were obtained by titrating β–LG solutions into 10 mM MES Buffer.

3.3 Results

3.3.1 Optimal pH for coacervation

Turbidity measurements were performed between pH 5.0 and 6.0 in order to select the pH of maximum co-assembly of LF with either β–LG A, β–LG B or β–LG (A+B) (Figure 3.1). Under the pH range investigated, the protein stock solutions had no detectable turbidity. The two β–LG isoforms exhibited different pH values for maximum turbidity. β–LG A + LF mixture showed an optimum turbidity value at pH 5.50 which shifted to pH 5.75 for β–LG B + LF mixture. The turbidity of β–LG A + LF was always higher than the one of β–LG B + LF at both pH values. Turbidity values close to those for β–LG A + LF was found for β–LG (A+B) + LF mixture at pHs 5.50 and 5.75. For all tested pHs, the turbidity of the mixture of β–LG (A+B) + LF was different from the sum of the half of the one presented by β–LG A + LF and β–LG B + LF mixtures. For instance, the turbidity of β–LG (A+B) + LF mixture appears to be dictated by β–LG A.

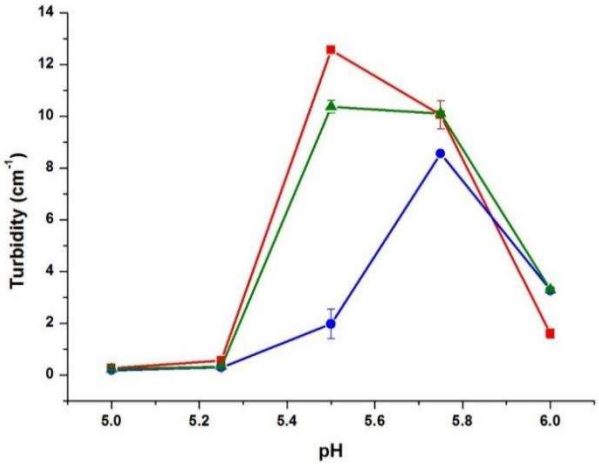

Figure 3.1. Change in turbidity of mixtures containing 40 µM of LF and 500 µM of (■) β–LG A, (●)β–LG B or (▲)β–LG A+B in 10 mM MES buffer at different pHs.

The shape of the formed supramolecular structures changed with the pH of the mixtures (Figure 3.1). Small aggregates (< 1 µm) were observed at pH 5.00 and 5.25, while coacervates were observed between pHs 5.50 and 6.00. The size of coacervates formed at pH 5.50 and 5.75 varied from 2.5 to 7.5 µm against less than < 2.5 µm at pH 6.00 exhibited. Mixtures containing aggregates exhibited a turbidity lower than the mixtures with coacervates. Despite the larger size of the coacervates compared to the aggregates, the difference in turbidity is probably also related to a higher proportion of proteins involved into formed coacervates. The determined optimum pH values are valid for the studied protein molar ratio and may vary by changing this ratio. This experimental procedure was chosen to better illustrate the differences in the behavior between the two β–LG isoforms. Studies of the next sections were conducted at pH 5.50 and pH 5.75, the optimal pH values for coacervation of LF with β–LG A and β–LG B, respectively. Hence the obtained results are valid for chosen protein concentrations used under these pH conditions. All the experiments were performed in MES buffer 10 mM and not in water to avoid pH drift during complexation and titration experiments.

3.3.2 Formation of coacervates as a function of protein concentration

Phase boundaries were built-up to identify the coacervation domain as a function of β–LG and LF concentrations at selected optimum pH values (Figure 3.2). We checked that no self-aggregation occurred in protein stock solutions used for these experiments. Three different concentration domains were distinguished on the phase boudaries: i- the black domain where no supramolecular structures were detected; ii- the gray domain where aggregates were observed (Figure 3.2 G); iii- The colored domains where coacervation i.e. formation of microsphere occurred (Figure 3.2 H). The coacervation domain was almost systematically surrounded by a concentration domain where aggregates were observed. Hence, by increasing β–LG concentration at a fixed concentration of LF, a domain with no detectable supramolecular structures was first crossed followed by aggregation and coacervation domains. A new aggregation domain was observed for the highest β–LG concentrations (highest β–LG/LF molar ratio). Hence, for all mixtures and pH conditions tested, the high impact of protein molar ratio on the coacervation process is clearly evidenced. The optimal protein concentrations for coacervation were found at the diagonal of the presented phase boundaries.

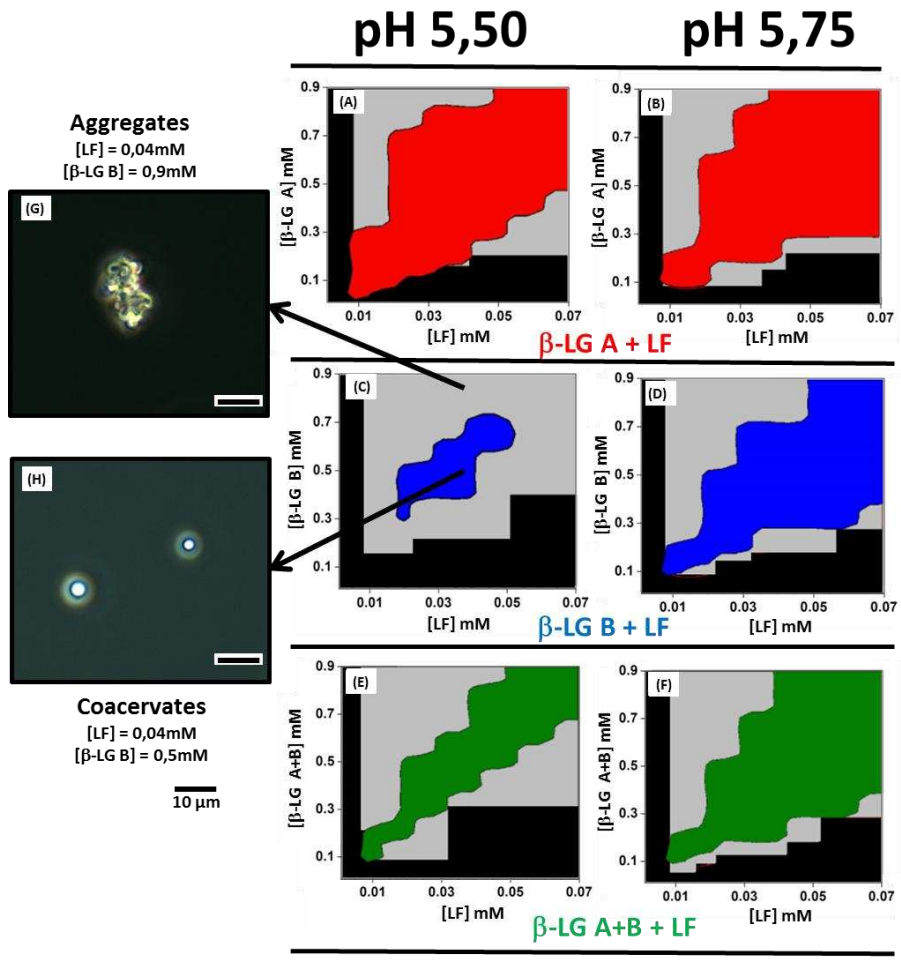

Figure 3.2. Phase boundaries of co-assembly of LF with β–LG isoforms at pH 5.50 and pH 5.75. (A,B): LF - β–LG A; (C,D): LF - β–LG B; (E,F) LF - β–LG AB. Black zones: domains without detectable supramolecular structures; Gray zones: aggregation domains. Red, Blue and Green zones: coacervation domains. Optical microscopy of aggregates formed by mixing for example 40 µM LF and 900 µM β–LG B at pH 5.50 (G) versus coacervates formed by mixing for example LF 40 µM and β–LG B 500 µM at pH 5.50 (H).

At pH 5.50, the area of the coacervation domain for β–LG A + LF was significantly larger than that obtained with β–LG B + LF (Figure 3.2 A, C). The coacervation domain of β–LG (A+B) + LF exhibited intermediary area. The area of the coacervation domain increased significantly from pH 5.50 to pH 5.75 for β–LG B (Figure 3.2 D, F), concomitantly to the

increase of its negative charge. The observed enlargement of the coacervation domains is particularly visible for the higher protein concentrations tested except for β–LG B + LF at pH 5.50. An overlap of the coacervation domains of the three mixtures at both pH is presented in Figure 3.3. The coacervation domain of β–LG A + LF was larger than that found for the two other mixtures, encompassing them entirely. β–LG B + LF mixture exhibited the smallest coacervation domain in particular at pH 5.50.

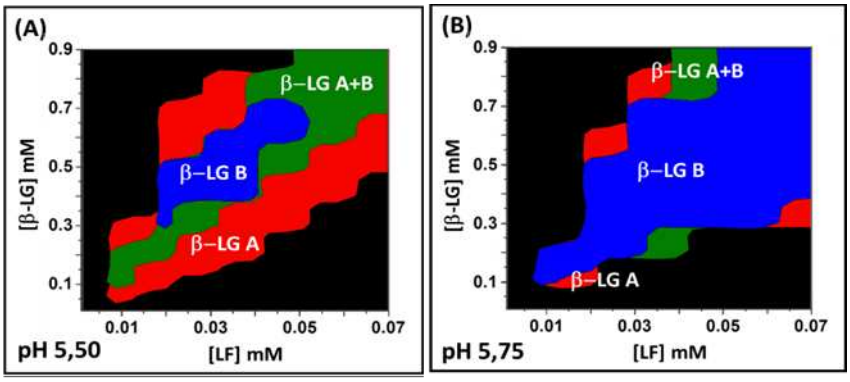

Figure 3.3. Superposition of the coacervation domains obtained by mixing LF and β–LG A (red), β–LG B (blue) or β–LG A+B (green) at pH 5.50 (A) and pH 5.75 (B). Co-assembly experiments were conducted at 25°C in MES buffer 10 mM.

3.3.3 Protein recovery and stoichiometry in formed coacervates

Protein recovery and stoichiometry were determined for the coacervation domains after separation of dense and diluted phases. For all tested conditions, total protein recovery was close to 100 %. The results are presented below in term of two-dimensional contour graphs of recovered protein in the coacervates i.e. the ratio between the amounts of protein (LF or β–LG) in the dense phase to the total protein amount in the initial mixture. For all tested concentrations, no centrifugable proteins were detected in pure protein solutions (axis of the phase boundaries).

Figure 3.4 reports the fraction of LF recovered in the dense phase for each condition tested (coacervation efficiency). The fraction of β–LG in the dense phase showed similar trends as for LF (data not shown). Whatever the conditions, the fraction of LF in the dense phase never reached 100%. For the β–LG A + LF mixtures, the fraction of LF recovered in the dense phase reached a maximal value around 75 - 82 % at both studied pHs. In contrast, when mixed with β–LG B, the LF fraction recovered in the dense phase increased drastically between the two pH conditions reaching up to 35-42% at pH 5.75 versus 6% at pH 5.5. For β–LG (A+B) + LF mixtures, LF recovery in the dense phase being intermediate, with maximum values between 45 - 55 % at pH 5.50 and between 55 - 65 % at pH 5.75. Protein ratios for optimal recovery of LF in the dense phases matched perfectly for the 3 protein mixtures and for both pHs.

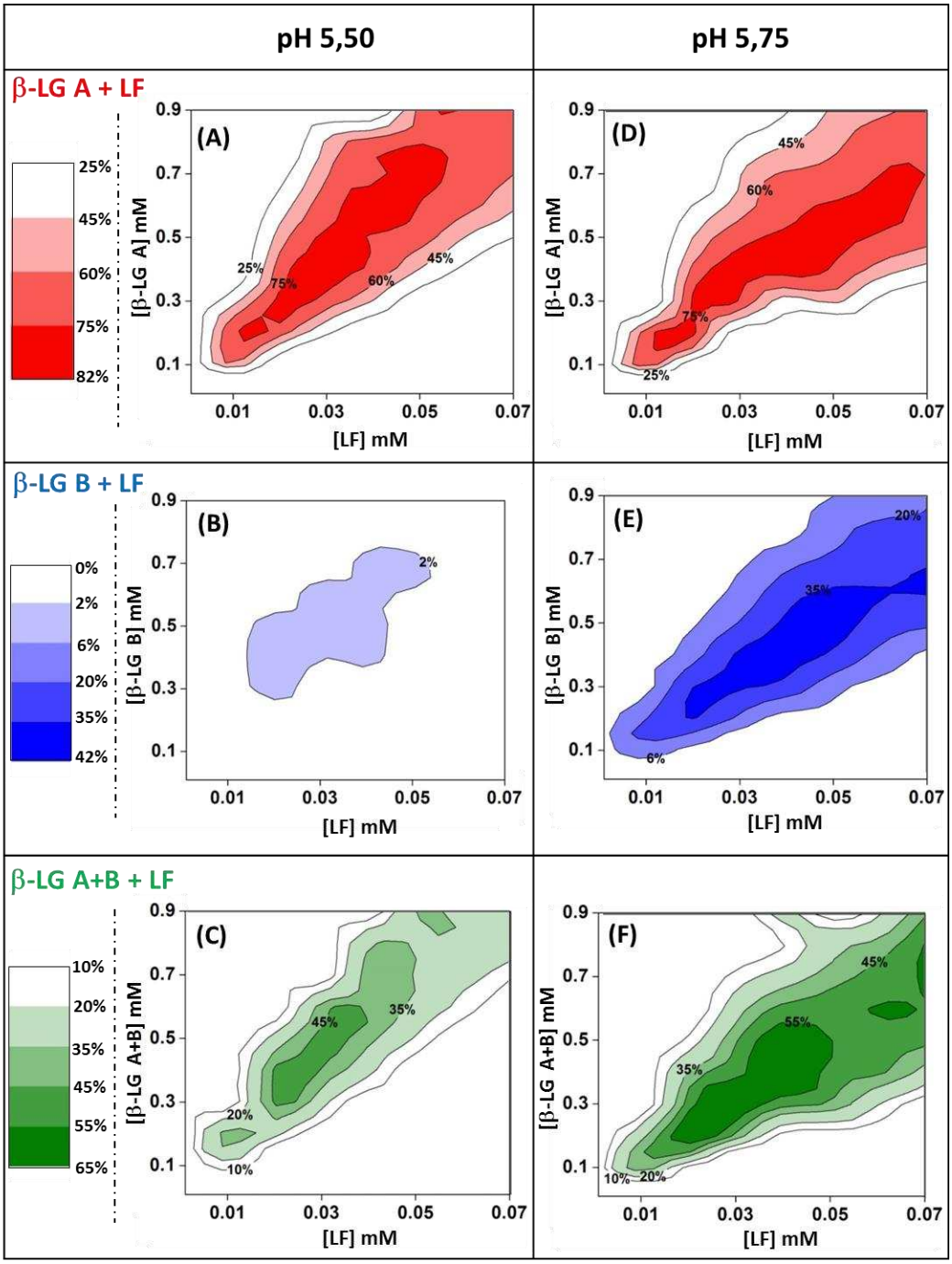

Figure 3.4. Fraction of LF recovered in the coacervates (dense phase) formed with β–LG A (A and D), β–LG B (B and E) or β–LG A+B (C and F) at pH 5.50 and pH 5.75 in 10 mM MES buffer and at 25°C.

The proportions of each β–LG isoform recovered in the dense phase of the β–LG (A+B) + LF for both pHs were quantified by reverse phase-HPLC. Figure 3.5 presents such proportions

for all tested initial protein concentrations in the coacervation domains. The small standard deviations underline that the proportion of β–LG A and β–LG B in the coacervates was independent on the initial total protein concentration. Interestingly both β–LG isoforms coexisted in the dense phase of β–LG (A+B) + LF mixtures at pH 5.75 and at pH 5.50 even for some protein combinations for which no coacervation occurred between LF and β–LG B. Isoform A predominated at both pHs and represented approximately 60% of β–LG in the dense phase. The higher ability of β–LG A to form coacervates with LF was checked by varying the relative proportion of the two β–LG isoforms in the initial mixtures. The ratio β–LG A/β–LG B in the dense phase was systematically higher than in the initial mixture (data not shown).

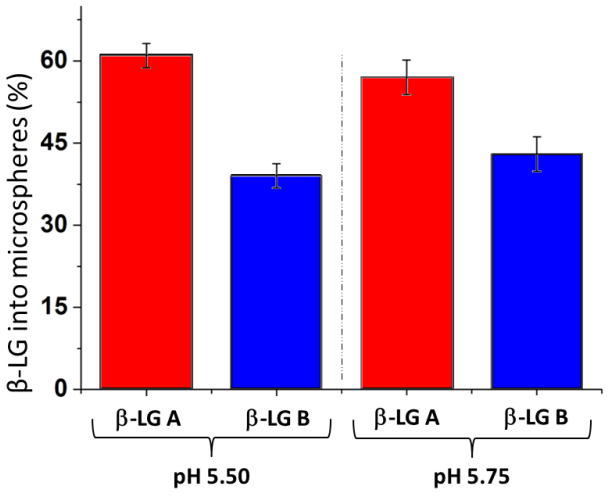

Figure 3.5. Average of the relative proportion of β–LG A and β–LG B quantified in the coacervation domains of mixture containing LF + β–LG A+B at pH 5.50 and pH 5.75 in 10 mM MES Buffer.

The β–LG/LF molar ratio in the coacervates was not constant in the whole range of mixed protein concentrations. At a fixed concentration of LF, increasing the concentration of β–LG induced a gradual increase of β–LG/LF molar ratio in the coacervates. A minimal β–LG/LF

molar ratio of 4 was found in coacervates formed between 10 µM LF and 50 µM β–LG A. By increasing β–LG concentration in protein mixtures, the β–LG/LF molar ratio in the coacervates slightly increased to reach optimal values of 6 to 8 at the center of the coacervation domains (diagonals of the phase boundaries).

3.3.4 β–LG and LF interaction at molecular level

ITC measurements were performed to quantitatively compare at molecular level the interaction parameters of LF with the two isoforms of β–LG. Figure 3.6 shows the binding isotherms resulting from successive injections of either β–LG A or β–LG B into the LF solution at pH 5.50 and pH 5.75. The relatively short period needed for the system to reach equilibrium between two injections ≈ 200 s showed a relatively fast binding kinetics. The binding isotherms obtained with two β–LG isoforms exhibited similar complex and exothermic profiles. In a first step, the energy released in the sample cell first decreased during the titration procedure up to a β–LG/LF molar ratio of 1-1.5 where it level off with β–LG A at pH 5.50 or increased again for the other cases. In a second step, the energy released decreased up to a β–LG/LF molar ratio of ~ 4. The variation of enthalpy between the first injection and the saturation point (plateau at β–LG/LF molar ratio of ≈ 4) was similar for both isoforms at both studied pHs (Figure 3.6). The obtained isotherms where fitted with sequential independent binding sites model (ORIGIN Software) to determine the thermodynamic parameters (Table 3.1). β–LG binds to two binding sites on LF with a stoichiometry of 1 for each site. The enthalpies and the binding constants for both isoforms were higher at the first step than at the second step. Figure 3.6 also shows the classical well-known dissociation of β–LG once injected in buffer solution (dilution). The dissociation of β–LG dimers is an endothermic process with a flux energy greatly lower than that linked to LF - β–LG interaction. Since it is not certain that the dissociation energy of β–LG dimers

remains the same in the presence of LF, no subtraction was performed before ITC data analysis.

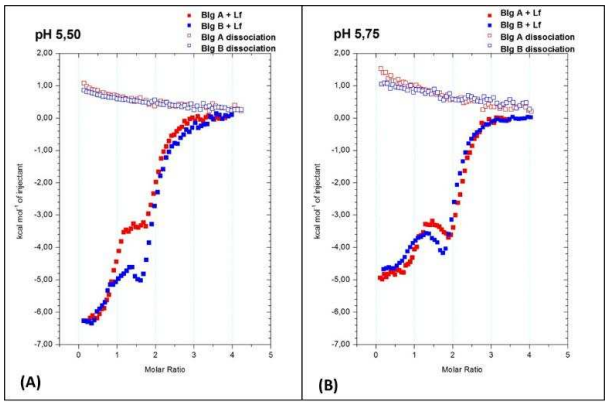

Figure 3.6. Binding isotherms of LF with (■) β–LG A or (■) β–LG B and dissociation isotherms upon dilution of (□) β–LG A and (□) β–LG B dimers. LF 0.1 mM was titrated with successive injections of β-LG 2 mM. ITC experiments were conducted at 25 °C in 10 mM MES buffer at pH 5.50 (A) and pH 5.75.

Table 3.1. Thermodynamic parameters of the interaction of LF with the two β-LG isoforms at 25°C in 10 mM MES buffer. ITC data were fitted with two independent binding sites.

Thermodynamic parameters	**pH 5.50**		**pH 5.75**	
	β-LG A + LF	**β-LG B + LF**	**β-LG A + LF**	**β-LG B + LF**
χ^2	8.9×10^3	35.9×10^3	22.4×10^3	31.2×10^3
N_1	0.87 ± 0.01	0.62 ± 0.04	0.95 ± 0.02	0.71 ± 0.05
Ka_1 (M^{-1})	$(4.7 \pm 0.9) \times 10^7$	$(4.6 \pm 4.4) \times 10^7$	$(1.8 \pm 1.0) \times 10^8$	$(2.9 \pm 4.8) \times 10^8$
ΔH_1 (kcal mol^{-1})	- 6.3 ± 0.05	- 6.3 ± 0.13	- 4.8 ± 0.05	- 4.6 ± 0.08
$T\Delta S_1$ (kcal mol^{-1})	4.2 ± 0.06	4.1 ± 0.27	6.4 ± 0.34	6.9 ± 0.50
ΔG_1 (kcal mol^{-1})	-10.4 ± 0.11	-10.4 ± 0.39	-11.2 ± 0.40	-11.5 ± 0.58
N_2	1.2 ± 0.01	1.4 ± 0.04	1.4 ± 0.02	1.4 ± 0.05
Ka_2 (M^{-1})	$(5.2 \pm 0.6) \times 10^5$	$(4.1 \pm 0.6) \times 10^5$	$(8.5 \pm 1.4) \times 10^5$	$(7.4 \pm 1.3) \times 10^5$
ΔH_2 (kcal mol^{-1})	- 3.5 ± 0.06	- 5.1 ± 0.11	- 3.5 ± 0.06	- 3.9 ± 0.07
$T\Delta S_2$ (kcal mol^{-1})	4.3 ± 0.01	2.5 ± 0.02	4.6 ± 0.04	4.1 ± 0.04
ΔG_2 (kcal mol^{-1})	- 7.8 ± 0.06	- 7.6 ± 0.08	- 8.1 ± 0.98	- 8.0 ± 0.11

3.4 Discussion

3.4.1 Selective interaction of LF with β-LG isoforms

LF and β-LG co-assemble and form well-organized microspheres called coacervates at low ionic strength in narrow range of pH and well defined protein concentration and protein molar ratio domains. The co-assembled proteins in the formed coacervates (dense phase) are in equilibrium with the proteins in the dilute phase. A maximum of 80% of the limiting protein was recovered in the dense phase under tested conditions indicating a complex coacervation behavior between these two oppositely charged proteins. Remarkably, the optimal conditions and the yield of coacervation differed significantly for the isoform A and B of β-LG. Selective coacervation of LF with β-LG A, the more negatively charged isoform, was evidenced in particular at pH 5.50 but also at pH 5.75. The observed selectivity in favor of β-LG A was expressed in the term of protein concentration domain leading to coacervation; the area of LF - β-LG A being systematically higher than that of LF - β-LG B (Figure 3.3), but also in term of the higher coacervation yield reached at both pH 5.50 and 5.75. Up to 75% of initial LF was recovered in the LF - β-LG A coacervates against only 2% and 35% in LF - β-LG B coacervates at pH 5.50 and pH 5.75, respectively (Figure 3.4). Indeed, when mixed isoforms were used for coacervation, the relative fraction of β-LG A/ (β-LG A+ β-LG B) recovered in the coacervates was always higher than in the initial mixtures. As all the coacervation experiments were conducted strictly in the same experimental conditions, the observed selectivity is attributed to the only differences between the two β-LG isoforms i.e. substitution of Ala118 and Gly64 in isoform B by Val118 and Asp64 in isoform A, conferring one more negative charge to β-LG A monomer. In our previous work on the formation of coacervates between LYS and α-LA two oppositely charged proteins, we have underlined the crucial role of protein conformation and flexibility of α-La (apo versus holo form of α-La) for the coacervation process [131]. On our knowledge, this is the first study evidencing selective

coacervation between two oppositely charged globular proteins originated from subtle amino acid substitution. Dubin and co-workers have already reported selective coacervation of the two β-LG isoforms with both a cationic gold nanoparticle –TTMA [149] and a linear cationic polyelectrolyte –PDADMAC [21]. In both cases, lower onset pH value for complexation and stronger binding affinity to cationic species were found for β-LG A. Based on simulated electrostatic potential around each isoform, the authors attributed the selective binding of cationic molecules to β-LG A to the presence of additional aspartate in the negative domain of β-LG. Similarly, difference in charge anisotropy could explain the preferential coacervation of LF with isoform A of β-LG observed here. Combined together, these results confirm and reinforce those disclosed for LYS/α-LA, other couple of globular proteins that showed experimentally (NMR) [131] and theoretically (Monte Carlo simulations) [150] that anisotropic electrostatic interactions are important for driving protein self-assembly into coacervates.

Unlike the systems described by Dubin and co-workers, the selective coacervation of LF with the two β-LG isoforms we observed here at macroscopic scale was not confirmed quantitatively at molecular level by ITC measurements. In fact, the interactions of β-LG isoforms with the TTMA and PDADMAC were found to be endothermic with systematically larger binding constant for β-LG A [21, 149]. Inversely, the binding of LF to the two β-LG isoforms is an exothermic enthalpy driven process with pronounced entropic contribution at both studied pHs. The exothermic nature of the binding indicate the predominance of favorable electrostatic interactions as generally found during complexation of oppositely charged protein and polyelectrolyte systems [151]. We failed to detect any difference between β-LG isoforms as their interaction with LF showed similar complex ITC profiles at both pHs in the used buffering conditions. The measured enthalpy (ΔH) values and derived binding constants at given pH are comparable suggesting that the interactions are rather of similar

nature. The slightly higher initial ΔH value at pH 5.50 versus pH 5.75 is probably due, from an enthalpic point of view, to the stronger electrostatic attraction of β-LG molecules by more positively charged LF. Also, the negative Gibbs free energy (ΔG) values (≈ - 10 kcal mol^{-1}) support the spontaneous character of the initial interaction between LF and β-LG isoforms.

The interaction β-LG - LF shows a complex binding isotherm with an uninterpretable, non-isoenthalpic region between two visual steps characteristic of at least two different events, with the occurrence of an atypical shoulder (Figure 3.5). The observed shoulder is not due to buffer-related energetic contribution since it occurred also when titration experiment was conducted in water (result not shown). A two-steps complexation (biphasic isotherm) has been reported for the formation of β-LG - pectin coacervates [152]. For this system, the two steps were assigned to the formation of intrapolymer soluble complexes followed by their aggregation in interpolymer complexes. The occurrence of these types of structures during our ITC experiments seems unlikely because the ITC stoichiometry values deduced for the two steps are much lower than those required for LF/β-LG coacervation (Figure 3.2). Consequently, the two ITC steps are fitted as indicative of two independent binding sites of β-LG on LF (Table 3.1). Accordingly, oligomers with 2 β-LG molecules per LF were formed during the titration experiments. This result is not without consequence on the mechanism of interaction/coacervation between LF and β-LG as discussed below.

3.4.2 Coacervation of lactoferrin - β-lactoglobulin

Apart from the present study, two other research groups have worked on the coacervation process of lactoferrin/β-lactoglobulin system. The results were published recently by Yan et al. [139] in October 2013 and by Anema and de Kruif [140] available online in June 2014 at the time of writing this article. Table 3.2 summarizes the main results of the three studies. Although the system is nominally the same, the comparison reveals important differences that

could be linked to experimental conditions. Two main experimental factors, certainly insufficient to explain the observed differences, deserve to be addressed: i- Protein source and quality: the presence of denatured/aggregated species promotes self-aggregation of β-LG and then impairs the coacervation process as it was the case in Yan et al. [139] study. Also, based on our previous results on the coacervation between LYS and apo or holo α-LA [130, 131], iron saturation degree of LF may affects the flexibility and the coacervation ability of the protein; ii- Coacervation medium: The already published works were conducted in water with significant evolution of pH during protein mixing. This probably complicates the kinetic of ionic equilibria which is known to be crucial for the coacervation. Ionic strength and pH range for coacervation and protein stoichiometry in formed coacervates are the main resulted differences: i- The coacervation between the two proteins occurs at narrow pH range and very low ionic strength for us and Yan et al. [139], against a broader pH range and relatively high ionic strength for Anema and de Kruif [140]. The difference in the effect of salt means that the decrease in the Debye-Huckel length needed to suppress the coacervation is twofold higher in this last study; ii- Protein stoichiometry β-LG/LF in the coacervate phase varies from one study to another (from 3 to 8). The stoichiometry increased with total protein in our work while it remained constant for the two other studies.

Table 3.2. Comparison of the experimental conditions and the main results obtained here and by others on the coacervation of β-LG/ LF system.

	Parameters		Yan et al.	Anema & de Kruif	Present study
Experimental conditions	**Protein origin & quality**	**β-LG**	Commercial β-LG AB 97%; presence of partially denatured forms	Lab-purified β-LG B (Purity > 95%)	Lab-purified β-LG A and β-LG B (Purity > 95%). Total elimination of denatured-aggregated forms
		LF	Commercial LF (> 90%) Iron saturation: 20%)	Commercial LF (purity 97%; Iron saturation: not specified)	Commercial LF. (purity 90%; Iron saturation: 10-20%)
	Co-aggregation of β-LG in the tested conditions		Yes	No	No
	Reaction medium		Water	water	MES buffer
Main results	**Coacervation pH**		5.7 to 6.2 pH evolves after protein mixing	5.0 to 7.3 pH evolves after protein mixing	5.5 to 6.0 Stable pH
	Maximal ionic strength for coacervation		≤ 20 mM (NaCl)	≤ 100 mM (NaCl)	≈ 25 mM (MES + NaCl)
	β-LG/LFmolar ratio in the coacervate phase		4 Proposed model: $LF(\beta\text{-}LG_2)_2$	3	4 to 8 (Function of total protein concentration)

To explain their β-LG/LF ratio of 4, Yan et al. [139] suggested the formation of complexes between LF and two β-LG dimers [$LF(\beta\text{-}LG_2)_2$] as the precursor of the coacervation. Based on the coacervation domains of β-LG B and β-LG (A+B), our work provides additional evidence to support this assumption. More explicitly, the presence of high proportion of β-LG B in the coacervate phase of LF - β-LG (A+B) in the protein domain where no coacervation was detected with LF - β-LG B mixture in particular at pH 5.50 supports the idea that β-LG dimer (homo or heterodimer) is needed for the coacervation process. Indeed, the occurrence of a complex involving one LF molecule (83 kDa, charges +22 to +24) [153] and 4 β-LG (18,3 kDa, charges -5 to -6) [153] is a good candidate of coacervation between oppositely charged

proteins which requires both charge and size compensation already suggested for other couple of proteins [53]. Thus, The apparent discrepancy between β-LG/LF molar ratio of 4 to 8 calculated from protein quantification in the coacervates and that of around 2 from ITC could be due to the concentration range used is these two separate experiments: large excess of β-LG in the initial mixture in the first case against only four times excess of β-LG at the end of ITC experiments.

3.4.3 Proposed mechanism

The presence of [LF(β-LG_2)$_2$] as part of the coacervate phase discussed above does not mean that LF interact initially with dimeric form of β-LG. ITC data are rather in favor of an initial binding of two β-LG monomers on two distinct sites of LF leading to the formation of a first entity LF(β-LG)$_2$. Combining our quantitative, macroscopic and ITC results with those already published, we may summarize the interaction/coacervation process between LF and β-LG as follows, see Figure 3.7. After mixing, a fraction of the proteins forms trimers LF(β-LG)$_2$ through binding of two β-LG monomers on LF. No coacervation occurs under excess of LF conditions. Increasing β-LG concentration favors the binding of two β-LG dimers at the LF surface forming the complex [LF(β-LG_2)$_2$], the precursor of the coacervation in agreement with what was suggested by Yan et al. [139].

Further increase of β-LG concentration leads to gradual increase of β-LG/LF molar ratio in the coacervate until a value of 8. This result is rather unexpected since this ratio would be constant if we consider charge compensation and charge balance effects. Similar finding was reported for coacervates formed between polysaccharides and either β-LG [154] or isolate of whey proteins [155]. It was attributed to a charge adjustment due to the high flexibility of coacervate systems originated from mass action effect which led to the phase separation of the molecule initially in large excess. At very high total protein concentration, self-suppression of

coacervation occurs with a transition from coacervates to aggregates. Suppression of β-LG - LF coacervation above a total protein concentration of 50 g L^{-1} at fixed protein weight ratio of 1 was also reported [139]. The disappearance of coacervates above a critical polymer concentration is well described for polyelectrolyte systems and is well predicted by successively modified coacervation theory including Tainaka theory (for details see Burgess [114]).

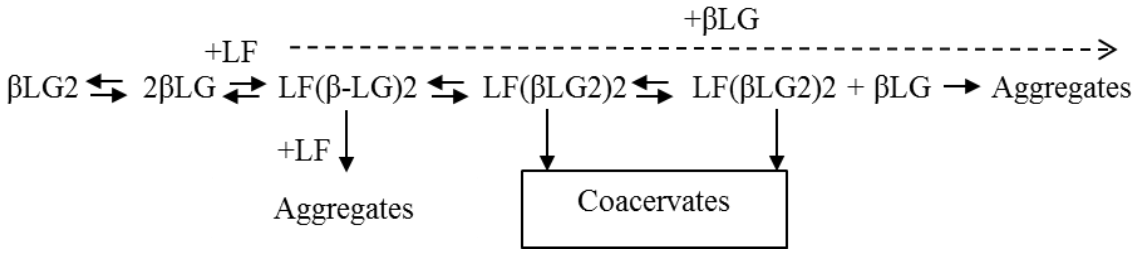

Figure 3.7. Proposed steps for the coacervation process involving LF and β-LG co-assembly.

3.5 Conclusion

Coacervation and phase separation in oppositely charged protein systems could be of great interest for the creation of self-assembled, biodegradable and edible materials. In this study, we conducted experiments to gain knowledge on the coacervation process between LF and β-LG and especially on the impact of minor changes in β-LG structure on the overall coacervation process. Coacervates between these two proteins are formed in particular under specific conditions of pH and initial protein ratio. The relative concentrations for coacervation were found to be disproportionate since a large excess of β-LG, the negatively charged protein of the lower molecular weight is required. The minimal protein molar ratio of 4 is recovered in the coacervates corresponding probably to pentamer [LF(β-LG_2)$_2$] as the primary unit of the co-assembly into coacervate. This heterocomplex with a mass ratio β-LG/LF of 1 is a good candidate as primary unit for coacervation between oppositely charged proteins which

requires both charge and size compensation as we already suggested for other couple of proteins.

Preference and selective coacervation of LF with β-LG A, the slightly more negative isoform is evidenced in the present work at pH 5.50 but also at pH 5.75. This important finding confirms and points toward the high sensitivity of coacervation to a small difference in the net protein charge (one more aspartic acid residue in isoform A).

ITC experiments showed an exothermic interaction of LF with both β-LG isoforms with both enthalpic and entropic contributions. Given the complexity of the binding isotherms, these experiments failed to reveal any difference between LF and the two β-LG isoforms. The interactions involve at least two sequential steps that were fitted as two independent binding sites. However, further studies are needed to better understand the thermodynamic events behind the interaction and coacervation between these two oppositely charged proteins. Also, we intend to further scrutinize the driving force for selective coacervation of β-LG isoforms with LF and other basic proteins. In particular, as protonation/deprotonation of buffer molecules contribute to the overall enthalpy, ITC experiments in other buffers may help to better understand the selective complexation of LF with the two β-LG isoforms.

3.6 Acknowledgements

Financial support from INRA and the federal Brazilian funding agency CNPq is acknowledged.

PART 2: MOLECULAR MECHANISM OF β-LACTOGLOBULIN AND LACTOFERRIN COMPLEX COACERVATION

PREAMBLE

The heteroprotein complex coacervation seems to be divided in two steps. The first step corresponds to the interaction between the proteins with the formation of the building blocks (heteroprotein complex) of the coacervates. The second step leads to the formation of the coacervate phase by the self-assembly of the preformed building blocks. The results presented in the first part showed a variation of the β-LG/LF molar ratio in the coacervate phase as a function of the initial β-LG/LF molar ratio. Concomitantly to this work and under different experimental conditions, Dubin's group suggested the formation of one well-defined building block initiating the complex coacervation between β-LG - LF. Therefore, the goal on this second part of the Chapter 1 was to understand the origin of the observed variable β-LG/LF molar ratio in the coacervates by a direct and detailed study of the heteroprotein complex structure forming the β-LG – LF coacervate phase.

Our questions:

- What are the molecular species (composition) of β-LG - LF coacervates and their overall dynamic?
- What are the building blocks of β-LG – LF complex coacervation under studied experimental conditions?

Compared to other published work on this system, the results presented in this part come from experiments conducted directly on the coacervate phase. The internal structure and quantity of the heteroprotein complexes forming the coacervates were determined by combining *in silico* approach (Docking Simulations) to evaluate the stability of different heterocomplexes formed between LF and β-LG and experimental characterization of the dynamics of labelled β-LG by

FRAP (fluorescence recovery after photobleaching) and the rotation diffusion coefficient of the molecular entities in the coacervates by ^{1}H NMR spectrum (nuclear magnetic resonance).

Our main results:

- LF presents two binding sites of different affinity for β-LG.
- LF interact either with monomers or dimers of β-LG.
- Three different protein complexes co-exist in equilibrium in the coacervate phase: (i) β-LG (monomer/dimer); (ii) LF(β-LG_2)$_2$ and (iii) (LF β-LG_2)$_n$.

Molecular mechanism of proteins complex coacervation: Case of β-lactoglobulin and lactoferrin

The content of this first part of the chapter is in preparation for submission to Soft Matter

Paulo D.S. Peixoto, Guilherme M. Tavares, Thomas Croguennec, Aurélie Nicolas, Pascaline Hamon, Claire Roiland, Saïd Bouhallab

Abstract

Under specific conditions, the mixture of β-lactoglobulin (β-LG), an acidic protein, and lactoferrin (LF), a basic protein, induces a liquid-liquid phase separation by complex coacervation. The comprehension of the molecular mechanism controlling the formation of this two phase system is necessary to improve its properties for targeted industrial applications. Moreover, such knowledge contributes to the more general comprehension of protein complex coacervation. Thus, to better understand the molecular mechanism(s) that stabilize the coacervate phase, in the current work, we have investigated the structure and the dynamics of the hetero and homocomplexes forming the coacervate. *In silico* calculations (docking simulations) and fluorescence recovery after photo bleaching (FRAP) experiments indicate that each LF can strongly bind one β-LG dimer (forming a very stable trimeric complex) and, less strongly, a second β-LG dimer (forming a more unstable pentameric complex). Rotation diffusion coefficients measured by NMR indicate the presence of three different complexes in dynamical equilibrium in coacervate phase: homocomplexes formed by free β–LG (β–LG_2) and heterocomplexes formed by one LF and two β-LG dimers LF(β-$LG_2)_2$ or quite large complexes (30 to 60 nm of diameter) formed by several LF and β-LG

dimer $(LF\beta\text{-}LG_2)_n$. The number of β−LG implicated in each one of these complexes is roughly equivalent. This work reveals the main key factors (in terms of structure and equilibrium dynamics) stabilizing the coacervate phase.

Keywords: Heteroprotein coacervation, β-lactoglobulin, lactoferrin, building blocks, molecular diffusion, NMR

3.7 Introduction

Complex coacervation results from the interaction of two oppositely charged colloids leading to a liquid-liquid phase separation. The denser phase is called coacervates and the other phase is the lean phase or the equilibrium phase. There are numerous examples of complex coacervation between oppositely charged (bio)polymers but the complex coacervation involving oppositely charged proteins (heteroprotein coacervation) is rather rare. The mechanism of heteroprotein coacervation, not completely elucidated, exhibits some specificity compared to complex coacervation involving polyelectytes. Heteroprotein coacervation is observed in very narrow ranges of pH, ionic strength, protein concentration and stoichiometry. However, some common features for heteroprotein coacervation exist even if the number of heteroprotein systems studied up to now is too limited to established general rules.

It is assumed that the formation of well-defined primary complex (building block) constitutes a preliminary step to heteroprotein coacervation [130, 131, 139, 142]. The driving force for building block formation is mainly electrostatic interactions with a contribution of the increase of entropy due to counter-ions release. The building blocks have to be close to charge neutrality for liquid-liquid phase separation to occur and consequently coacervation is only observed between the pI of the proteins involved in the coacervation process. Protein size

compensation is another requirement for heteroprotein coacervation as two proteins of opposite charge but equal magnitude do not form coacervates if they have different molecular size [53]. It is also observed that the flexibility of at least one protein favors heteroprotein coacervation [98, 133, 156]. Protein flexibility could stabilize the building block by an optimal exposition of amino acids involved in the interaction [131].

Once formed, the building blocks separate into a dense phase. Such mechanism suggests that protein stoichiometry in the coacervates is constant and correspond to the protein stoichiometry of the building block. This was observed for most of the system studied up to now but for LF - β-LG system results are unclear. Under selected conditions, Anema and de Kruif [140] proposed a β-LG/LF molar ratio of 3 while other authors proposed a molar ratio of 4 [139, 142]. This difference was first explained by the origin of the proteins used for coacervation experiments. Note that in these studies β-LG/LF molar ratio in the coacervates were determined indirectly. By using the same protein source, we determined by direct quantification of the proteins in the coacervates that the protein molar ratio in the coacervates varied from 4 to 6-8 by modifying the protein stoichiometry in the mixture [6]. From the complexes in the lean phase, Flanagan et al. [142] proposed that the building block for LF - β-LG heteroprotein coacervation was a pentamer LF(β-LG_2)$_2$ including two β-LG dimers bound to one LF. However, the structure of the coacervate was analyzed by SANS and the results indicate that the proposed model does not exactly fit with the experimental data [141]. These authors proposed that the building block (or primary blocks) may adopt different configuration and that some of them may associate into higher order equilibrium structures. The purpose of this study is to gain further insight into the internal structure and the dynamic of the fascinating coacervates formed throughout specific interactions between LF and β-LG. Here we investigate the molecular interactions and the diffusion properties of the proteins in the coacervate phase using Nuclear Magnetic Resonance (NMR), Fluorescence Recovery after

Photo Bleaching (FRAP) and docking simulations. We confirm that LF can bind two β-LG dimers with different affinities. From NMR measurements, we show the presence of three different complexes in dynamical equilibrium in the coacervate phase.

3.8 Experimental section

3.8.1 Sample preparation: Reagents and Solutions

Bovine beta-lactoglobulin (β-LG), containing genetic variants A and B, was provided by a confidential industrial source. The protein powder was dispersed in deionized water (45 g/L), adjusted to pH 5.2 with 1M HCl and kept at 30°C for 5 min, in order to precipitate non-native forms of β-LG. The dispersion was centrifuged at 20,000*g* at room temperature for 10 min (Heraeus Biofuge Primo, Thermo Scientific, Waltham, MA, USA) and the supernatant containing only native β-LG was adjusted at pH 7.0 with 1 M NaOH, freeze-dried and stored at – 20 °C until use. Bovine lactoferrin (LF) (purity of 90% and iron saturation of 10 - 20 % according to technical specification) was purchased from Fonterra Cooperative Group, New Zealand. MES hydrate buffer was purchased from Sigma-Aldrich (St. Louis, MO, USA) and all other chemicals were from VWR (Radnor, PA, USA).

β-LG and LF protein powders were solubilized in a 10 mM MES buffer, pH 5.5, at about 5.0 mM and 0.7 mM respectively and filtered through a 0.2 µm membrane (cat. no. 4612, Pall Corporation, Ann Arbor, MI, USA). The exact protein concentration was determined by absorbance at 280 nm (SAFAS UV MC2, Safas, Monaco) using 0.96 L g^{-1} cm^{-1} and 1.47 L g^{-1} cm^{-1} as extinction coefficients for β-LG and LF respectively. No sign of protein self-aggregation was detected in the stock solutions that were translucent.

3.8.2 Preparation of β-LG-LF coacervates

The coacervates were obtained by mixing an appropriate volume of the protein stock solutions

to reach β-LG and LF final concentration of 0.6 mM and 0.06 mM respectively. These optimal concentrations were defined in accordance with our previously work [6]. The solution was prepared respecting the following order of mixing: MES buffer + β-LG stock solution + LF stock solution. Immediately after mixing the solution evolved in a system containing two liquid phases in equilibrium: (i) a dilute phase (lean phase) and (ii) a dense phase dispersed in the lean phase, called coacervates. As described by Tavares et al. [6] the coacervates were separated from the lean phase by centrifugation (Heraeus Biofuge Primo, Thermo Scientific, Waltham, MA, USA) at 20,000g for 10 min. Proteins in the coacervates were quantified by reverse phase chromatography as previousely described by [6].

The coacervate samples studied here were a translucent, slightly pink and viscous liquid containing around 150 g/kg of LF and 130 g/kg of β-LG, i.e. a β-LG/LF molar ratio about 4, which is in accordance with the ratio observed by other authors.

3.8.3 Evaluation of β-LG and LF heterocomplex by rigid docking

A rigid docking experiment was conducted to determine the structure and the abundance of complexes potentially present in a mixture containing β-LG and LF using the web server pyDockWeb [157]. In this kind of experiment the software creates 10,000 different complexes by changing the relative position of the partners (LF and β-LG dimer noted β-LG_2) involved in the association and evaluates their relative stability (score energy). The most stable complexes are assumed to be the ones that display the longer lifetime and thus the most abundant. However, the relation between the complex stability, predicted by docking experiment and its actual abundance in solution is not straightforward. This is mainly because the rigid docking simulation does not take into account the internal dynamics of the protein, a serious drawback for flexible molecules. Nevertheless β-LG and LF are globular proteins presenting a relatively rigid structure [1] and the main driving forces associated to β-LG_2 and

LF interaction are long range forces, especially electrostatic [15] limiting the impact of the internal dynamics of each protein and the entropic contribution on the simulation. However, to support the docking results they were confronted to other experiments. This point is further discussed in the Discussion section.

3.8.4 FRAP: analysis of β-LG binding to LF

Theory:

FRAP analysis was used to characterize the binding between FITC (Fluorescein isothiocyanate) labeled β-LG and LF. In solution where a fluorescent molecule displays a classical diffusion behavior, the radius of a Gaussian bleached spot increases with time after photo-bleaching [158]. FRAP recovery curve can be then used to estimate the molecular diffusion constant of the fluorescent molecule. In contrast, in a solution where the fluorescent molecules are strongly bound to immobile obstacles, the radius of a spherical bleached spot does not increase with time [158]. In this reaction dominant regime, the time of diffusion of a "free" fluorescent molecule is shorter than the diffusion time of a complex (with bound fluorescent probe). Thus, the large scale fluorescent probe diffusion measured by FRAP is exclusively dictated by the time that the probe remains bound to the obstacle. Therefore, FRAP recovery curve informs on the probe-obstacle dissociation rate (κ_{off}) and on the concentration of fluorescent probes bound to the obstacle (C_{eq}). For reaction dominant regime, the FRAP recovery data can be fitted by the following equation:

Eq. 3.1. $$frap(t) = F_{eq} + C_{eq1}\left(1 - e^{-k_{1off}t}\right)$$

Where *frap(t)* is the fluorescence intensity at time *t* and F_{eq} is the concentration of unbound fluorescent molecule [159].

This equation only fits the experimental data if all different probe-obstacle complexes present the same dissociation rate. However, we found a dependence between the lifetime of the

LF(β-LG_2)$_n$ complexes and the number of β-LG_2 bound to LF in the current work. Considering that β-LG_2 binds to LF in two different affinity sites [6, 139] FRAP data must be fitted using a double exponential equation:

Eq. 3.2.

$$frap(t) = F_{eq} + C_{eq1}\left(1 - e^{-k_{1off}t}\right) + C_{eq2}\left(1 - e^{-k_{2off}t}\right)$$
$$= 1 - C_{eq1}e^{-k_{1off}t} - C_{eq2}e^{-k_{2off}t}$$

The Eq. 3.2 parameters are the same than in the first equation and the indices 1 and 2 refers to the complexes with longer and short lifetimes, respectively.

Complementarily, it is also possible that one of the two β-LG_2 bound to LF presents a too weak affinity to be considered in the reaction dominant regime. In this case, the fraction of β-LG_2 strongly bound to LF presents a reaction dominant regime, while the other fraction presents a different regime characterized by a significant diffusion time of free β-LG_2 between LF-β-LG_2 complexes (obstacles). In this case, the following equation must be used:

Eq. 3.3. $$frap(t) \approx \left(F_{eq} + C_{eq1}\right)\left[e^{\frac{-\tau 1eff}{2t}}\left(l_0\left(\frac{\tau 1eff}{2t}\right) + l_1\left(\frac{\tau 1eff}{2t}\right)\right)\right] + C_{eq2}\left(1 - e^{-k_{2off}t}\right)$$

The last term in Eq. 3.3 describes the contribution of the β-LG_2 bound to the LF site of highest affinity (identical term of the Eq. 3.2). In contrast, the first term of the equation describes the contribution of the β-LG_2 fraction bound to the LF site of weakest affinity. The equation parameters are the same previously described and τ_{eff} is defined as:

Eq. 3.4. $$\tau 1eff = \frac{w^2}{D_{1eff}} = \frac{w^2}{D_f}\left(1 + \frac{k_{1on}}{k_{1off}}\right)$$

Where w is the radius of the bleached spot, D_{eff} and D_f are the effective diffusion (the hindrance induced by diffusion and binding) and the pure diffusion (the hindrance induced by diffusion only) respectively and k_{on} is the association rate.

Finally, the LF(β-LG_2)$_n$ complexes are not totally immobile and their diffusion is significant regarding the time range of the experiment. The diffusion of these complexes themselves was

followed and treated as a classical but slow diffusion behavior. If a fraction of β-LG_2 forms a stable complex with LF in the time range of the experiment (strongly bound) and another fraction displays a dynamical association (weakly bound) with LF, the Eq. 3.3 can be used to model the fluorescence recovery curve.

Basically, the coacervate phase for the FRAP experiments was prepared as described above but with few adjustments. The proportion of 1% of the bulk β-LG concentration was replaced by the FITC labeled β-LG. The FITC-β-LG was obtained as described by Silva et al. [160]. Briefly the protein was solubilized in phosphate buffer pH 8.0 and covalently labeled with FITC by addition of the fluorescent probe to the protein solution for 90 min at 20 °C. The solution was then dialyzed (6–8 kDa cellulose membranes, Spectrum Laboratories Inc., Rancho Dominguez, CA) against Tris buffer (pH 7.3) containing 0.6 M of NaCl for 2 days to eliminate all free FITC and subsequently the solution was dialysed against deionized water before lyophilization. The labeling yield was around 30% was checked by mass spectroscopy (QSTAR XL, Applied Biosystems, Concord, ON, Canada).

The coacervate phase was placed between glass slide and a coverslip sealed with a small adhesive frame (25 µL capacity). The fluorescence recovery images were obtained using an inverted CLSM (Nikon, Champigny-sur-Marne, France). The observations were realised with a 40 times magnification oil immersed objective at 30 µm from the coverslip. The labeled β-LG in the coacervate phase was excited with 50 mW sapphire laser system at a wavelength of 488 nm and detected from 500 to 530 nm. The fluorescence before photobleaching was recorded using 0.1% of the maximum laser intensity. The photobleaching was realized using 100 % of the laser intensity in an 85 µm² spot and the recovery of fluorescence was followed during 60 min. Obtained images were treated using ImageJ free software.

3.8.5 NMR: Estimation of hydrodynamic radius and relative abundance of the different β-LG/LF complexes

Solid state ^{13}C and ^{1}H NMR spectra of the coacervate phase were obtained using a Bruker Avance III 600 SB spectrometer (14T) operating at Larmor frequencies of 150.9 and 600.1 MHz for ^{13}C and ^{1}H respectively. The spectra were obtained under magic angle spinning (MAS).

The hydrodynamic radius (Rh) of β-LG_2, LF and the complexes formed by these two proteins was estimated from their rotation correlation time (τ_c), which is strongly correlated to the ^{1}H translation relaxation times, T_1 and T_2. In diluted solution, τ_c is related to Rh of the molecule as described below:

Eq. 3.5. $$\tau_c = 48\pi\eta(Rh)^3(k_bT)^{-1}$$

Where η is the solvent viscosity, k_b is the Boltzmann constant and T is the temperature.

In dense solution, the hydrodynamic interactions between particles are affected by the solvent viscosity (η), the determination of which is not trivial in particular for polydisperse systems [161]. The value of η increases with the molecular crowding and the size of the diffusive particles. Theoretical studies [162] showed that the molecular motion of small particles (~1 to 7 nm of radius) displays a quasi-linear relationship with Rh at short time scales (pico to nano-seconds, in the time range of the present study) in protein density range equivalent to the ones of the present study (250 to 350 g/L). Thus, even if it is not possible to exactly determine η (since the composition of the medium is unknown) the quasi-linear relationship between the size of the molecule and τ_c can be used to estimate a relative Rh for the different species under study.

In the present work, both T_1 and T_2 were measured to increase the accuracy of the estimation of Rh. $1/T_2$ is always roughly inversely proportional to τ_c; $1/T_1$ is inversely proportional to τ_c only for particles displaying fast-to-moderate rotational motions. Below a given τ_c, $1/T_1$

becomes directly proportional to τ_c. Note, that T_1 and T_2 are also sensitive to the local dynamics of the protein or complexes and not only to the global molecular tumbling. To consider the global dynamics only, T_1 or T_2 was calculated using many different protons species (the methyl protons of the protein). The use of the same exponential curve to fit protons with different chemical shifts indicates that the global dynamics dominates T_1 and T_2.

Determination of the relative abundance of the different β-LG/LF complexes from the NMR ^{1}H spectrum.

The peak width in NMR is very sensitive to the dynamics of the molecular species in solution. If the association/dissociation rate of the complexes is slow regarding NMR time scales (pico to nanoseconds), peaks with different widths are observed on a 1D ^{1}H spectrum: complexes with slow dynamics produce broad peaks while their building blocks having fast dynamics exhibit narrow peaks. Based on this, the relative abundance of the complexes was directly estimated by measuring the signal intensity of each peak in a 1D ^{1}H spectrum. Two molecular species displaying close values of τ_c dynamics cannot be distinguished according to the width of their ^{1}H NMR peaks. However, their dynamic can be distinguished based on their relaxation time T1 or T2 using a multi-exponential fit.

3.9 Results

3.9.1 β-LG and LF complexes: rigid Docking

The energy of 10,000 different complexes formed by one β-LG dimer (β-LG_2) and one LF has been evaluated. Electrostatic interactions being the main driving forces of protein association. The score energy of the different complexes displays a Gaussian-like shape centered at a score energy of 10, a width at half height of 30 and a (non Gaussian) long “tail” in the direction of the most stable complexes (Figure 3.8A) . The most stable complexes (with score energies

between -70 and -40) are formed by the association of β-LG_2 on a specific site of LF (called S, for single, in Figure 3.8B). The S site of LF exhibited a very high density of positively charged residues (inset of Figure 3.8B) explaining the strong interaction.

In the next simulation, the association energy of β-LG_2 with already formed LFβ-LG_2 complex was evaluated. The histogram (Figure 3.8C) displays a Gaussian-like shape (no "tail" is observed) centered at the score energy of 20. This indicates that most of the complexes formed during this second docking simulation are less stable than the ones obtained during the first simulation. The most stable complexes presented by the second simulation (with score energies going from -25 to -10) are formed by the association of β-LG_2 at different sites on LFβ-LG_2 (called sites M, for multiple, Figure 3.8D).

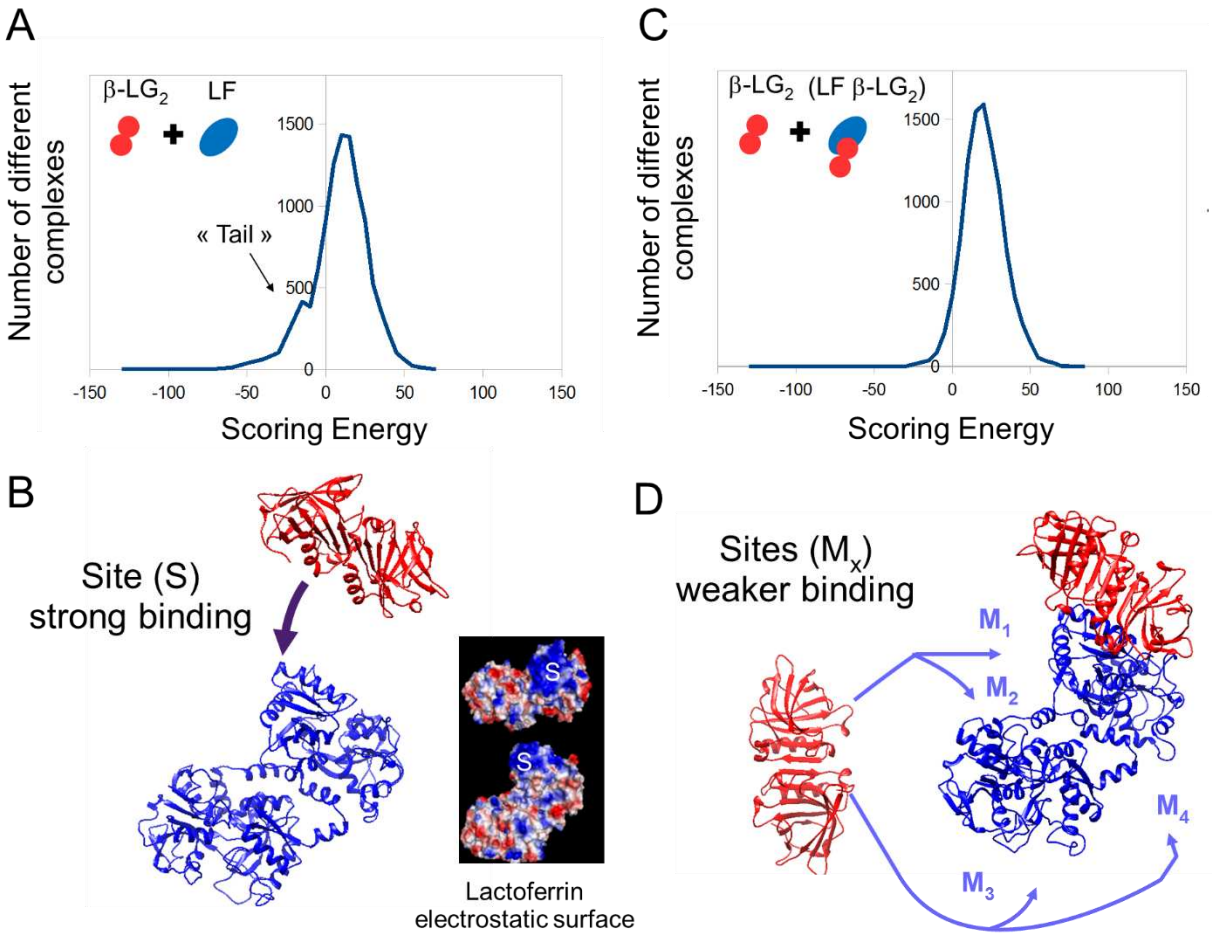

Figure 3.8. Molecular docking between β-LG_2 and LF (A, B), and between β-LG_2 and already formed LFβ-LG_2 complex (C, D).

Histogram of the energy scores of 10,000 complexes formed either by β-LG_2 and LF (A) or by β-LG_2 and LFβ-LG_2 complexes (C). The complex LF(β-LG_2)$_2$ is less stable than LFβ-LG_2 complex. (B): Structures of β-LG_2 in red and of LF in blue. β-LG_2 is located in a specific site S, in most stable complex (-70 to -40 in score energies). The inset shows that the S site on LF exhibits a huge density of positively charged residues (blue) in contrast to the other parts of the protein where the relative density of positively (blue) and negatively (red) charged residues is more homogeneous. (D): Illustration of the different sites on LF (called site M's) where the second β-LG_2 binds to the LFβ-LG_2 complex.

The self or co-association of the complexes presented in Figure 3.8 was also evaluated. Figure 3.9A displays the histogram of the energy scores for the association between two pentamers LF(β-LG_2)$_2$ complexes (forming a larger complex of ten proteins). The energy score histogram for the formation of this complex is centered at 30, showing that this complex is less stable than the precedent ones (Figure 3.8). Moreover, a small "tail" could be observed in the direction of most unstable complexes (representing ~5% of the total number of complexes with score energies between 50 and 80). The complexes formed by eight proteins (co-association of LF(β-LG_2)$_2$ and LFβ-LG_2 complexes, Figure 3.9B) and by six proteins (self-association of two LFβ-LG_2 complexes, Figure 3.9C) are centered at a score energy around 20-25. This indicates that these complexes are as stable as the ones resulting from the association of β-LG_2 and LFβ-LG_2 (Figure 3.8C). For the most stable complexes LF is always in direct interaction with β-LG_2 and two LF or two β-LG_2 molecules are never in direct contact.

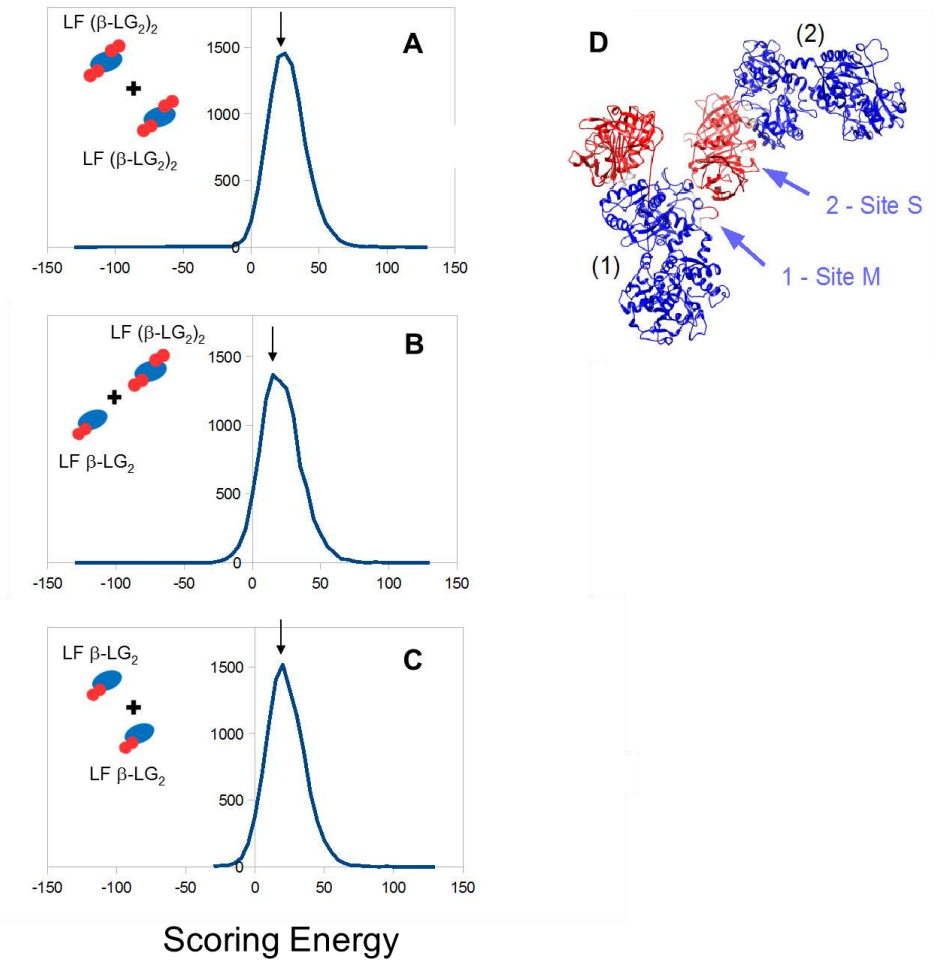

Figure 3.9. Molecular docking between trimeric and pentameric complexes of LF and β-LG_2. Histogram of the energy scores of 10,000 large complexes formed by association of different complexes of β-LG_2 (red) and LF (blue). Docking results for the association between two LF(β-LG_2)$_2$ complexes (A), LFβ-LG_2 and LF(β-LG_2)$_2$ (B) and two LFβ-LG_2 complexes (C). (D) Example of one stable complex resulting from the docking of two LFβ-LG_2 complexes (called 1 and 2). The β-LG_2 of the complex 2 makes the bridge between the two LF. The arrows show the site M and S on the complexes 1 and 2 respectively.

The docking simulations indicate that the strongest association is found for a complex formed by LF and one β-LG_2 bound on site S (forming an LFβ-LG_2 complex). The second most stable complexes are formed either by the association of LFβ-LG_2 with β-LG_2 (forming the LF(β-

$LG_2)_2$ complexes with one β-LG_2 on site S and another on site M), or by the association of LFβ-LG_2 with LFβ-LG_2 or with LF(β-$LG_2)_2$ (forming LF_2(β-$LG_2)_2$ or LF_2(β-$LG_2)_3$ complexes respectively). The most unstable complex results from the self-association LF(β-$LG_2)_2$.

3.10 β-LG binding within coacervate phase: FRAP analysis

Figure 3.10A shows a bleached spot profile, immediately (0.5 s) and one hour after bleaching. Figure 3.10B shows the corresponding FITC labeled β-LG fluorescence recovery curve. The radius of the bleached spot profile displays only a small increase one hour after bleaching indicating that the diffusion of β-LG_2 within the coacervates is dominated by the binding of β-LG_2 to immobile obstacles (reaction regime, see experimental section for details). Only 70% of initial β-LG fluorescence intensity was recovered one hour after bleaching. This is a remarkable slow recovery even for a system as dense as this one [159, 162] indicating that (i) β-LG binds to the obstacles for a long time and (ii) the obstacles are large enough to consider their diffusion negligible after one hour.

Since the bleached spot analysis indicates that the system is reaction dominated, the recovery curve has been fitted assuming a model in which the complexes formed by β-LG_2 and LF dominate the diffusion. A model in which one single dissociation time for all complexes is considered did not correctly fit the experimental data (Figure 3.10B, red line). Proper fits were obtained with models considering either two different dissociation times for the complexes (Figure 3.10B, green continuous line) or both the diffusion of β-LG and its binding to complexes (Figure 3.10B, green dotted line). The fitting parameters of the last two cited models are displayed in Table 3.3.

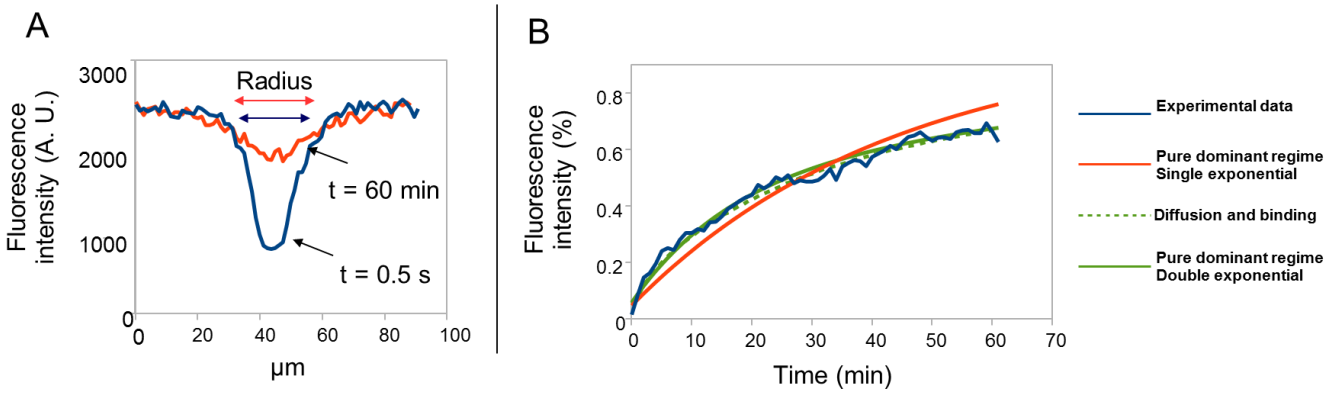

Figure 3.10. FRAP analysis of the FITC labeled β-LG within the coacervate phase.

(A): Time evolution of the bleached spot profile from a FRAP experiment using an initial bleached radius of 5.2 µm. (B): Typical FRAP recovery curve (blue) and the fits using the models described in materials and methods section. The red line represents the best fit using the model considering the diffusion of β-LG_2 dominated by binding and that all complexes display the same lifetime. The green continuous curve represents the best fit using a model considering the diffusion of β-LG_2 dominated by its binding to complexes which display two different lifetimes. The green dotted curve represents the case where both, β-LG_2 diffusion and its binding to complexes were considered for the fluorescence recovery.

Table 3.3. FRAP fitting parameters

	Reaction dominant	***Reaction/Diffusion***
F_{eq} (%)	6	70*
C_{eq1} (%)	45	70*
C_{eq2} (%)	49	30
$k_{1\,off}$ (s^{-1})	1.0×10^{-3}	8.6×10^{-3}
$k_{2\,off}$ (s^{-1})	1.2×10^{-4}	5.2×10^{-4}
$k_{1\,on}$ (s^{-1})	-	30
D_f ($\mu m^2/s$)	-	15

* In the reaction/diffusion model, F_{eq} and C_{eq1} (see equation 3.3 in experimental section) cannot be distinguished; the value of 70% corresponds to both F_{eq} and C_{eq1}.

The dissociation rates k_{1off} and k_{2off} range from 1 to 8 ms^{-1} and 0.1 to 0.5 ms^{-1} for the pure reaction and reaction/diffusion models, respectively (Table 3.3). The dissociation times are slightly lower in the pure reaction model than in the reaction/diffusion model. However, in both models, the first dissociation rate (k_{1off}) is more than one order of magnitude higher than the second constant (k_{2off}). In contrast, the relative number of β-LG molecules (C_{eq}) associated to k_{1off} and k_{2off} is quite different. The number of molecules associated to both rates is around 50/50 in the reaction dominant model. In contrast, more molecules are associated to the first dissociation rate (70%) than to the second in the reaction/diffusion model.

3.10.1 Rotation diffusion coefficients show the presence of three different complexes: NMR analysis

Three main signals were distinguished in the ^{1}H spectrum of the coacervate phase (Figure 3.11A): a large signal with a full width at half maximum (fwhm) of about 40 ppm, a second signal with 10-15 ppm of fwhm and a narrow signal of 1-2 ppm of fwhm. The narrow signal displays the typical pattern of water and the two others signals are assigned to protons of proteins. Usually, protons with the largest fwhm also present the slowest dynamic. Thus, based on their dynamics, 2 types of protein complexes could be distinguished on the ^{1}H spectrum of the coacervates. This was further confirmed on the 2D ^{1}H-^{13}C cross-polarization (CP) spectrum (Figure 3.11B) on which only the protons displaying a very slow dynamics appeared. The CP spectrum displays the signal of the largest Gaussian with a fwhm of 40 ppm (see green dotted lines in Figure 3.11A). A focus at the center of the ^{1}H spectrum (Figure 3.11C) shows individual peaks assigned to the amino acids of the proteins composing the second signal and the underneath spectrum of the slowest species described above. Figure 3.11D shows that the signal of the slowest species is completely extinguished after 20 µs

using an echo experiment (that measures T_2). In contrast, the intensity of the second signal barely changed confirming that their relaxation times (consequently their dynamics) are extremely different. The deconvolution of the ^1H spectrum gave the fraction of protons assigned to the slowest species. The peak of the slowest species (largest signal) represents about 50% of the total ^1H NMR signal intensity of the proteins.

Figure 3.11E and F show the spectra of the solutions of β-LG (Figure 4E) and LF (Figure 3.11F) at 150 g/L, under the same conditions of pH and temperature. A comparison of the spectrum of Figure 3.11D with the spectra on Figure 3.11E and 3.11F indicates that the second peak in the coacervate phase cannot be associated to only one of the proteins. Similar results are obtained when denser solutions (~300 g/L) of β-LG or LF were analyzed.

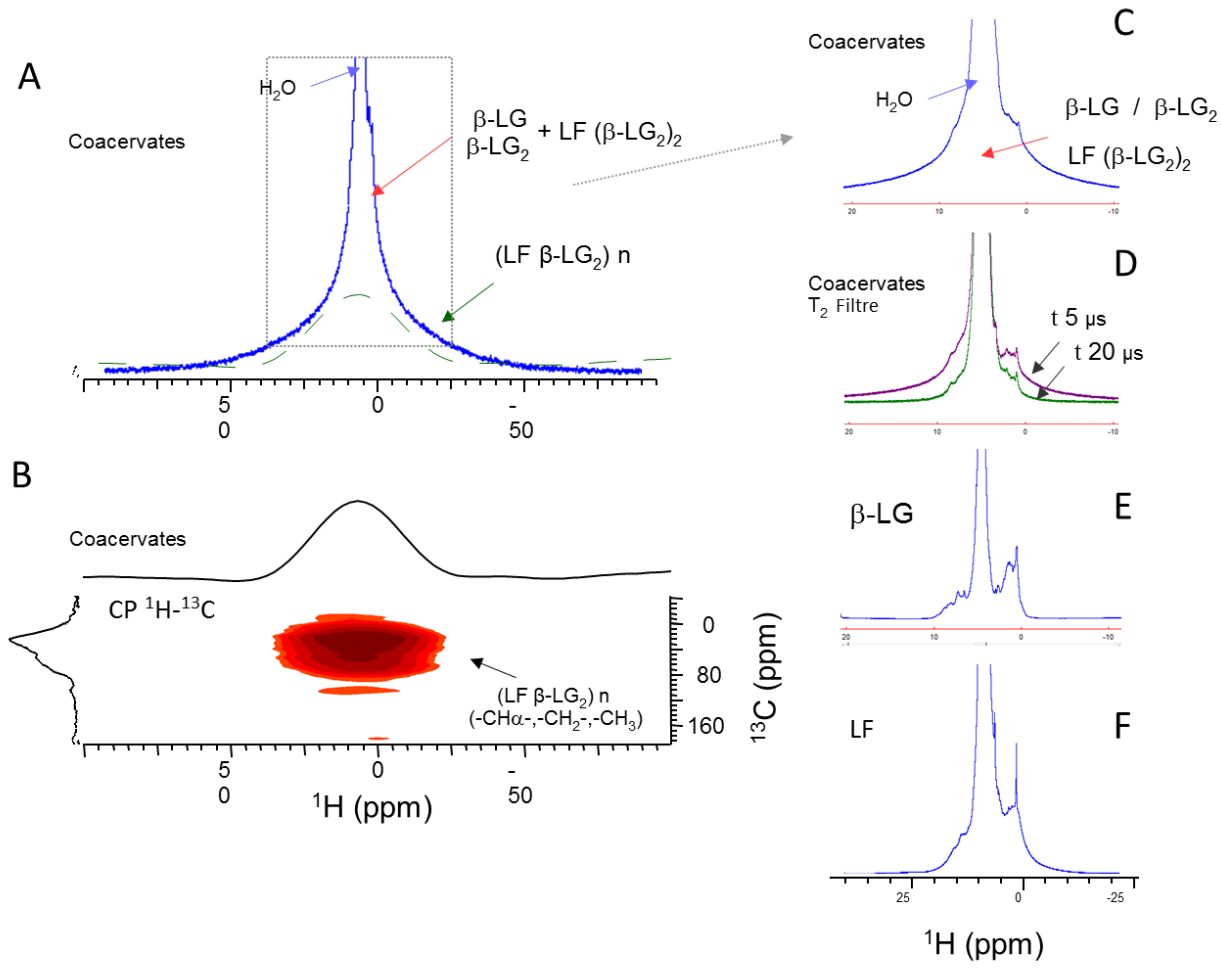

Figure 3.11. NMR signal Assignments.

(A): Three main signals detected in ^{1}H spectrum of the coacervate phase: the largest signal is assigned to the association of several LF and β-LG_2 molecules i.e. (LFβ-LG_2)$_n$, the second signal is assigned to β-LG /β-LG_2 and LF(β-LG_2)$_2$ and the third signal is assigned to water molecules (see below for details). (B): 2D ^{1}H-^{13}C cross polarization spectrum of the coacervate phase. In the spectrum only the protons having a very slow dynamic display a reasonable intensity. (C): Zoom at the center of the spectrum A focusing on the peaks emanating from β-LG_2 and LF(β-LG_2)$_2$. (D): ^{1}H spectrum using echo filter. In the spectrum between 5 and 20 µs the signal of the largest peak is completely eliminated without affecting significantly the intensity of the other peaks (the water and the second peak corresponding to β-LG_2 and LF(β-LG_2)$_2$. (E) and (F), ^{1}H spectra of dense β-LG and LF solutions respectively.

The measurement of the spin relaxation times T_1 and T_2 gives access to quantitative data about the protein dynamics (notably the protein rotational correlation time, see experimental section for details). Figure 3.12A shows the spectra at different delays (from 0 to 3 s) used to measure T_1. Since the two signals have different dynamics, the measurement of the T_1 of each signal can be determined independently (see experimental section for details). For the largest signal, the time evolution echo curve can be roughly fitted with a mono-exponential curve indicating that this signal can be associated to proton species displaying roughly the same slow dynamics. The best fit gives a $1/T_1$ value of 35 seconds. Based on hydrodynamic radius calculation (Table 3.4), the largest signal is associated to complexes composed of several LF and β-LG_2 noted (LFβ-LG_2)$_n$ with a Rh ~ 30-60 nm (see discussion for assignment). In contrast, the second signal cannot be fitted only with one specific $1/T_1$ value (Figure 3.12B). The use of two different $1/T_1$ values, 1.25 and 4.85 seconds, gives a very good fit (green and yellow curbs in Figure 3.12C). These values were used to calculate the Rh of the molecular species responsible for such signal (Table 3.4). Molecular species with calculated Rh of 2.0

and 7.3 nm (corresponding to $1/T_1$ values of 1.25 and 4.85 seconds, respectively) were assigned to β-LG /β-LG_2 and LF(β-LG_2)$_2$ (see discussion for explanation), respectively (as indicated in Figure 3.11D). Moreover, the fit of the relaxation of the second signal gives access to the relative proportion of protons of β-LG / β-LG_2 and LF(β-LG_2)$_2$ (1:2, respectively) (Table 3.4).

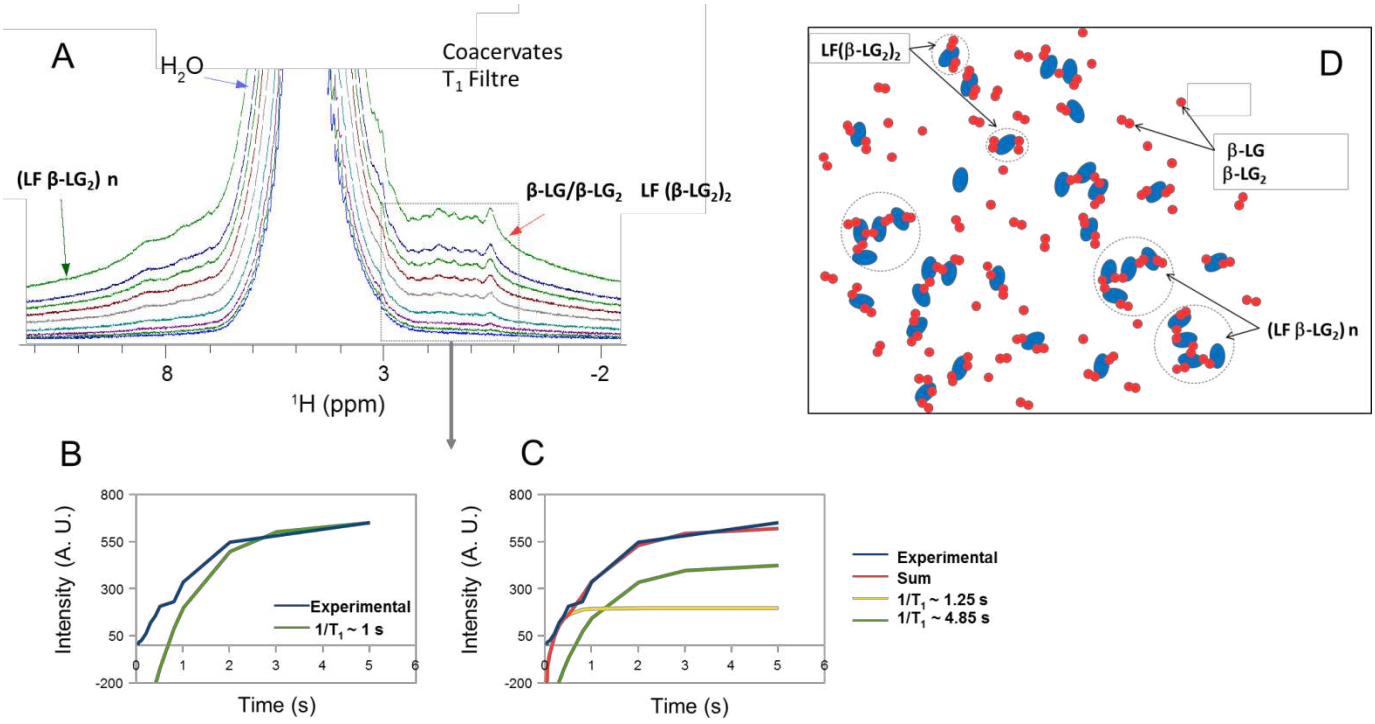

Figure 3.12. Assignment of NMR signals to different complexes in the coacervates.

(A): Spectra corresponding to the different delays used to calculate T_1 (delays from 0 to 3 s). (B): Experimental relaxation of the second signal (blue) and the best mono-exponential fit using 1s for $1/T_1$ (green curb). (C): Experimental relaxation of the second signal (blue) and best fit using a double exponential function (red curb). The green and yellow curves, associated with value of $1/T_1$ of 1.25 and 4.85 seconds respectively, represents the two exponential functions used in the fit. (D): Two-dimensional representation of the coacervate phase composed of LF (blue full ellipses) and β-LG (red full sphere). Dark circles represent some large complexes containing several LF and β-LG_2 (LFβ-LG_2)$_n$. The red circle and show a free LF(β-LG_2)$_2$ complex. The ratio of each species is derived from NMR data as described

in the text (Table 3.4).

Table 3.4. Abundance (w/w) and dynamics of complexes in the coacervate phase.

	*% Protons**	*$1/T_1$ (s)*	*% β-LG*	*Rh (nm)***
β-LG/β-LG_2	17	1.3	≈ 33	2.0
LF(β-LG_2)$_2$	33	4.9	≈ 33	7.3
(LFβ-LG_2)$_n$	50	35.0	≈ 33	30-60

* %β-LG indicates the relative number of β-LG in each complex, calculated based on the NMR data.

**Rh was calculated using the values of T_1 (see experimental section for details).

3.11 Discussion

We and others have published on the fascinating coacervation behavior of LF-β-LG mixture with somewhat different results. The present study aimed to elucidate the exact molecular mechanisms of LF-β-LG association behind such liquid-liquid phase separation. In some aspects related to charge and size compensations as prerequisite to LF-β-LG coacervation, this system conforms to systems we have studied previously [15]. But, one major difference is that the protein molar ratio in LF-β-LG coacervates varied with the physicochemical conditions of the medium. This suggests that LF-β-LG coacervates are not formed by only one type of heteroprotein complexes but rather involve several entities. In this discussion we will first address the most probable building blocks responsible for the observed liquid-liquid phase separation. Secondly, we will detail the composition of the coacervates under used experimental conditions. Finally, we confront our results to proposed mechanism for LF-β-LG coacervation and give some elements to explain the extreme sensitivity of the coacervates to

experimental conditions.

3.11.1 Building blocks of the coacervates

It has been postulated that LF-β-LG coacervates result from the association of heterocomplexes formed by LF and β-LG_2. The characterization of these heterocomplexes (building blocks) is a preliminary step to understand the basic molecular mechanisms that allow two oppositely charged proteins to form a thermodynamic stable two phase system with coacervates dispersed in a lean phase. Docking simulations showed that each LF molecule is able to bind 2 β-LG_2. The first β-LG_2 always bind to the same site of higher affinity on LF surface (site S, Figure 3.8B). In contrast, the second β-LG_2 can bind on different sites of lower affinity, called M sites, located all around LF surface. The theoretical evidence of the existence of two sites of different affinity for β-LG (sites S and M) on each LF confirms the results obtained previously by isothermal calorimetry (ITC) [6] and electrostatic modeling [142]. Hence, the most probable building blocks leading to coacervate formation are the heterocomplexes LFβ-LG_2 and LF(β-LG_2)$_2$. The coexistence of these heterocomplexes was already addressed by Flanagan et al. [142]. Their relative abundance depends on β-LG/LF initial molar ratio.

Given the strong affinity of LF S-site for β-LG_2, the probability of having free LF in the coacervates should be weak under molar excess of β-LG compared to LF. NMR data indicate that β-LG distributes equally to the various species in the coacervate i.e. the free β-LG and the two heterocomplexes LF(β-LG_2)$_2$ and LFβ-LG_2 (see below). According to HPLC quantification, 7.2 mM β-LG was found in the coacervates meaning 2.4 mM in each of the above species. Hence, the concentrations of LF involved in LF(β-LG_2)$_2$ and LFβ-LG_2 heterocomplexes are estimated at 0.6 mM and 1.2 mM, respectively. LF quantification in the coacervates (1.87 mM) suggests that less than 5% of LF exists as free entity in the coacervate

phase, confirming previous assumption.

In support to Docking simulation, FRAP experiments show that β-LG bind to immobile obstacles with two quite different affinities. The immobile obstacles could be either an individual LF monomer or a LF bound to a larger complex (see below). The fit of FRAP data reveals dissociation rates of about 1 to 8 ms^{-1} for sites M and 0.1 to 0.5 ms^{-1} for the site S. Both these values correspond to a relative weaker binding strength compared to the ones described for most biological complexes displaying a specific binding (dissociation rate of about 10^{-3} ms^{-1} for protein receptors, [159].

3.11.2 Identification of the structures and quantification of the main species in the coacervates

Based on NMR analysis, mainly 3 types of molecular entities with specific dynamics and Rh seem to be present in LF-β-LG coacervates. The smaller one is assigned to β-LG_2 and β-LG monomers (Rh = 2.0 nm). Considering a dissociation constant Kd of 5.5×10^{-4} M at working pH of 5.5 [6], the β-LG_2/β-LG molar ratio is roughly 60/40 for the non-complexed β-LG in the coacervates (2.4 mM). The other entities with Rh of 7.3 nm or ~ 30-60 nm are assigned to heterocomplexes involving LF and β-LG_2. Their most probable structure in solution was addressed by complementary docking experiments thanks to a theoretical evaluation of their stability. Docking shows that each LF molecules is able to bind 1 or 2 β-LG_2 as indicated above. Docking also suggests that larger complexes (formed by six to ten protein molecules) can exist in the coacervates. The formation of complexes of six to eight proteins (LF_2(β-LG_2)$_2$ and LF_2(β-LG_2)$_3$, respectively) (Figure 3.9) is energetically as favorable as the association of β-LG_2 on one site M of LF (Figure 3.8C). In contrast, the complexes formed by ten proteins (association of two LF(β-LG_2)$_2$) are less stable then less probable. On LF(β-LG_2)$_2$ the 2 binding sites of LF are occupied by β-LG_2. Moreover, in most stable larger complexes, two β-

LG_2 or two LF molecules are never in close contact. Thus, the formation of complexes involving two $LF(\beta\text{-}LG_2)_2$ is not favorable energetically due to stronger repulsions between β-LG_2 in close vicinity. In contrast, for complexes involving LFβ-LG_2, one binding site on LF surface is still available for the association of another complex (LFβ-LG_2 or $LF(\beta\text{-}LG_2)_2$). In this case one β-LG_2 acts as a bridge between 2 LF. This favor the growth of the complexes composed by a number of proteins larger than 6 i.e. $(LF\beta\text{-}LG_2)_n$. Hence, from the docking experiments, we assumed that the species of medium size (7.3 nm) determined by NMR are mainly composed of $LF(\beta\text{-}LG_2)_2$ because of their inability to further associate. This result could explain why $LF(\beta\text{-}LG_2)_2$ was proposed as building block of LF - β-LG coacervates. We suggest that complexes with Rh ranging from about 30 to 60 nm results mainly from the association of several LFβ-LG_2 units i.e. $(LF\beta\text{-}LG_2)_n$. As indicated above, $LF(\beta\text{-}LG_2)_2$ is able to associate with LFβ-LG_2 and hinders the growth of the $(LF\beta\text{-}LG_2)_n$ complexes. This could explain why the Rh distribution of $(LF\beta\text{-}LG_2)_n$ is quite large. The presence of free LFβ-LG_2 which has a Rh close to the one of $LF(\beta\text{-}LG_2)_2$ in the coacervates is not excluded. But for a sake of simplification, we assume from NMR data that the main entities in the coacervates are β-LG_2, $LF(\beta\text{-}LG_2)_2$ and $(LF\beta\text{-}LG_2)_n$ with a relative proportions, based on proton assignment, of 17%, 33% and 50% respectively (Table 3.4). Since the number of protons of β-LG represents ~50% and ~33% of the total number of protons in $LF(\beta\text{-}LG_2)_2$ and $(LF\beta\text{-}LG_2)_n$ respectively, we deduced that β-LG molecules in the coacervates distributes almost equally between the three entities. Based on the protein composition in the coacervates determined by NMR, a rapid calculation of the β-LG/LF molar ratio gives ~4, a value in agreement with the stoichiometry found by RP-HPLC protein quantification previously reported [6, 139]. A composition of the coacervates is displayed in Figure 3.12D, with the larger complexes evidenced by NMR represent $(LF\beta\text{-}LG_2)_n$. The number of building blocks that forms these

complexes has been chosen considering a Gaussian distribution. They are diluted in a "sea" of β-LG_2 and LF(β-LG_2)$_2$ complexes. Under our conditions the number of β-LG_2 is close to twice the number of LF(β-LG_2)$_2$.

3.11.3 Specific thermodynamic equilibrium governs the stability of the coacervates

It has been proposed that the stability of the coacervates depends exclusively on the specific interaction between the heterocomplexes LF(β-LG_2)$_2$ which would display self-attraction, at long range, and self-repulsion, at short range [141]. Such units were suggested to generate a liquid-liquid phase separation because the short range repulsions allow molecules to move in solution (keeping the liquid properties of the coacervate) and the long range attractions prevents the complete dilution of the coacervate in the dispersing lean phase. For several reasons, this explanation does not completely fit with our results: (i) depending on protein concentration, the β-LG/LF molar ratio in the coacervates varied from 4 to 6-8 [6]. Under other experimental conditions Anema and de Kruif [140] observed a β-LG/LF molar ratio of 3 in the coacervates. Such molar ratios are not compatible with LF(β-LG_2)$_2$ as the only building blocks of the coavervates. (ii) LF(β-LG_2)$_2$ had to be very abundant in solution and consequently very stable if these complexes were the main building blocks of the coacervates. Consequently the conditions of formation of LF-β-LG coacervates should be quite resistant to variations in protein concentration and β-LG/LF molar ratio. Experimentally we observed that random aggregates instead of coacervates are formed in mixtures containing high β-LG/LF molar ratio (> 20) [6]. Increasing β-LG concentration in LF solution should drive the binding equilibrium toward the saturation of the LF binding sites resulting in larger amount of LF(β-LG_2)$_2$ but these conditions do not favor LF-β-LG coacervation.

The new results brought by the present study give an explanation to previous observations. We suggest that the coacervates result from the coexistence of three metastable entities: β-

LG_2, $LF(\beta\text{-}LG_2)_2$ and larger complexes $(LF\beta\text{-}LG_2)_n$. These entities are probably in equilibrium in the coacervates but not completely with the lean phase as unlike $LF(\beta\text{-}LG_2)_2$ and $LF\beta\text{-}LG_2$, the size corresponding to larger entities i.e. $(LF\beta\text{-}LG_2)_n$ was not detected in the lean phase [142]. Any subtle change of these equilibria by modifying the physicochemical conditions (protein concentration, β-LG/LF molar ratio, ionic strength and pH) could change the relative abundance of each entity. This could explain the reported evolution of the β-LG/LF molar ratio in the coacervation domain and also the transition from coacervates to aggregates for larger changes [6]. It could also explain the extreme sensitivity of LF-β-LG coacervation by changing ionic strength and pH when compared to similar liquid-liquid systems involving large colloids and polyelectrolytes. Ionic strength and pH conditions affect the equilibrium between electrostatic forces responsible for the long/short range attraction/repulsion in most liquid-liquid systems. The properties of LF-β-LG coacervates are dictated by the balance of the interaction between entities and their relative abundance. Any changes in the physico-chemical parameters have a double impact on the present system: it modifies the self-repulsion/attraction properties of each complex (as for colloids and polyelectrolytes) but also their relative abundance. This explains why the present system is much more sensitive to changes in physicochemical conditions than the ones composed by more stable units (colloids or polyelectrolytes).

3.12 Acknowledgements

The financial supports from INRA, CNRS, Université de Rennes 1 and federal Brazilian funding agency CNPq and are acknowledged.

3.13 Additional Data: Characterization of the coacervates thermal-stability

The denaturation temperature of the proteins used in the present work was determined using Differential Scanning Calorimetry (DSC). Coacervate phase and concentrated β-LG and LF solutions (~300 g/L) were submitted to a temperature range of 20 – 120 °C at a rate of 2 °C min^{-1} under nitrogen flow using the DSC Q1000 (TA instruments). Aluminium pans were filled with around 90 mg of each sample and sealed for analysis. An aluminium pans filled with the MES buffer was used as reference. The obtained thermograms are shown in Figure 3.13.

The denaturation temperature determined for β-LG (77.60 ± 0.47 °C) and LF (major peak at 59.07 ± 1.07 °C (apo-LF) and minor peak at 86.34 ± 0.42 °C (holo-LF)) solutions were consistent with those described in the literature [163, 164]. Interestingly, a shift was observed in the denaturation peaks of the proteins in the coacervate phase compared to the proteins in solutions, especially for β-LG. Compared to denaturation temperature of the proteins in solution, the denaturation temperature of the major peak of LF (60.79 ± 0.14 °C) was slightly higher and the denaturation temperatures of β-LG (70.31 ± 0.15 °C) and of the minor peak of LF (79.75 ± 2.02 °C) were significantly lower in the coacervate phase.

The shift of the protein denaturation temperature induced by complex coacervation with other molecules, especially polysaccharides, has been described in the literature. Bokkhim et al. [164] reported the increase of the denaturation temperature of the major peak of native LF induced by the coacervation with alginate. These authors attributed the increase of the denaturation temperature of LF to the presence of the large number of electrostatic interactions between LF and alginate molecules which contributes to increase the LF thermal-stability. Other authors reported a decrease of the denaturation temperature of lysozyme when complexed to heparin in a coacervate phase. They suggested that heparin had a higher affinity for the partial unfolded lysozyme compared to the native form [165, 166]. Similarly, it is

possible that the complex coacervation induces the partial unfolding of β-LG and that LF presents higher affinity for partially unfolded β-LG rather than for native β-LG. But it is also possible that the denaturation of LF during the DSC analysis of the coacervates induces "premature" denaturation of the β-LG explaining the large shift in its denaturation temperature.

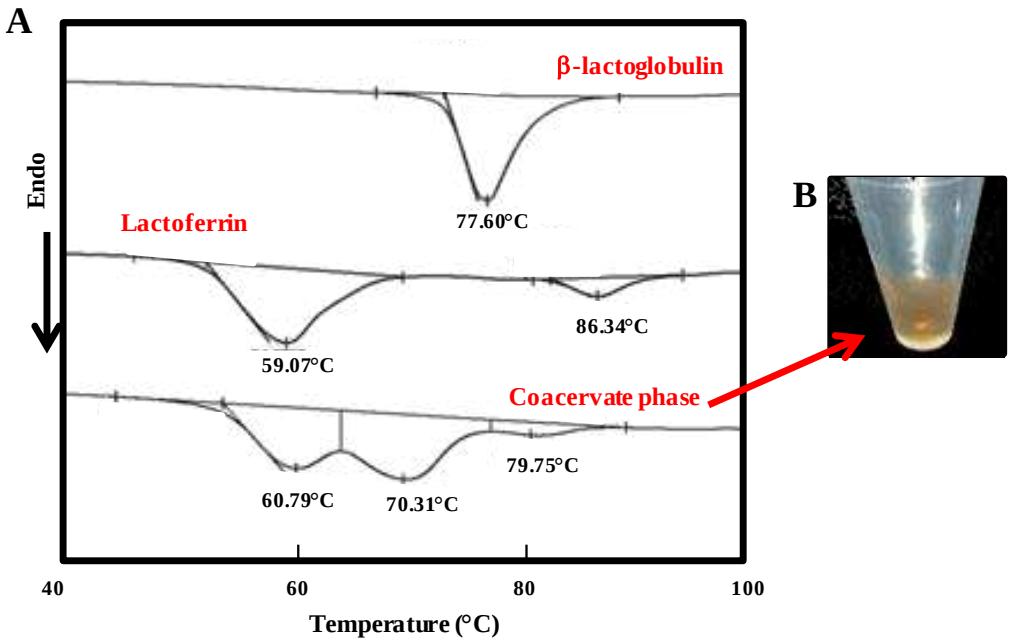

Figure 3.13. (A) DSC thermograms of the β-LG (~300 g/L), LF (~ 300 g/L) and the coacervate phase (β-LG ~150 g/L + LF ~150 g/L). (B) Image of the coacervate phase.

4 CHAPTER 2: How the presence of a small molecule affects the complex coacervation between lactoferrin and β-Lactoglobulin

PART 1: HOW THE PRESENCE OF ANS AFFECTS THE COMPLEX COACERVATION BETWEEN LACTOFERRIN AND β-LACTOGLOBULIN

PREAMBLE

As physico-chemically non inert substances, small ligands such as bioactives can affect the structure and surface properties of proteins and consequently their coacervation process. Our goal in the Chapter 2 was to investigate the potential interaction of small ligands with β-LG and LF and how their presence affects the heteroprotein complex coacervation. In this first part of the chapter 2 we used ANS (8-Anilinonaphthalene-1-sulfonic acid) as a model hydrophobic ligand. ANS was chosen because of its fluorescent properties and its structural similarities to various bioactives (small organic molecule presenting several functional groups). ANS is known as probe of hydrophobic regions of protein surface through its anilinonaphthalene group and can also form ion pairs with positively charged residues of proteins through its sulfonate group.

Our questions:

- Does ANS interact with β-LG or LF under conditions of coacervation and if yes what are the structural changes and the interacting parameters?
- How is the overall process of β-LG – LF complex coacervation affected by the presence of increasing concentrations of ANS?

Isotherm titration calorimetry was used to monitor the binding of ANS to β-LG and to LF. In parallel, we verified the effect of various ANS concentrations on the structure and the surface net charge of the proteins. No interaction of ANS with β-LG was detected in the present work as assessed by ITC experiments and DLS measurements. Studies of the effect of ANS concentration on β-LG - LF complex coacervation took into account the mixing order among the three molecules. The morphology of the formed supramolecular structures and the

partition of proteins and ANS between dense phase and equilibrium solution (lean phase) were determined as a function of total ANS concentration.

Our main results:

- Under the used conditions ANS does not interact with β-LG but interacts with LF inducing self-association (aggregation) of formed ANS-LF complexes into nanoparticles with reduced surface charge.
- The increase of ANS concentration favored a shift from coacervation to aggregation regime.
- In the coacervation regime, the increase of ANS concentration reduced the amount of proteins recovered in the coacervate phase.
- Without further optimization, a loading capacity of about 40 mg of ANS per gram of LF in the coacervate phase was obtained.

How the presence of a small molecule affects the complex coacervation between lactoferrin and β-lactoglobulin

The content of this first part of the chapter is in preparation for submission to Food Chemistry

Guilherme M. Tavares, Thomas Croguennec, Olivia Lerideau, Pascaline Hamon, Antônio F. Carvalho[c], Saïd Bouhallab

Abstract

Complex coacervation corresponds to the formation of two liquid phases in equilibrium induced by the interaction of two oppositely charged colloids. The more concentrated phase known as coacervate phase, has attracted interest from several fields of science due to its potential applications for example for encapsulation and delivery of bioactives. Prior such application, it is necessary to understand how the presence of small ligands affects the complex coacervation. In this work, we reports on the interaction of small ligand with individual proteins β-lactoglobulin (β-LG) and lactoferrin (LF) and consequences on their coacervation. ANS (8-Anilinonaphthalene-1-sulfonic acid), a fluorescent probe, was used as model ligand. Although ANS did not interact with β-LG, it presented two set of binding sites with LF inducing its self-aggregation. Depending on its concentration, ANS modulated the shape of β-LG-LF assembly. Coacervates were observed for ANS/LF molar ratio < 25 against amorphous aggregates for higher ANS/LF molar ratio. The maximum loading capacity of around 40 mg of ANS per gram of LF on the coacervates was reached.

Keywords: complex coacervation, β-lactoglobulin, lactoferrin, binding, ANS, ITC

4.1 Introduction

The coacervation corresponds to the equilibrium phenomenon of a colloidal system leading to the formation of two distinct liquid phases, one more concentrated in colloid known as the coacervate phase and the other, more diluted, known as the equilibrium solution (dilute phase) [108]. When this phase separation is induced by the interaction of two oppositely charged colloids, the phenomenon is called complex coacervation [108]. The complex coacervation of various polyelectrolytes/colloids has been extensively studied [115, 123]. However, compared to the other systems, the complex coacervation between proteins has been much less described [15]. The protein complex coacervation, especially involving food protein, starts to be the focus of several research teams from different science fields mainly because of its potential applications such as formation of protein films and the encapsulation/transport of bioactives [4].

The complex coacervation is very dependent on the protein nature, but certain parameters governing this phenomenon are universal [15]. Among other factors, the anisotropy of charge presented by the proteins makes their complex coacervation more difficult to be predicted compared to the systems involving uniform and homogeneous surface charges. Protein complex coacervation requires conditions (pH and protein molar ratio) allowing a compensation of charge and size between the proteins involved [53] and also a protein conformation state allowing the access to the interaction sites as demonstrated for the coacervation between α-lactalbumin (α-LA)/lysozyme (LYS) [130, 131].

Recently several research teams reports on the coacervation between β-lactoglobulin (β-LG) and lactoferrin (LF) [6, 139, 140]. The complex coacervation of these two proteins is particularly interesting because (i) both proteins are from milk, allowing elaboration of structures compatible with dairy matrices; (ii) β-LG (~ 18,3 kDa) been the major soluble acidic protein (pI ~ 5.2) of cow milk can easily be obtained and (iii) LF (~ 83 kDa), the major

basic protein (pI ~ 8.5) of cow milk, presents several biological activities (i.e. immunomodulatory, anti-inflammatory) and a high nutritional and industrial value (infant formula) [28].

The binding of bioactive to the proteins can alter their properties such as protein aggregation [167], changes of the protein conformation [168] or increase of protein thermo-stability [22]. Hence, before considering the use of protein coacervates for encapsulation purposes, it is necessary to understand how small ligands affect the coacervation process. For such purpose, we used ANS (8-Anilinonaphthalene-1-sulfonic acid), a hydrophobic and charged probe as a model molecule. The ANS is a probe that exhibits low fluorescence in water, but becomes quite fluorescent in non-polar environments and for this reason is widely used as probe to detect changes in protein conformation [169]. ANS has a molecular weight (299.34 g mol^{-1}) consistent with the molecular weights of different bioactives (vitamins, polyphenols). ANS is able to interact with hydrophobic residues of proteins through its anilinonaphthalene group [170] and also with positively charged residues through its sulfonic group [171]. Several studies tried to elucidate how ANS interacts with proteins. While ANS is able to strongly interact with non-native β-LG, the interaction is largely reduced with the protein in its native state [172] and although there is no description in the literature about the ANS-LF binding, a strong correlation between the number of positive charges of basic proteins and the ANS binding stoichiometry was demonstrated [171].

In this paper we confirmed that ANS does not interact with native β-LG, while two different sites could be evidenced on LF. The increase of the ANS binding induced LF self-aggregation, affecting consequently the shape of formed assemblies (coacervates/aggregates) in the presence of β-LG. A maximum loading capacity of around 40 mg of ANS per gram of LF on the coacervates was obtained.

4.2 Materials and Methods

4.2.1 Reagents and Solutions

Bovine lactoferrin (LF) (purity of 90% and iron saturation of 10 - 20 % according to technical specification) was purchased from Fonterra Cooperative Group, New Zealand. Bovine beta-lactoglobulin (β–LG), containing genetic variants A and B, was provided by a confidential industrial source. The industrial powder was dispersed in deionized water (45 g/L), adjusted to pH 5.2 with 1M HCl and kept at 30°C for 5 min, in order to precipitate non-native forms of β-LG. The dispersion was centrifuged at 20 000*g* at room temperature for 10 min (Heraeus Biofuge Primo, Thermo Scientific, Waltham, MA, USA). The supernatant containing only native β-lactoglobulin was adjusted at pH 7.0 with 1 M NaOH, freeze-dried and stored at – 20 °C until use.

The variant A of beta-lactoglobulin (β–LG A) was purified from the native β-lactoglobulin as described by Tavares et al. [6]. Briefly, ion-exchange purification was performed on a Q-Sepharose Fast Flow resin (GE Healthcare, Velizy-Villacoublay, France) eluted using a NaCl gradient. The collected β–LG A fraction was concentrated and then diafiltrated with deionized water on a 5.0 kDa ultrafiltration membrane. The protein solution was then freeze-dried and stored at – 20 °C until use. ANS probe (8-Anilino-1-naphthalenesulfonic acid, purity ≥ 97%) and MES hydrate were purchased from Sigma-Aldrich (St. Louis, MO, USA) and all other chemicals were from VWR (Radnor, PA, USA).

LF, β–LG and β–LG A stock solutions at approximately 0.2 mM, 2.0 mM and 2.0 mM respectively were prepared by solubilizing the protein powders in 10 mM MES buffer containing or not 50 mM of NaCl. The solutions were adjusted at pH 5.50 with 1 N HCl and then filtered through a 0.2 µm pore-size membrane (cat. no. 4612, Pall Corporation, Ann Arborn, MI, USA). Final stock solutions concentrations were determined by measuring the absorbance at 280 nm (SAFAS UV MC2, Safas, Monaco) using as extinction coefficients

1.47 L g^{-1} cm^{-1} for LF stock solution and 0.96 L g^{-1} cm^{-1} for β–LG and β–LG A stock solutions.

ANS stock solution was prepared by solubilizing 5.0 mM ANS in 10 mM MES buffer. After filtration through a 0.2 µm pore-size membrane (cat. no. 4612, Pall Corporation, Ann Arborn, MI, USA) the solution was adjusted to pH 5.50 with 1 N NaOH and then filtered through a 0.02 µm pore-size membrane (cat. no. 6809-2002, Whatman, Germany). Final ANS concentration was determined on the basis of its extinction coefficient value of 4950 M^{-1} cm^{-1} at 350 nm reported in the literature [173]. No sign of self-aggregation was detected in the stock solutions that were translucent.

4.2.2 Preparation of the coacervates

Based on our previous work, the final concentrations of LF and β-lactoglobulin (β–LG or β–LG A) for coacervation were fixed at 0.05 mM and 0.5 mM respectively [6]. To verify the effect of ANS on the coacervation process, different mixtures containing LF, β-lactoglobulin (β–LG or β–LG A) and different concentrations of ANS were studied. The final concentration of ANS was defined as a function of the LF concentration, to cover the ANS/LF molar ratio from 0 to 45. To avoid problems linked with the differential dilution of the mixtures by adding different volumes of ANS stock solution, pre-diluted ANS solutions were prepared to standardize the ANS volume used whatever the ANS/LF molar ratio. Three different order of mixture were tested: (1) β–LG + LF + ANS; (2) β–LG + ANS + LF and (3) LF + ANS + β–LG. Control mixtures replacing β–LG and/or LF by MES buffer were prepared.

4.2.3 Isothermal titration calorimetry (ITC)

The interaction between ANS and each protein (LF and β–LG) was characterized using ITC. ITC experiments were performed on a VP-ITC microcalorimeter (Microcal, Northampton

MA). LF and β–LG solutions at 0.05 mM and ANS solutions at 4.25 mM, prepared from the stock solutions, were degassed under vacuum before titration experiments. The reference cell was filled with 10 mM MES buffer pH 5.50 and the sample cell (1.425 mL) was filled with LF or β–LG solution. The protein solutions were titrated with 58 successive 5 µL injections of ANS. Each injection lasted 10 s with an interval of 200 s between consecutive injections in order to reach thermodynamic equilibrium. During the titration, the solution in sample cell was stirred at 310 rpm to ensure its complete homogeneity. For each ITC experiment, a reference titration was performed by titrating ANS solutions directly into 10 mM MES Buffer containing or not 50 mM of NaCl. The area under each injection peak was integrated and plotted versus the ANS/protein molar ratio using the software Origin 7.0.

4.2.4 Hydrodynamic diameter (Dh) measurement

The evolution of the hydrodynamic diameter (Dh) of mixtures of β–LG+ANS and LF+ANS, and of the structures remaining in dilute phase (supernatant of the mixtures containing β–LG/LF/ANS) at various ANS/protein molar ratios was verified by dynamic light scattering (DLS) using a Zetasizer NanoZS (Malvern Instruments, Malvern, UK). Dh was calculated using the Stokes – Einstein equation, assuming that the complexes have a spherical shape. The dynamic light backscattering was detected at 173° and a refractive index of 1.45 for the complexes was used for volume-size representation.

For the Dh measurements of the solutions containing one protein (β-LG or LF) and ANS, various volumes of ANS stock solution were added to a 0.05 mM β–LG or LF solution in a 10 x 10 mm polystyrene cell (Sarstedt, Nümbrecht, Germany) to reach the required ANS/protein molar ratio. Dh measurements were performed after an equilibration time of 2 min at 25 °C in absence or in presence of 50 mM of NaCl. Results were the mean of at least 13 runs and all samples were analyzed in triplicate.

For Dh measurements in the dilute phase after separation of the coacervates, the supernatants were filtered through a 0.8 µm pore-size membrane (cat. no. 4608, Pall Corporation, Ann Arborn, MI, USA) to ensure the absence of coacervates or large aggregates.

4.2.5 ζ-potential measurement

The evolution of the ζ-Potential of mixtures of β–LG+ANS and LF+ANS at various ANS/protein molar ratios was determined at 25 °C using the same equipment as the one described for Dh analysis. Each ANS/protein molar ratio corresponded to an individual sample preparation. The samples were prepared by mixing the required volume of ANS stock solution with 0.05 mM β–LG or LF solution. The samples were put into a folded capillary cell (DTS1061, Malvern, United Kingdom) and after 2 min of equilibration an electric potential of 150 V was applied. The dielectric constant and the refractive index of the solvent were set at 78.5 and 1.333 respectively. The electrophoretic mobility was calculated applying the Henry equation and the ζ-Potential was calculated using the Smoluchowski approximation.

4.2.6 Turbidity measurements

Turbidity measurements were performed at 600 nm (A_{600nm}) with the spectrometer FLX-Xenius (Safas, Monaco) to monitor the interaction between LF, β–LG and ANS. Absorbance measurements were converted to turbidity using the following relationship: $\tau = (2.303A_{600nm})/l$, where τ is the turbidity (cm^{-1}) and l is the light path length (0.26 cm) corresponding to the height of the liquid column (100 µL) into the microplate well. Proteins and ANS mixing was performed directly into the microplate wells respecting the different orders described above. Absorbance measurements started immediately after mixing and the turbidity evolution was monitored during 60 min. No evolution of turbidity was detected for the control mixtures (i.e. mixtures without β-LG or LF).

4.2.7 Optical microscopy observation

The formation of coacervates, amorphous aggregates or the absence of suprastructures for all different mixtures containing β-LG, LF and ANS was determined at room temperature using a phase contrast optical microscope equipped with an epifluorescence module (Olympus BX51TF, Olympus, Hamburg, Germany) set at the magnification 100x. The control mixtures (i.e. mixtures without β-LG or LF) do not present any detectable supramolecular structures formation.

4.2.8 Quantification of proteins and ANS in dense and coacervate phases

The partition of the proteins and ANS in between the coacervate and dilute phases was quantified by liquid chromatography. For this purpose, a volume of 1000 µL of all different mixtures was prepared. Dilute and coacervate phases were separated by centrifugation (Heraeus Biofuge Primo, Thermo Scientific, Waltham, MA, USA) at 28000*g* for 30 min. Proteins and ANS in both phases were quantified using a PLRPS column (S/N 1006329-5, Varian Inc., Shropshire, UK) connected to a Waters 26 95 HPLC. Milli-Q water containing 1.06 ‰ (v/v) of trifluoroacetic acid and an 80/20 acetonitrile/milli-Q water (v/v) mixture containing 1.0 ‰ (v/v) of trifluoroacetic acid were used for elution. The absorbance at 280 nm was measured during the elution using a Waters 2487 detector. Less than 1.5 % of protein or ANS were recovered in the dense phase of the control mixtures.

4.3 Results

4.3.1 Characterization of the ANS-β-LG and ANS-LF interactions

Before performing complex coacervation between β-LG and LF in the presence of ANS, we checked the interaction of ANS with each of the two proteins. Binding experiments were

performed by injecting small volumes of ANS stock solution into protein solutions. Figure 4.1 shows the binding isotherms obtained by the titration of ANS into LF, β-LG or in MES buffer (dilution effect).

A negligible exothermic signal was associated to the injection of ANS into buffer solutions. Likewise, a flat exothermic isotherm was obtained from the titration of ANS into β-LG, indicating no detectable binding between ANS and β-LG under these experimental conditions. However, a quite complex binding isotherm was obtained by titration of LF with ANS, showing an exothermic signal with a release of energy associated to the first injection of around - 6.0 kcal mol^{-1} of injected ANS. The obtained ANS-LF binding isotherm clearly shows two distinct regions. The first one, until ANS/LF molar ratio of 5 was characterized by a continuous decrease of the energy released between two successive injections. The second region, for ANS/LF molar ratios above 5, was characterized by the formation of a "cavity" due to successive increase-decrease of released energy as a function of increasing ANS concentration. We note that full saturation was not reached at the end of our titration experiment i.e ANS/LF molar ratio of 20. Both regions were affected by increasing the high ionic strength even if the overall titration profile remained unchanged (Figure 4.1). With 50 mM NaCl, the first region showed a less exothermic signal, reducing its slope. The second region was also significantly affected, the ITC signal became closer to the baseline and the "cavity" was less visible and seems to be shifted to the higher molar ratios.

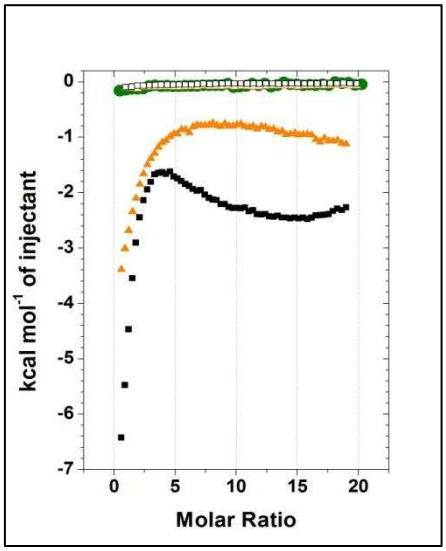

Figure 4.1. Binding isotherms of the titration of LF 0.05 mM and β-LG 0.05 mM with 4.25 mM ANS in MES buffer pH 5.5 at 25 °C. LF without (■) and with (▲) 50 mM NaCl; β-LG without NaCl (●). Injection of ANS in the MES buffer without (□) and with 50 mM NaCl (Δ).

To relate thermodynamic titration to structures, the evolution of the hydrodynamic diameter (Dh) and the ζ-potential were monitored as a function of ANS/LF molar ratio (Figure 4.2). The ANS stock solution presented a Dh of 0.76 ± 0.15 nm. The measured Dh remained unchanged for low ANS/LF molar ratios. However, increasing the ANS/LF molar ratio, a continue increase of the Dh of the complexes was observed. Above a ratio of 5, a progressive increase of the Dh was observed until a value of 18.9 ± 0.30 nm reached for ANS/LF molar ratio of 50.

Concomitantly, ζ-potential decreased progressively during titration from + 10.17 ± 0.86 mV, the value of pure LF, to reach + 1.74 ± 0.18 mV at ANS/LF molar ratio of 50. A negative value of – 9.80 ± 0.68 mV was found for the ANS stock solution. For comparison, titration of β-LG with ANS in the conditions did not affect the Dh nor the ζ-potential (data not shown).

The increase of ionic strength by adding 50 mM NaCl moderately affected the Dh increase of ANS/LF complex. A significant Dh increase started at ANS/LF molar ratio of 10 to reach a

17.3 ± 0.25 nm at ANS/LF molar ratio of 50, a value lower than that reached in the absence of added NaCl.

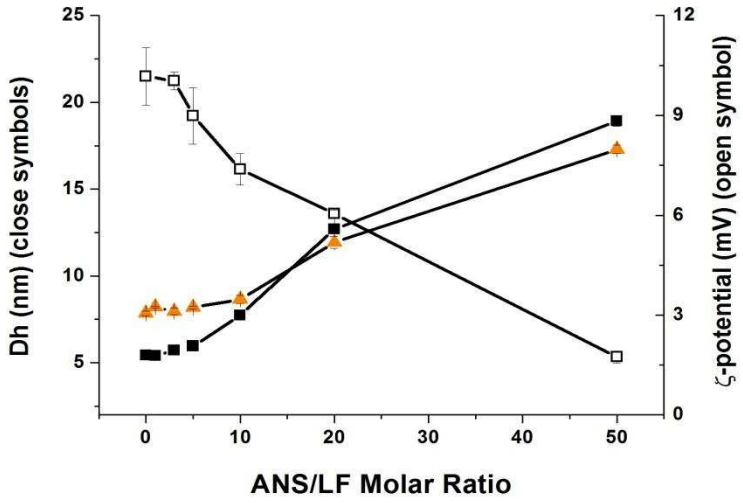

Figure 4.2. Evolution of the hydrodynamic diameter Dh and ζ-potential of the complexes as a function of the initial ANS/LF molar ratio at 25°C without added NaCl (■, □) and in the presence of 50 mM of NaCl (▲).

4.3.2 Coacervation process in the presence of ANS

The effect of ANS on the β-LG - LF coacervation was investigated for the three different mixing orders: (1) β–LG + LF + ANS; (2) β–LG + ANS + LF and (3) LF + ANS + β–LG. Figure 4.3 shows the turbidity of the mixtures carried out for various ANS/LF ratios whatever the mixing order. Mixtures with ANS/LF molar ratios of 10 and 20 showed the same behavior as without ANS. The mixtures showed a maximum of turbidity immediately after mixing which decreased with time tending to zero after 60 min. A different behavior was presented by the mixture at ANS/LF molar ratio of 45, the turbidity immediately after mixing was lower than for the other mixtures, but increased with time to stabilize after 20 min. However, the turbidity level presented by this mixture did not reach the maximum turbidity levels found for the other mixtures.

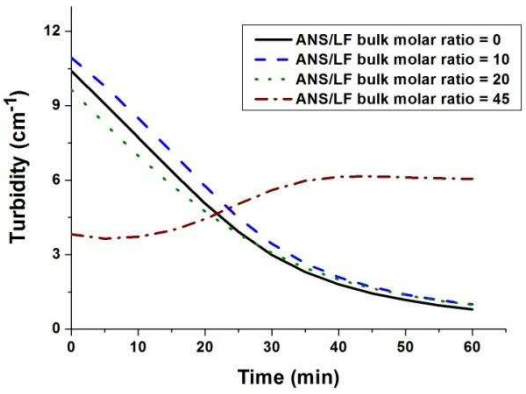

Figure 4.3. Evolution of the turbidity of mixtures containing 0.5 mM of β-LG, 0.05 mM of LF and variable concentrations of ANS. Different ANS/LF molar ratios were tested: 0 (straight line), 10 (dashed line), 20 (dotted line) and 45 (dash-dotted line). These results correspond to mixtures performed according to the order 2 (β-LG+ANS+LF), given than the same behavior was found for orders 1 and 3.

The morphology of formed assemblies depended on the ANS concentration as determined from phase contrast microscopy and epifluorescence images (Figure 4.4). Until the ANS/LF molar ratio of 25, the mixtures formed microspheres (coacervates) dispersed in the dilute phase as without added ANS (Figure 4.4A). For ANS/LF molar ratio of 30, the formation of clusters of coacervates was observed (Figure 4.4C). For ANS/LF molar ratio of 40, the complex coacervation was suppressed and instead amorphous aggregates were formed (Figure 4.4E).

The incorporation of ANS molecules into formed supramolecular structures was evidenced using epifluorescence microscopy, showing fluorescence co-localized with formed objects (Figure 4.4 B, D and F). Similar effect of ANS was obtained whatever the mixing order.

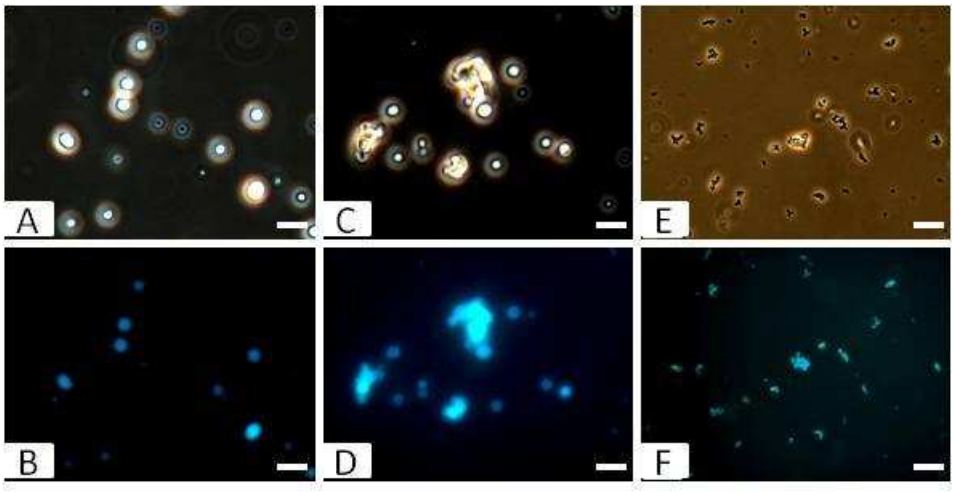

Figure 4.4. Optical microscopy images in phase contrast mode (A, C, E) and epifluorescence mode (B, C, E) for mixtures containing 0.5 mM of β-LG, 0.05 mM of LF and different concentrations of ANS according to mixing order 2. Different ANS/LF molar ratios were tested: 25 (A, B), 30 (C, D) and 40 (E, F).

4.3.3 Partition of proteins and ANS between dilute and coacervate phases

The partition of ANS and its effect on the protein equilibrium between dilute and coacervate phases were determined for variable ANS/LF molar ratio and fixed total protein concentration. In the absence of ANS and regardless the order of mixing, 34.2 ± 1.5% of initial LF was recovered in the coacervate phase, consistent with the LF yield we already reported [6]. The increase of ANS concentration induced a gradual decrease of LF recovered in the coacervates reaching 26.2 ± 1.7% for ANS/LF molar ratio of 20. The LF recovery in the dense phase was much lower (less than 6%) for ANS/LF molar ratio of 45, mixtures forming amorphous aggregates. The recovery of β-LG in the dense phase showed similar trend than LF. The β-LG/LF molar ratio in the coacervate phase (ANS/LF bulk molar ratio ≤ 20) was almost constant around 7.9 ± 0.3, against 4.1 ± 0.2 when amorphous aggregates were favored i.e. ANS/LF molar ratio of 45. The proportion of ANS and corresponding evolution of the

ANS/LF molar ratio in the dense phase as a function of the initial ANS/LF molar ratio are depicted in Figure 4.5A.

ANS/LF molar ratio in the dense phase evolved almost linearly with the ANS/LF initial molar ratio. In the coacervation regime (ANS/LF initial molar ratio ≤ 20), about 23.1 ± 1.1% of the initial quantity of ANS was recovered in the coacervate phase for the mixtures containing an ANS/LF initial molar ratio of 1. This proportion decreased to 15.9 ± 1.2% of the mixture containing ANS/LF initial molar ratio of 20, corresponding to 39.2 ± 1.0 mg of ANS per g of LF in the coacervate phase. In the aggregation regime (ANS/LF initial molar ratio = 45) the proportion of ANS recovered in the dense phase was much smaller (less than 3.5 %). Note that no significant effect of mixing order was observed.

To check that the ANS recovery in the coacervate phase is associated to protein yield and not to unspecific phenomenon such as co-precipitation, we performed the same experiment using β-LG isoform A. β-LG A is known to shift the equilibrium of the coacervation with LF leading to higher coacervation yield compared to β-LG (native, containing the two isoforms A and B) [6]. As expected, the LF recovery in the coacervate phase was 70.4 ± 1.2%, i.e. 2.6 times higher than the LF recovered for the mixture prepared with β-LG (native). The ANS recovery in the coacervate phase with β-LG A was 30.9 ± 0.7%, almost twice the ANS recovered with β-LG (native). In contrast, a slightly lower ANS amount i.e. 30.9 ± 0.8 mg instead of 39.2 ± 1.0 mg ANS per g of LF was recovered when β-LG (native) was substituted by β-LG A.

Figure 4.5B shows the Dh of the molecular entities remaining in the dilute phase and its evolution as a function of the ANS/LF initial molar ratio. The measured Dh value without ANS was 12.2 ± 0.17 nm and remained relatively constant until ANS/LF molar ratio of 20. Larger complexes with Dh of 17.2 ± 0.6 nm were detected for higher ANS/LF molar ratios. Mixing order did not affect the observed evolution of Dh.

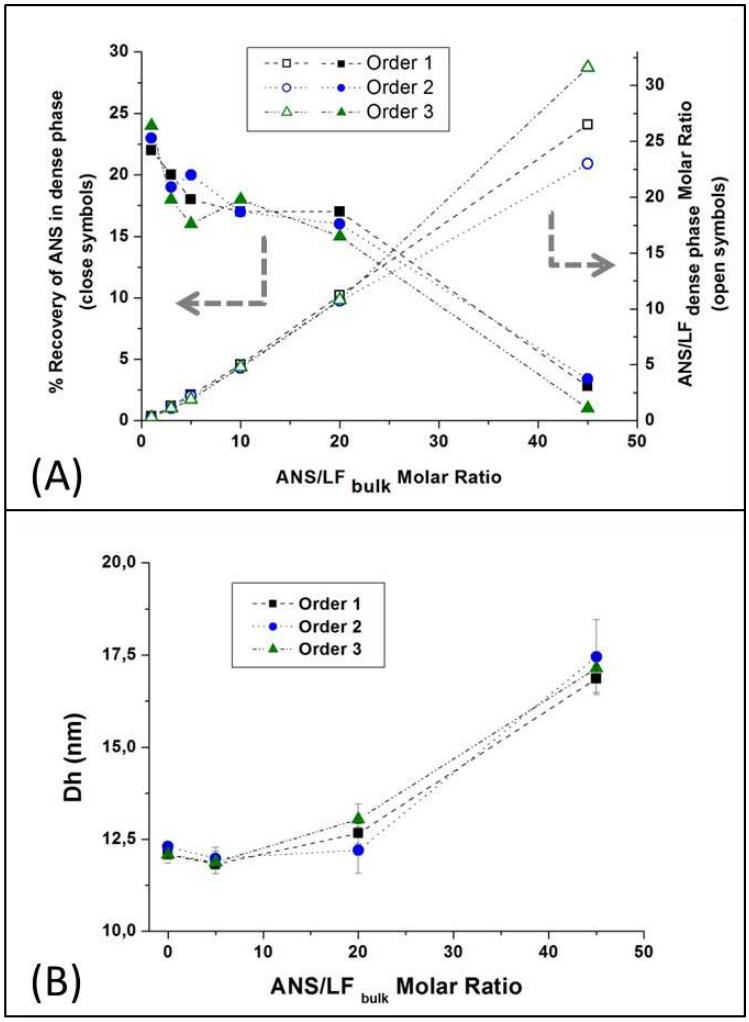

Figure 4.5. Evolution of recovered ANS (in %) and corresponding ANS/LF molar ratio in the dense phase (A) and of Dh of the structures remaining in the dilute phase after centrifugation of the mixtures (B) as a function of the initial ANS/LF molar ratio. Protein concentrations were 0.05 mM for LF and 0.5 mM for β-LG. The squares, circles and triangles correspond to mixing order 1, 2 and 3, respectively.

4.4 Discussion

4.4.1 ANS-LF binding versus β-LG-LF coacervation

Immediate increase of turbidity after mixing β-LG and LF under after defined physico-chemical conditions and protein stoichiometry underline spontaneous protein coacervates dispersed in continuous dilute phase. The characteristic subsequent decrease of turbidity

indicates coalescence and sedimentation of the coacervates over time. The presence of small hydrophobic molecule such as ANS until an ANS/LF molar ratio of 20 did not affect the turbidity profile and consequently the coacervation kinetic. At higher ANS/LF molar ratio, the protein assembly leads to the formation of amorphous aggregates with different turbidity profile [6, 139].

According to the ANS concentration, various structures including coacervates, clusters of coacervates and aggregates were obtained in which ANS molecules are incorporated (Figure 4.2). Hence, ANS starts to exercise a structural effect when present at 20-fold excess compared to LF. The clustering of individual coacervates at intermediary at ANS/LF molar ratios is assumed to be induced by the increase of the surface hydrophobicity of the coacervates throughout ANS binding. As shown in the Figure 4.5A, the ANS/LF molar ratio in dense phase is proportional to the initial (bulk) ANS/LF molar ratio.

As evidenced by ITC, while ANS does not interact with native β-LG under studied physical-chemical conditions, it presented a quit complex binding profile with LF. This binding process presents a first, more energetic region corresponding to a specific binding site of ANS to LF, and a second region which corresponds probably to the superposition of the energetic contributions of a nonspecific binding of ANS and of subsequent LF aggregation as evidenced from DLS measurements. The two interaction regions were affected but not abolished by an increase of ionic strength. Addition of 50 mM NaCl decreased the enthalpy of the first injection in the first region from ~ - 6.5 to -4.5 kcal/mole of ANS and also decrease considerably the exothermic signal linked to the second interacting region. Higher concentration of NaCl further decreases the intensity of the signal in the two regions (not shown). Similar unusual ITC profile with two distinct regions was reported for the interaction of ANS with BSA at acidic pHs [171]. These authors proposed that the primary determinant of binding of ANS to BSA is electrostatic with ion pair formation between positive charge of

the protein and sulfonate SO^-_3 group of ANS. However, is this study, the occurrence of other phenomena during the titration such as subsequent aggregation was not checked. Given the limited effect of NaCl we observed here, it is difficult to attribute the events occurring in the two ITC regions to a kind of given interaction electrostatic versus hydrophobic. Indeed, other forces, involving or not water molecules may be involved in the ANS-LF binding such as hydrogen bonds and or the van der Waals interactions (both associated with an exothermic behavior). The effect of the ANS on the β-LG - LF coacervation would probably be more intense if electrostatic interactions constitute the main driving forces in ANS-LF interaction.

The effect of ANS on β-LG - LF coacervation process as well as coacervation yield seems to be independent on the mixing order, suggest a thermodynamic equilibrium between the proteins and ANS molecules in dilute and dense phases. Nevertheless, these results are quite unexpected. As ANS interact spontaneously with LF inducing its self-assembly, we would expect a specific effect consecutively to the addition of β-LG. In fact, until ANS/LF ratio of 25, for which coacervation still occurs, ANS affects in the same manner both already formed coacervates (order 1) and coacervation between β-LG and pre-formed ANS-LF complexes (order 3). The effect on the mixing order starts to be detected for ANS/LF ratio as high as 40.

Taking together the above results, a mechanism relating the effects of ANS concentration on the co-assembly between β-LG and LF is proposed (Figure 4.6). Until ANS/LF molar ratio of 25, the formed ANS-LF nanoparticles of ~12 nm still interact with an excess of β-LG to form coacervates. Above this ratio, the increase of the ANS concentration favoured the clustering of formed ANS-containing coacervates. For ANS/LF molar ratio higher than 40, the high excess of ANS prevents the coacervation process leading to the formation of aggregates with smaller size. We assume that until a critical ratio, ANS binds to LF without affecting the immediate environment of two binding sites reported for β-LG [6]. At high excess of ANS concentration relatively to LF, ANS compete with or displaced β-LG from its binding sites

thus impeding the coacervation. Under these conditions, formation of amorphous aggregates is favoured with a predominance of nanoparticle with Dh ~17 nm recovered in the supernatants as well as after mixing ANS and LF in the absence of β-LG.

At low concentrations (ANS/LF molar ratio ≤ 5), ANS did not affect the Dh of the particles found in dilute phase which exhibited a value around 12 nm, in agreement the Dh values found by others in the absence of ANS [139, 142]. Similar Dh value was found in dilute phase of samples with ANS/LF molar ratio of 20, in which both coacervation and ANS-induced LF self-association occur.

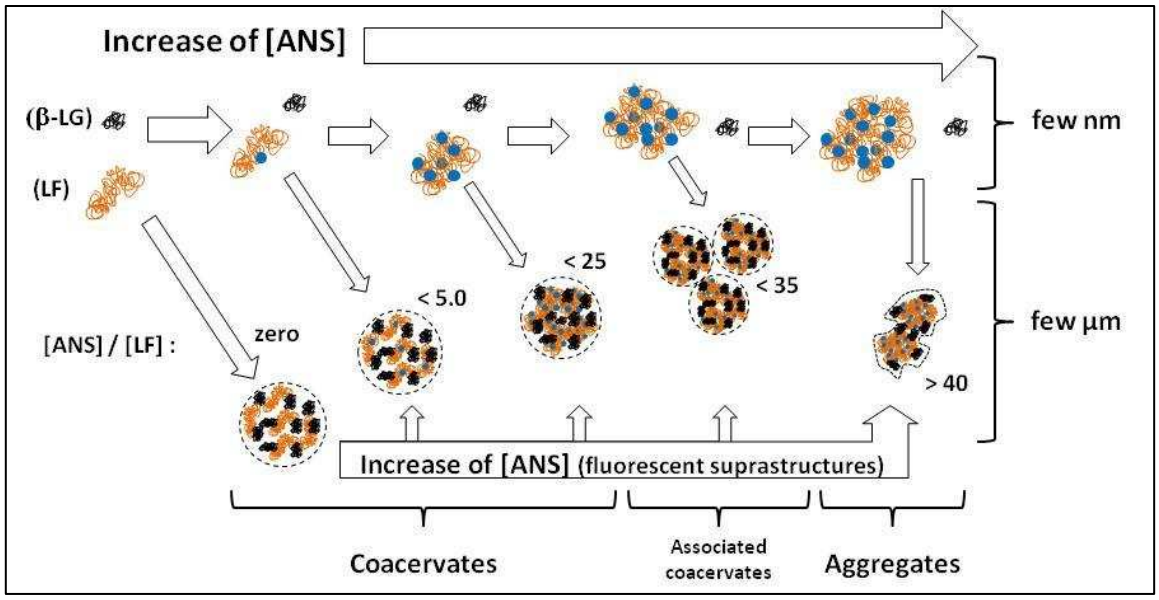

Figure 4.6. Proposed mechanism describing how increasing ANS concentration (represented by the blue circle) affects β-LG-LF coacervation process at constant protein concentration.

The proportion of recovered proteins in the coacervate phase decreased by increasing ANS concentration, supporting the fact that bound ANS affects β-LG-LF interaction/coacervation yield. The recovery of ANS in the coacervate phase is directly linked to the protein recovery. The ANS recovery in the coacervate was significantly increased by increasing the protein recovery throughout substitution of β-LG by β-LG A isoform. Approximately 30 - 40 mg of

ANS per g of LF were recovered in the coacervate phase corresponding to a maximum ANS recovery of about 30% under used experimental conditions.

We show that the presence of such molecules affects the thermodynamic equilibrium of protein coacervation. In particular because small ligands affect the global electric charge and or size (aggregation) of the proteins, two key parameters governing protein coacervation [53]. As the binding of small ligands to proteins is also based on a thermodynamic equilibrium, precise determination of the physico-chemical conditions and relative stoichiometry of protein/protein and ligand/proteins interactions becomes essential. The ability of β-LG and lysozyme to form coacervates in the presence of vitamin D_3 was recently published (Diarrassouba et al. [138]. However these authors focused their work on the stability of vitamin D_3 rather than on the mechanism of the overall coacervation process.

4.5 Conclusion

As a preliminary step towards the use of protein coacervates for encapsulation purpose for small molecules, we reports on how small molecules induced changes on the proteins affect the kinetics and yield of coacervation. ANS was chosen as a model molecule in this study to mime potential bioactive molecules (size, charge, hydrophobicity). The LF charge reduction and self-aggregation induced by the ANS affect the β-LG-LF interaction and consequently the coacervation process. For ANS/LF molar ratios below 25 the sites of interaction between β-LG and LF were not impaired and the coacervation still occurred. Nevertheless, for ANS/LF molar ratios higher than 40, the formation of amorphous aggregates was observed probably due to the obstruction of the β-LG sites on LF induced by LF aggregation. Interestingly, the behavior of the mixtures containing ANS, β-LG and LF was independent on the mixing order indicating the thermodynamic equilibrium of the system, crucial for the optimization of the protein coacervation. Studies are in progress to better understand the ITC profile, the nature of

the interactions involved in the overall exothermic signal and to better define the exact role of formed nanoparticles in the coacervation – aggregation processes.

4.6 Acknowledgements

The financial supports from INRA, Trinity College Dublin (Biochemistry Department), Université Européenne de Bretagne (Collège Doctoral International), Conseil Régional de Bretagne and the federal Brazilian funding agency CNPq are acknowledged.

PART 2: HOW THE PRESENCE OF FOLIC ACID AFFECTS THE COMPLEX COACERVATION BETWEEN LACTOFERRIN AND β-LACTOGLOBULIN

PREAMBLE

To complete the study of the effect of ANS, a hydrophobic substance, on β-LG - LF complex coacervation, the second part of chapter 2 focuses on the effect of Folic Acid (FA) used as model of hydrophilic ligands. Our objective was to extract some critical parameters able to modulate the heteroprotein complex coacervation in the presence of small ligands. The FA, known as vitamin B_9, is essential for human beings presenting several biological functions. The research questions and the experimental approach are similar to those for ANS (part 1 of this chapter). However a greater focus was directed to the thermodynamic characterization of FA-LF interaction and subsequent aggregation of formed complexes. Only results with LF were reported as no interaction of FA with β-LG was detected in the present work as assessed by ITC and filtration experiments as well as by DLS results showing a constant Dh for β-LG around 5 nm independent of the concentration of FA.

Our main results:

- Under the used experimental conditions, FA does not interact with β-LG (flat ITC profile, constant Dh) but interacts electrostatically with LF forming nanoparticles of definite size of around 16 nm.
- FA-LF interaction exhibits an exothermic signal with an affinity constant value of $\approx 10^5\ M^{-1}$.
- The nanoparticles present a FA/LF molar ratio of 10 and seem to be stabilized by a slight accumulation of positive charges on their surface.
- Experimental and simulation approaches support a two steps mechanism: i- FA-LF interaction until a critical stoichiometry; ii- subsequent aggregation of formed complexes.

This page was intentionally left blank.

Binding of folic acid induces specific self-association of lactoferrin into nanoparticles: thermodynamic characterization

The content of this part of the chapter has been submitted for consideration in Langmuir

Guilherme M. Tavares, Thomas Croguennec, Sébastien Lê, Olivia Lerideau, Pascaline Hamon, Antônio F. Carvalho, Saïd Bouhallab

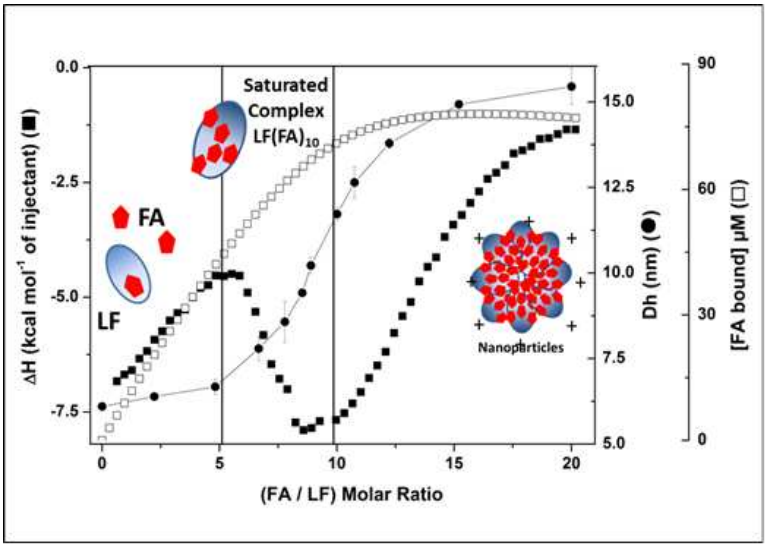

Graphical Abstract: Superposition of FA-LF binding isotherm, evolution of bound FA concentration, evolution of the Dh of FA-LF complexes and schematic representation of the formation of FA-LF nanoparticles.

Abstract

In the study presented here, we investigated the interaction at pH 5.5 between folic acid (FA), and lactoferrin (LF) a positively charged protein. We found a binding constant K_a of 10^5 M^{-1} and a high stoichiometry of ten moles of FA per mole of LF. The size and charge of the complexes formed evolved during titration experiments. Increasing the ionic strength to 50

mM completely abolished the ITC signal, suggesting the predominance of electrostatic interactions in the exothermic binding obtained. We developed a theoretical model that explains the complex triphasic ITC profile. Our results revealed a two-step mechanism: FA-LF interaction followed by self-association of the complexes thus formed. We suggest that ten FA molecules bind to LF to form saturated reactive complexes (FA_{10}/LF) that further self-associate into nanoparticles with a finite size of around 16 nm. There is thus a critical saturation degree of the protein, above which the self-association can take place. We present here the first results that provide comprehensive detail of the thermodynamics of FA-LF complexation-association. Given the high stoichiometry, allowing a load of 55 mg FA/g of LF, we suggest that FA-LF nanoparticles would be an effective vehicle for FA in fortified drinks.

4.7 Introduction

The demand for products that enhance consumers' health and well-being is increasing throughout the world. Consumer demand for such products provides substantial challenges for the food sector as it aims to propose bioactive molecules in the form of functional foods. Producing such functionally-enhanced products is not without obstacles because of the high sensitivity of bioactive molecules to the conditions applied during food processing, formulation and storage. Despite the relatively small quantities of bioactive molecules required by the body, the challenge is to find specific and adapted formulations for effective delivery of native soluble bioactive molecules (micronutriments, nutraceuticals). Many research groups have therefore explored the possibilities of using food proteins as carriers due to their high affinity for small bioactive molecules [174]. β-lactoglobulin and serum albumin, natural ligand binding proteins from cow's milk, are the most extensively studied proteins as carriers for several bioactive molecules, including polyphenols [175]; fatty acids [176]; aroma

[66] and vitamins [177]. Most of these studies have been carried out at physiological pH, i.e. neutral.

Among bioactive molecules, the vitamin B family has always received considerable attention owing to its crucial biological role. Folic acid (FA), currently known as vitamin B_9, is essential for several human body reactions and is thus an essential dietary component. FA is a co-enzyme in carbon metabolism pathways, including the biosynthesis of several amino acids, and is effective in decreasing the risk of several diseases [178]. Because of its physiological functions, and since humans cannot synthesize folates, there is a need to develop fortified foods and drinks. However, from a technological point of view this is not always easy because of the poor solubility and the precipitation of FA. Although hydrophilic and negatively charged, FA is poorly soluble at acidic pH [179]. This limits the use of this vitamin for food fortification, particularly acidified drinks.

We hypothesized that lactoferrin, a positively charged milk protein, could interact efficiently with FA under acidic pH conditions and could thus improve its solubility and its subsequent bioavailability.

Lactoferrin (LF) is an iron-binding glycoprotein with 689 amino acids and a molar mass of about 83 kDa. LF is folded into two symmetrical lobes (the N-lobe and C-lobe), which are highly homologous to each other. The two lobes are connected via a hinge region which confers flexibility to the folded molecule [28]. LF is one of small number of proteins that carries a net positive charge at neutral and acidic pH (pI of 8.6–8.9). The charge distribution on the surface of LF is uneven, with some highly positive patches on the N-lobe and the interlobe region [23]. LF is a multifunctional protein with immunomodulatory, antimicrobial and antioxidant properties [28].

In the present study, we investigated the ability of positively charged LF to form a complex with negatively charged FA at pH 5.5 with view to designing a natural carrier for FA.

4.8 Material and Methods

4.8.1 Reagents and Solutions

Bovine lactoferrin (LF, purity 90% and iron saturation level 10 – 20% according to the manufacturer's specifications) was purchased from the Fonterra Cooperative Group, New Zealand. Folic acid (FA, purity ≥ 97%) was purchased from Sigma-Aldrich (Sigma Aldrich, St. Louis, MO, USA). Sodium citrate (tri-sodium citrate dehydrate, purity 99%) was purchased from Carlo Erba reagents (Val de Reuil, France). MES hydrate was purchased from Sigma-Aldrich and all other chemicals were from VWR (Radnor, PA, USA).

LF solutions were prepared by solubilizing the protein powder in 10 mM MES buffer with or without 50 mM NaCl. The solutions were adjusted to pH 5.50 with 1 N HCl and then filtered through a 0.2 µm pore-size membrane (Cat. No. 4612, Pall Corporation, Ann Arbor, MI, USA). The final LF concentration was determined by measuring the absorbance at 280 nm (SAFAS UV MC2, Safas, Monaco) using 1.47 L g^{-1} cm^{-1} as extinction coefficient.

FA stock solution was prepared by dispersing 1.0 mM of FA in deionized water at pH 11. After filtration through a 0.2 µm pore-size membrane (Cat. No. 4612, Pall Corporation, Ann Arbor, MI, USA), the solution was adjusted to pH 5.50 with 1 N HCl and then filtered through a 0.02 µm pore-size membrane (Cat. No. 6809-2002, Whatman, Germany). Final FA concentration was determined using the extinction coefficient value of 25100 M^{-1} cm^{-11} at 283 nm [180]. Stock solution of 2 mM sodium citrate was prepared by solubilizing the tri-sodium citrate dehydrate powder in 10 mM MES buffer pH 5.5.

4.8.2 Isothermal titration calorimetry (ITC)

A VP-ITC microcalorimeter (Microcal, Northampton MA) was used to assess the energy of the binding of FA or sodium citrate to LF at various temperatures from 20°C to 32°C. LF

solutions ranging from 0.01 to 0.06 mM, and stock solutions of FA and sodium citrate, were degassed under vacuum before titration experiments. The reference cell was filled with 10 mM MES buffer, pH 5.50, and the sample cell (1.425 mL) was filled with LF solution. LF was titrated with 58 successive injections of 5 µL FA (or sodium citrate). Each injection lasted 10 s with an interval of 200 s between consecutive injections in order to reach thermodynamic equilibrium. During titration, the solution in the sample cell was stirred at 310 rpm to ensure complete homogeneity. For each ITC experiment, a reference titration was performed by titrating FA (or sodium citrate) solutions directly into 10 mM MES Buffer. The FA (or sodium citrate) dilution data (reference experiment) were subtracted from the experimental data using Origin 7.0 software. The area under each injection peak was plotted as a function of the FA/LF (or citrate/LF) molar ratio.

4.8.3 Quantification of free and bound FA

A series of solutions of FA and LF with FA/LF molar ratios ranging from 0 to 15 were prepared by mixing appropriate volumes of FA stock solution with a fixed volume of LF solution (0.01 mM). After 10 min equilibration, free and LF-bound FA were separated by centrifugation at 28000*g* for 10 min (Heraeus Biofuge Primo, Thermo Scientific, Waltham, MA, USA) using a 10 kDa pore size membrane separator (vivaspin, Sartorius, Germany). Control experiments showed that LF was totally retained while FA crossed the membrane freely (permeate compartment) in the absence of LF, indicating the absence of non-specific interaction between FA and the membrane. FA concentrations in the initial mixtures [FA] and in the permeate compartment after centrifugal separation [FA_{free}] were determined by reversed-phase high-performance liquid chromatography (RP-HPLC). Briefly, FA was separated on a LiChrospher 100 RP-18 column (Art. 1509430001, Merck, Darmstadt, Germany) connected to a Waters 2695 HPLC system. FA was eluted at a flow rate of 0.4 mL min^{-1} using an isocratic gradient of Acetonitrile/milli-Q water 40/60 (v/v) containing 100

µL/L of 1M NaOH and quantified by absorbance at 283 nm. The retention time of FA was close to 3 min. The bound FA concentration [FA_{bound}] was calculated by subtracting [FA_{free}] from [FA]. Experiments were performed in duplicate.

The association constant (K_a) and the stoichiometry (n) of the interaction between LF and FA were determined using the Scatchard equation [181]:

Eq. 4.1. $$\frac{[\text{FA } bound]}{[\text{LF}]\,[\text{FA } free]} = \text{n Ka} - \text{Ka}\,\frac{[\text{FA } bound]}{[\text{LF}]}$$

4.8.4 Measurement of hydrodynamic Diameter (Dh)

The hydrodynamic diameter (Dh) of the complexes formed at various FA/LF molar ratios was determined by dynamic light scattering (DLS) using a Zetasizer NanoZS (Malvern Instruments, Malvern, UK). Dh was calculated using the Stokes – Einstein equation, assuming that the complexes were of spherical shape. The dynamic light backscattering was detected at 173°, and a refractive index of 1.45 for the complexes was used for volume-size representation. Various volumes of FA stock solution were added to a 0.01 mM LF solution in a 10 x 10 mm polystyrene cell (Sarstedt, Nümbrecht, Germany) to reach the required FA/LF molar ratio. Dh measurements were performed at 15, 25 and 32°C, after an equilibration time of 2 min. The results were the means of at least 13 runs and all samples were analyzed in triplicate.

4.8.5 ζ-Potential measurement

The ζ-Potential of the complexes formed at various LF/FA molar ratios was determined at 25°C using the same equipment as that described for Dh analysis. Each FA/LF molar ratio corresponded to an individual sample preparation. The samples were prepared by mixing the required volume of FA stock solution with 0.01 mM LF solution. The samples were put into a folded capillary cell (DTS1061, Malvern, United Kingdom) and after 2 min of equilibration

an electric potential of 150 V was applied. The dielectric constant and the refractive index of the solvent were set at 78.5 and 1.333, respectively. The electrophoretic mobility was calculated applying the Henry equation, and the ζ-Potential was calculated using the Smoluchowski approximation.

4.9 Results

4.9.1 Isotherm of FA-LF interaction

Isothermal calorimetric titration of LF with FA at pH 5.5 was first conducted at 20°C. Figure 4.7 (top) shows the raw signal of one representative isothermal calorimetric titration profile obtained from injection of FA stock solution into 0.01 mM LF. Each peak in the binding isotherm represents a heat change associated with a single injection of FA into the LF solution. The titration of FA into LF solution resulted in exothermic peaks. The energy contribution of the FA dilution (i.e. injection of the FA stock solution into the buffer) was very low compared to the heat exchange associated with the FA-LF interaction, indicating that an interaction between FA and LF had occurred. The integration of each peak provided the heat released per injection, allowing the construction of the binding isotherm shown in Figure 4.7 (bottom panel).

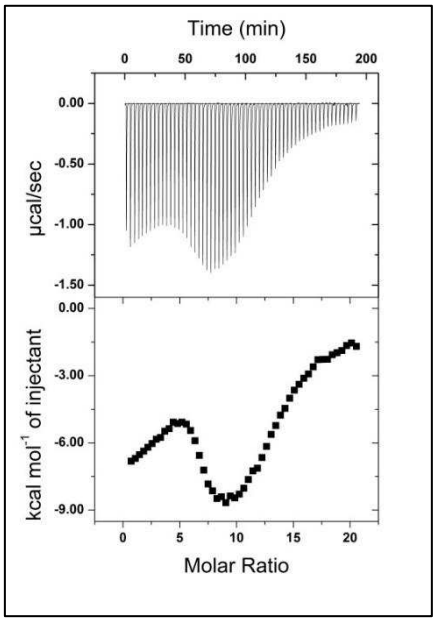

Figure 4.7. Representative raw data (upper panel) and binding isotherm (bottom panel) of the titration of 0.01 mM LF with successive injections of FA stock solution. The experiment was carried out at 20°C in 10 mM MES buffer, pH 5.5.

The FA-LF binding isotherm exhibited a complex profile far from that classically obtained for an exothermic ligand/protein interaction that is characterized by a continuous decrease in the heat released until total saturation of the binding site(s). This was the case for the citrate-LF interaction chosen as the comparative example in the present work (Figure 4.16, Supporting Information). The FA-LF binding isotherm evidenced three distinct zones in the range of the FA/LF molar ratio investigated. The first zone, below an FA/LF molar ratio of 5, was characterized by a continuous decrease in the exothermic signal. The second zone, between FA/LF molar ratios of 5 and 10, exhibited an opposite trend with an increase in the exothermic signal throughout the titration. Finally, the third zone where the exothermic signal decreased by increasing the FA/LF molar ratios from 10 to 20, a ratio at which saturation was reached. Given the complexity of the binding isotherm, the thermodynamic parameters for the FA-LF interaction could not be determined by the classical fitting models.

The complexity of the FA-LF binding isotherm was not linked to the iron saturation level of LF, as the same profile was obtained by substituting our LF sample (~ 15% saturation) by either fully iron-saturated (holo-LF) or iron-depleted (Apo-LF) forms (data not shown). The profile observed seemed to be specific to the FA-LF interaction, as the interaction of LF with citrate (another negatively charged ligand) showed a simple, classical ITC profile with well-defined interacting parameters (see Figure 4.16, Supporting Information).

4.9.2 Influence of physicochemical parameters on FA-LF interaction

We investigated the influence of three physicochemical parameters: temperature, LF concentration ([LF]) and ionic strength on the FA-LF binding isotherm, to understand the rather complex ITC profiles. Figure 4.8A shows the binding isotherms obtained during titration of the FA solution into LF (0.01 mM) at 20°C, 25°C and 32°C. In this temperature range, the FA-LF binding isotherms exhibited slight but significant temperature dependence. The titration profiles exhibited the same three zones as described above. However, the temperature affected the slope of the first zone; the transition between zone 1 and zone 2, and between zone 2 and zone 3, occurred at the same FA/LF molar ratios but the intensities of the exothermic signals were lower at higher temperatures. The slope of zone 2 was unchanged although slightly shifted to a higher FA/LF molar ratio when the temperature increased. The three binding isotherms overlapped in the third zone and converged to the same plateau value at the end of the titration.

Figure 4.8B shows FA-LF binding isotherms for two different [LF] and all other parameters of the titration remained unchanged (FA stock solution concentration, titration order and temperature). Binding isotherms exhibited the same complex profile for the two [LF] tested. Titration ended at a lower FA/LF molar ratio for a higher LF concentration in the sample cell. With increasing LF concentrations, the slope of zone 1 decreased and the transition between zone 1 and zone 2 occurred at a lower FA/LF molar ratio. Similarly, the slope of zone 2 was unchanged but the transition from zone 2 to zone 3 was more exothermic at higher [LF]. Both binding isotherms tended to overlap in zone 3.

Figure 4.8C shows the ITC profile of FA titration into LF solution without and with added NaCl. All the events observed involved in the interaction between LF and FA were completely abolished in the presence of 50 mM NaCl (flat isotherm).

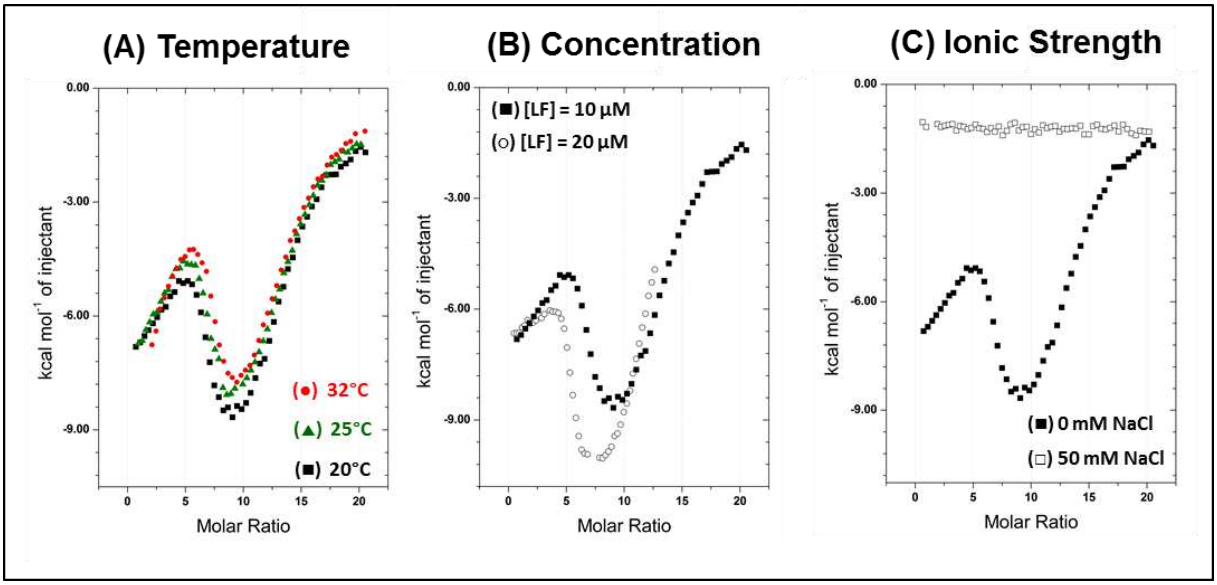

Figure 4.8. Experimental binding isotherms of the interaction of FA with LF at various: (A) Temperatures, titration of LF 0.01 mM with 1 mM FA; (B) Cell LF concentrations, titration with 1 mM FA at 20°C; (C) ionic strength, titration of LF 0.01 mM with 1 mM FA at 20°C. All experiments were carried out in 10 mM MES buffer, pH 5.5.

4.9.3 Independent determination of the FA-LF binding parameters

Given the complexity of the binding isotherm described above, ITC experiments were complemented by quantification experiments after separation at equilibrium of free FA from bound FA at different FA/LF molar ratios. The binding constant between FA and LF was estimated using the Scatchard equation. A plot of $[FA_{bound}]/[FA_{free}]$ [LF] versus $[FA_{bound}]/[LF]$ yielded a straight line, giving access to the interaction affinity (K_a) and stoichiometry (n) (Figure 4.9). The best fit of the experimental data provided values of $K_a = 2.09 \pm 0.36 \times 10^5$ M^{-1} and $n = 10.6 \pm 1.0$.

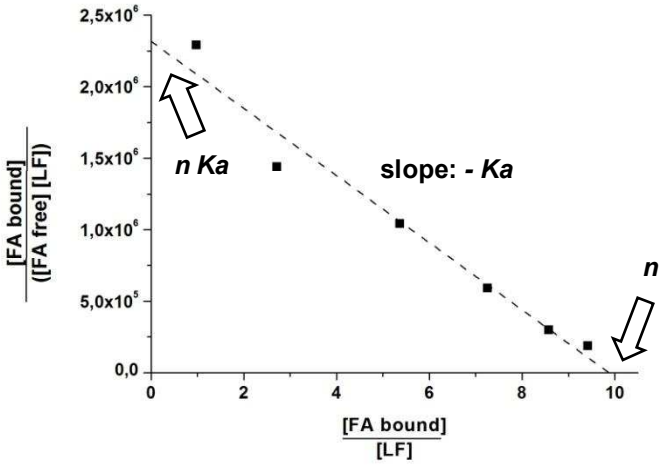

Figure 4.9. Scatchard plot for the interaction between LF (10 µM) and FA (0-150 µM) in 10 mM MES buffer, pH 5.5.

4.9.4 Characterization of FA-induced LF nanoparticles

Figure 4.10A shows the evolution of the size and the ζ-potential of FA-LF complexes as a function of the FA/LF molar ratio. The Dh measured for stock solutions were 6.1 ± 0.01 nm and 0.8 ± 0.08 nm for LF and FA, respectively. The evolution of the Dh of the complexes presented a sigmoid-like shape, with only a small increase in Dh until a FA/LF molar ratio of 5 was reached. Increasing this molar ratio further induced a rapid increase in the Dh of the complexes until the formation of nanoparticles presenting a final Dh value of around 15 - 16 nm was reached for the FA/LF molar ratio of around 15. Interestingly, the size of the nanoparticles levelled off at FA/LF molar ratios even greater than 20, as the same Dh was obtained for a FA/LF molar ratio as high as 72 (16.1 ± 0.01 nm). Increasing the initial LF concentration did not change the final Dh of the nanoparticles; with 0.06 mM LF (6 times more concentrated) and a FA/LF molar ratio of 13, the Dh value of the nanoparticles was 16.6 ± 0.38 nm. Considering particles of spherical shape, the change in the Dh measured corresponded to an increase in volume of about 18 times between the LF monomers and the FA/LF nanoparticles. Given the relatively small size of FA molecules, the size increase

observed was attributed to FA-induced self-association of LF. The increase in Dh profile and final particle size were independent of temperature in the temperature range tested (from 15°C to 32°C). However, the increase in Dh above a FA/LF ratio of 5 was steeper at lower temperatures (data not shown). In addition, at a specific FA/LF molar ratio the Dh of the complexes was independent of the titration direction (increasing or decreasing the FA/LF molar ratio), indicating that the system was at equilibrium. For comparison, it should be noted that no change in Dh was detected for the titration of LF with citrate (data not shown). The reversibility of the nanoparticles was also revealed by increasing the ionic strength (Figure 4.10B). The overall size of LF molecules was recovered after addition of 50 mM NaCl on pre-formed nanoparticles, indicating a complete dissociation of the complexes formed at relatively high ionic strength. The slight shift between curves 1 and 3 was due to the salt-induced increase in the LF Dh.

The evolution of the ζ-potential as a function of the FA/LF molar ratio is shown in Figure 4.10A. Under our conditions, LF alone exhibited a positive ζ-potential of +9.28 ± 0.93 mV, against a negative value of -8.11 ± 0.82 mV for FA. Addition of increasing concentrations of FA to the LF solution decreased the ζ-potential value. A sigmoid-like evolution of the ζ-potential was observed for increased FA/LF molar ratios. The ζ-potential of the complexes/nanoparticles was always positive for all FA/LF molar ratios tested, even with a considerable excess of FA in the protein solution. Major decreases in the ζ-potential of the complexes occurred for FA/LF molar ratios ranging from 3 to 13. The ζ-potential value tended to stabilize around +3.5 mV, indicating that above a ratio threshold, the additional FA does not seem to interact with already formed nanoparticles.

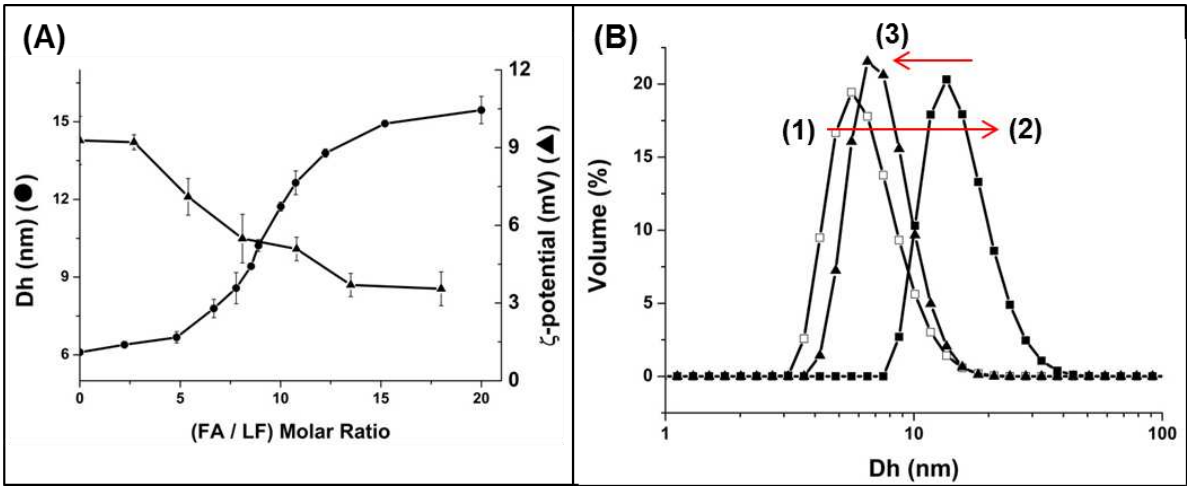

Figure 4.10. (A) Evolution of the hydrodynamic diameter Dh (●) and ζ-potential (▲) as a function of the FA/LF molar ratio at 25°C. (B) Particle size in MES 10 mM pH 5.5, 25 °C for (□) LF solution, (■) FA / LF nanoparticles at bulk molar ratio of 20 and (▲) FA/LF nanoparticles at bulk molar ratio of 20 in the presence of 50 mM NaCl.

4.10 Model to characterize the energy of FA-LF interaction

The complexity of the ITC profiles revealed the occurrence of several consecutive events during the titration of FA into LF. At least two events were clearly identified using complementary experiments: (i) the binding between the FA and LF, confirmed by the Scatchard plot of the titration of FA in LF solution (Scatchard plot gave a K_a in the order of 10^5 M^{-1} and n of around 10 molecules of FA per molecule of LF) (Figure 4.9) and (ii) the self-association of LF induced by addition of FA evidenced by the evolution of the Dh during titration (Figure 4.10A). The overlap of these events on the ITC signal prevented the use of classical interaction fitting models (one or more sets of binding sites).

However, it was clear that the onset of LF self-association with [LF] = 0.01 mM (ITC conditions) corresponded to the molar ratio of the transition between zones 1 and 2 on the binding isotherms (Figure 4.8A). The enthalpy contribution of LF self-association should therefore only be relevant for FA/LF molar ratios higher than 5. This might explain the slope

inversion between zones 1 and 2 in the experimental binding isotherm, and therefore zone 1 on the ITC profile would correspond mainly to the energy contribution of FA binding to LF (see below), while zones 2 and 3 would represent the overlap of the energy contributions of the binding of FA to LF and the self-association of complexes. A model based on the algorithm shown in Figure 4.11 was constructed to describe FA binding and subsequent self-association of FA-LF complexes, assuming that complete saturation of the LF binding site is required for self-association. FA-LF binding parameters from the Scatchard plot were used to model the energy contribution of FA binding to LF. The energy contribution of LF self-association induced by FA was achieved by simulation of the fraction of LF able to self-associate at each injection during ITC titration. The interaction enthalpy (cal mol^{-1} of bound FA) and the self-association enthalpy (cal mol^{-1} of saturated LF) were subsequently determined. More details are given in Supporting Information.

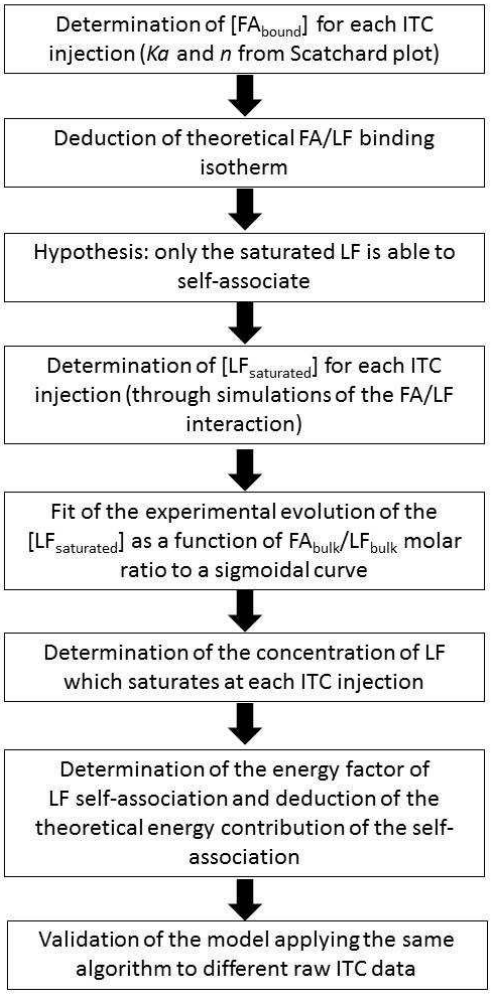

Figure 4.11. Algorithm used to develop the proposed model for FA binding to LF and subsequent self-association of FA/LF complexes.

4.10.1 Deduction of the theoretical FA-LF binding isotherm

The first step in constructing the theoretical isotherm of FA binding to LF was to discriminate the [FA $_{free}$] and [FA $_{bound}$] in the sample cell after each injection during the ITC analysis. From knowledge of the [FA] and [LF] at each injection and K_a and n, we calculated [FA $_{bound}$] as a function of the FA/LF molar ratio.

When the energy released during the ITC analysis (µcal per injection) was ascribed to the mole of FA bound to LF at each injection, a constant value of – 6,775.6 ± 325 cal mol^{-1} of FA bound was obtained for the injections in zone 1 (FA/LF molar ratio between 0 and 5). At

FA/LF molar ratios higher than 5, this value strongly diverged, confirming that the energy release in zone 1 (FA/LF molar ratio < 5) was mainly due to the binding step, with negligible contribution from LF self-association. At the end of zone 1, LF molecules were not saturated by FA. The contribution of the enthalpy of the binding of FA to LF was then extrapolated to the whole binding isotherm (zones 2 and 3) by multiplying the calculated fraction of FA bound to LF per injection by the number of calories released per mole of bound FA. The expected theoretical binding isotherm generated by FA binding, without the occurrence of other events, is shown in Figure 4.12 in comparison with the experimental binding isotherm. The theoretical FA/LF binding isotherm shows an ITC profile typical of an interaction presenting one set of binding sites [168, 182], similar in shape to the citrate/LF binding isotherm shown in Figure 4.16, Supporting Information.

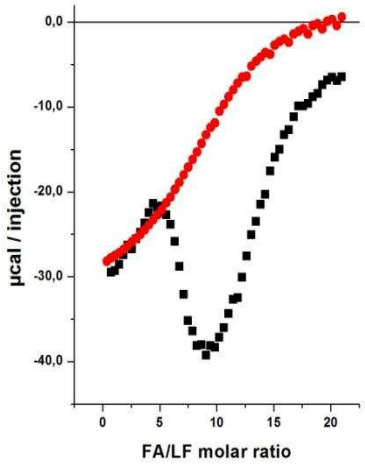

Figure 4.12. Superimposition of the experimental (■) and theoretical (●) FA/LF binding isotherms. Experimental titration of 0.01 mM LF was performed with FA in 10 mM MES buffer pH, 5.50, at 20°C.

4.10.2 Estimation of saturated LF concentration for each ITC injection

To prove that the difference between theoretical and experimental ITC signals was due to the energy contribution of FA-induced LF self-association, we determined the concentration of

LF species able to self-associate during titration. We assumed that only fully saturated LF molecules (i.e. with 10 bound FA) were able to self-associate.

The concentration of saturated protein [$LF_{saturated}$] for various FA_{bound}/LF molar ratios was simulated assuming a statistical law of binding to identical independent sites (Figure 4.17, Supporting Information). The results of simulation are presented in Figure 4.13. The proportion of saturated LF was close to zero for a FA_{bound}/LF molar ratio below 5, and then increased exponentially to 100% at a FA_{bound}/LF molar ratio of 10. When [$LF_{saturated}$] was represented as a function of the FA/LF molar ratio instead of FA_{bound}/LF molar ratio, a sigmoidal-like trend was observed (Figure 4.13A): a significant increase in [$LF_{saturated}$] was observed for FA/LF molar ratios between 5 and 15. From the equation fitting the sigmoidal evolution of the [$LF_{saturated}$] versus FA/LF molar ratio, it was possible to calculate the concentration of saturated LF between two successive FA injections (Figure 4.13B). The evolution of saturated LF per injection exhibited a pseudo-Gaussian behavior centered on the FA/LF molar ratio of around 10. At this molar ratio, LF self-association was at a maximum. Interestingly, this maximum rate of LF self-association corresponded to the FA/LF molar ratio of transition of the experimental binding isotherm between zones 2 and 3 (Figure 4.12).

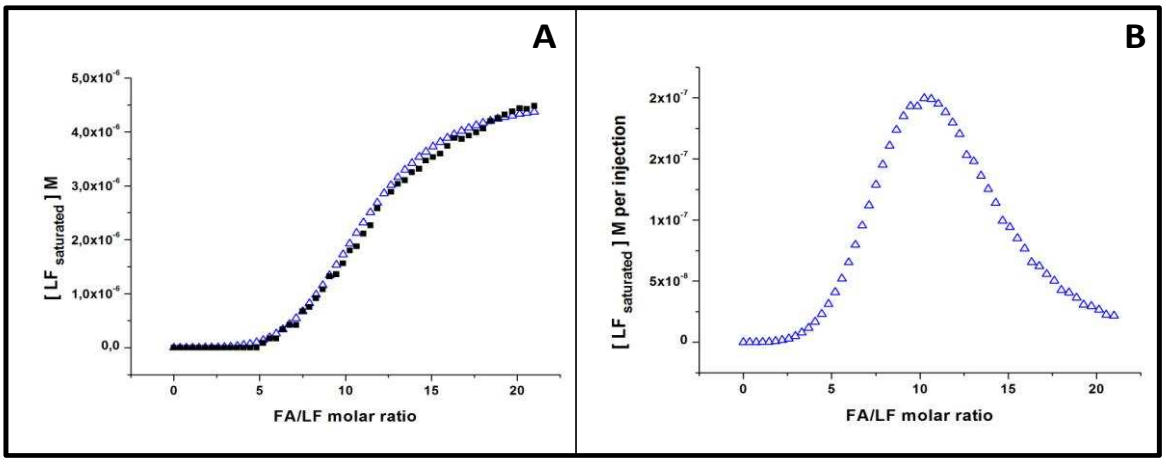

Figure 4.13. (A) Evolution of [$LF_{saturated}$] as a function of FA/LF molar ratio (■) and the sigmoidal curve fitted to the experimental data (Δ). (B) Concentration of LF which saturates at each ITC injection as a function of FA/LF molar ratio (data obtained from the fitted

sigmoidal curve).

4.10.3 Deduction of the energy contribution of the self-association step

The theoretical energy contribution of the self-association of saturated LF was obtained by multiplying the quantity of saturated LF per injection (mol of LF $_{saturated}$) by an enthalpy of self-association (cal mol^{-1} LF $_{saturated}$). The theoretical energy contribution best fitted the experimental binding isotherm when an enthalpy of self-association of 98 kcal mol^{-1} LF $_{saturated}$ was applied. Figure 4.14A shows the superimposition of theoretical energy contributions of FA/LF binding and of self-association of saturated LF to the experimental binding isotherm. Except for the slight gap between the model and experimental isotherms around the FA/LF molar ratio of 5.0, the proposed model satisfactorily described the experimental findings. The proposed model was further validated for a higher protein concentration [LF] = 0.02 mM (Figure 4.14B). A binding enthalpy of –6,750.4 ± 170.1 cal mol^{-1} of FA, not statistically different from that determined for [LF] of 0.01 mM, was calculated. Using the same enthalpy of self-association determined above, a good adjustment between experimental and theoretical isotherms was observed, validating the proposed model.

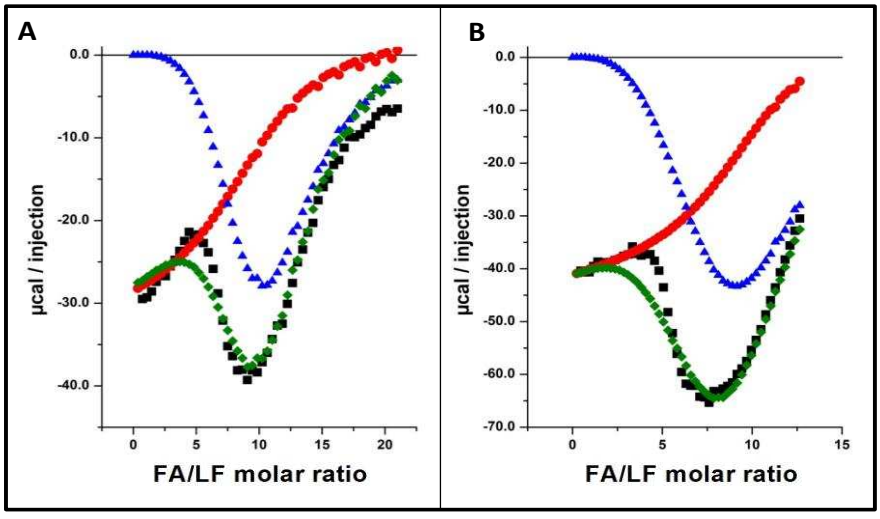

Figure 4.14. Superimposition of experimental binding isotherm (■), theoretical FA/LF binding isotherm (●), theoretical energy contribution of the LF self-association (▲) and the

theoretical global isotherm (binding + self-association) (♦). Results were obtained from the raw ITC data acquired at 20°C and (A) [LF] = 0.01mM and (B) [LF] = 0.02mM.

4.11 Discussion

4.11.1 Overview of the ITC isotherms and the proposed model

We have succeeded in interpreting the atypical ITC profile and therefore propose a mechanism of FA-induced LF self-association that follows two successive steps: FA binds first to LF (binding step) up to saturation of around 10 molecules of FA per LF molecule and then saturated LF molecules self-associate in nanoparticles of Dh ~16 nm (self-association step). This was achieved through the development of a statistical model that simulated the fraction of saturated LF in solution during the titration of LF with FA. The binding constant K_a value of 10^5 M^{-1}, used as feeding constant in the model and determined by another means, was in the order of magnitude of those obtained for the binding of FA to other milk proteins e.g. β-lactoglobulin, α-lactalbumin, BSA and β-casein [183, 184]. From the K_a and the enthalpy of FA/LF binding ($\Delta H = -6.8$ kcal mol^{-1}), the free energy ΔG of – 6.7 kcal mol^{-1} and the entropic contribution ΔS of $-2.5\ 10^{-4}$ kcal K^{-1} mol^{-1} were deduced using the equation: $\Delta G° = \Delta H - T\ \Delta S = - R\ T\ \ln Ka$.

The negative value for free energy indicates a spontaneous process, that is enthalpy driven, with strong participation of electrostatic interactions, as indicated by the effects of ionic strength on the ITC results and a very small unfavorable entropic contribution. Usually exothermic binding processes exhibit a decrease in *Ka* with increasing temperature [168, 185]. This is concordant with the temperature-dependent increase in the slope of zone 1 of the experimental binding isotherms (Figure 4.8A). However, the decrease in *Ka* observed in the temperature range tested was rather low, as also found for the FA-BSA binding [168]. The energy gap observed in zone 2 and at the transition between zones 2 and 3 of the experimental

binding isotherms shown in Figure 4.8A may be interpreted as an increase in the entropic contribution of the LF self-association at higher temperatures. The temperature increase results in an intensification of the hydrophobic interactions. The decrease in the enthalpic contribution is therefore a consequence of the enthalpy-entropy compensation usually observed for macromolecular interactions, such as the β-lactoglobulin-acacia gum complex coacervation [129].

For the same FA/LF molar ratio, more FA-LF complexes were formed at higher [LF] due to the shift in the binding equilibrium. Furthermore, the onset of self-association shifted toward a lower FA/LF molar ratio. Increasing [LF] thus induced both a decrease in the slope of zone 1 and an earlier transition between zones, as observed experimentally and well described by the model developed (Figures 4.8B and 4.14).

The model also accounted accurately for the energy contribution of the subsequent self-association step. The self-association enthalpy of saturated LF (– 98 kcal mol^{-1}) was about 15 times higher than the enthalpy of FA binding (– 6.8 kcal mol^{-1}). However, as 10 molecules of FA were required to saturate 1 molecule of LF to form nanoparticles, FA binding contributed to approximately 40% of the energy released compared to 60% for self-association of FA/LF complexes.

Although the proposed binding/self-association model for FA/LF exhibited good fitting to ITC data overall, some discrepancies should be noted. First, the model and experimental curves matched well except at the transition between zones 1 and 2, which could be attributed to the small differences between the experimental evolution of the [$LF_{saturated}$] and the fit shown in Figure 4.13A, especially at FA/LF molar ratios below 5. This resulted in premature onset of the energy contribution of the LF self-association to the theoretical binding isotherm (Figure 4.14). Secondly, calculation of the enthalpy related to the binding disregarded any potential energy contributions of FA-induced conformational changes in LF. Other authors

have reported small conformational changes in BSA induced by FA [168]. These conformational changes might explain the non-perfect matching of the theoretical and experimental binding isotherms in zone 1. Finally, we assumed a thermodynamically equivalent set of binding sites on LF. The potential occurrence of two or more sets of binding sites might affect the theoretical binding isotherms in zone 1 and at the transition between zones 1 and 2.

4.11.2 Specific features of FA-LF nanoparticles

The interaction of FA with LF at pH 5.5 exhibited a unique and specific binding self-association mechanism. A classical binding profile of FA to other proteins at neutral pH without subsequent aggregation has been reported for β-lactoglobulin and serum albumin [69, 168]. On the other hand, ligand-induced protein aggregation has been mainly found for a family of polyphenols, i.e. epigallocatechin gallate (EGCG). EGCG-mediated aggregation was reported for LF [167] and likewise for β-casein and a salivary proline-rich protein [186, 187]. Two main points illustrate the specificity of the FA-LF interaction mechanism: i) The initial binding step of FA to LF and the FA-LF nanoparticles formed are highly sensitive to ionic strength, underlying a predominance of electrostatic interactions. This suggests possible interactions between negatively charged groups of FA and positively charged domains of LF. In contrast, weak sensitivity to the overall protein charge and low dependence on the ionic strength have been reported for EGCG-induced aggregation processes [167]. Hydrogen bonds between EGCG and the protein have been suggested as the stabilizing forces [186, 187]. ii) For the EGCG-protein systems, the aggregate size increased with increasing initial protein and/or bioactive concentrations. A core/corona aggregation mechanism was proposed i.e. that the aggregates were formed by a core with EGCG-rich proteins and a corona containing proteins with fewer bound EGCG [186]. The FA-induced aggregation pathway of LF seemed

to be different as the final size and charge of the nanoparticles were not changed by increasing protein or bioactive concentrations. We suggest a two-step mechanism for the FA-LF interaction (Figure 4.15). The binding of negatively-charged FA to positively-charged LF induced a continuous reduction in net protein charge. At a critical saturation degree, FA_{10}/LF complexes that were still slightly positively charged self-associated by short-range attractions to form nanoparticles of definite size. Further growth was then prevented by sufficient long-range coulomb repulsions due the positive charges at the surface of the nanoparticles.

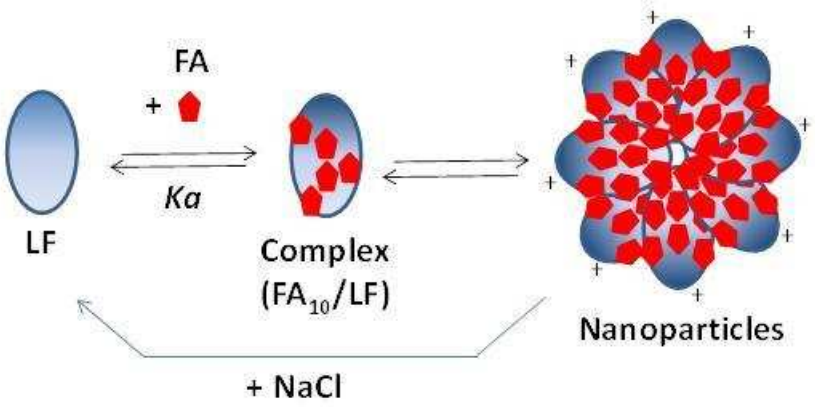

Figure 4.15. Proposed mechanism for the formation of folic acid/lactoferrin nanoparticles of finite size.

4.12 Conclusion

We demonstrated that folic acid interacts with lactoferrin at pH 5.5 to form stable, slightly positively-charged nanoparticles with a finite size of about 16 nm. The binding parameters suggest that LF binds tightly ten FA molecules per molecule through an exothermic process, with a Ka value in the order of 10^5 M^{-1}. This result supports our hypothesis concerning the fact that lactoferrin, a positively-charged protein, is a good putative carrier for FA below neutral pH. The FA-LF interaction and the stability of the nanoparticles are highly sensitive to ionic strength. We were able to elucidate a two-step mechanism in the formation of such nanoparticles by successfully modeling the ITC signal. FA binds to LF until saturation (step

1), generating “reactive” complexes able to self-associate into nanoparticles (step 2). The enthalpy associated with these two successive steps was deduced by combining experimental and theoretical calculations. Small angle X-ray and static light scattering experiments are in progress to determine the structure of FA-LF nanoparticles. These nanoparticles provide an opportunity to develop a novel ingredient that maintains FA solubility and bioaccessibility at acidic pH. A simple calculation determined from the binding stoichiometry indicates that up to 55 mg FA/g LF can be solubilized. However, for potential applications, future research should focus on the stability of FA-LF nanoparticles in formulated food products.

4.13 Acknowledgements

We are grateful for the financial support from INRA and the Federal Brazilian Funding Agency CNPq.

4.14 Supporting Information

Titration of lactoferrin with citrate (Figure 4.16); Details on the program and the algorithm used for the simulation of ITC profiles.

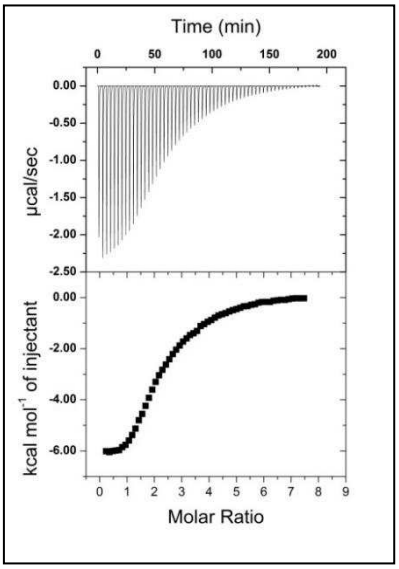

Figure 4.16. Raw data (upper panel) and binding isotherm (bottom panel) of the titration of

0.06 mM LF with successive injections of sodium citrate stock solution. The experiment was carried out at 25°C in 10 mM MES buffer, pH 5.5.

4.14.1 Determination of saturated LF concentration after each ITC injection

To put it simply, considering a system with only 2 LF molecules (bulk) and 10 bound FA molecules, i.e. a FA $_{bound}$/LF molar ratio of 5.0, the distribution of bound FA on the 2 LF molecules can be 10/0, 9/1, 8/2, 7/3, 6/4 or 5/5, but the probability of their random occurrence differs. In this case, the probability of having 10 FA molecules bound to the same LF molecule and the other LF molecule being free is very small but not nil. In our system, the number of LF molecules per liter was about 10^{18} (0.01 mM), which greatly increased the number of possibilities and made determination of the fraction of saturated LF for each FA_{bound}/LF molar ratio less than straightforward.

To overcome this hurdle we simulated the fraction of saturated LF for specific FA_{bound}/LF molar ratios using a program developed with software R (version 3.1.1) (Figure 4.17, Supporting Information). The [LF], the stoichiometry *n* and the [FA_{bound}] were the input variables for the simulation. For the sake of simplification the simulation was conducted using 100 LF molecules, each presenting a maximum capacity of 10 FA, and the amount of bound FA was selected in order to cover the FA $_{bound}$/LF molar ratio range of the ITC analysis. For each simulation, corresponding to one specific FA_{bound}/LF molar ratio, the number of draws was set at 1000. The premise of the simulation process was that the binding of FA on LF is random and the probability of having one FA molecule bound on a free LF binding site is the same, regardless of the number of FA molecules bound to LF up to 10. At the end of each simulation for a defined FA_{bound}/LF molar ratio (in the range of those encountered during ITC analysis), the proportion of saturated LF was obtained. It is important to note that varying the

number of LF molecules in the simulation but keeping both the stoichiometry and the FA_{bound}/LF molar ratio constant, the simulation response was unchanged.

The evolution of [$LF_{saturated}$] as a function of the FA/LF molar ratio was fitted by a logistic equation model (sigmoidal) using Origin 7.0 software:

Eq. 4.2. $$y = \frac{A_1 - A_2}{1+\left(\frac{x}{x_0}\right)^p} + A_2$$

where the values of A_1 (initial [$LF_{saturated}$]), A_2 (final [$LF_{saturated}$]), x_0 (FA/LF molar ratio when [$LF_{saturated}$]=50%) and p (power) are 0, 4.6×10^{-6}, 11 and 4.6, respectively. The χ^2 of the fitting was 1.6×10^{-14}.

```
#######################################################################

stsg <- function(number_lf,number_sites,number_fa,nbsimul)
{
nbfull <- c(rep(0, nbsimul))
dist <- c(rep(0,number_lf+1))


for (j in 1:nbsimul){
prob <- c(rep(1,number_lf))
init <- c(rep(0,number_lf))

for (i in 1:number_fa){
a <- rmultinom(1,1,prob)
num_lf <- which(a==1)

if (init[num_lf]==number_sites) {
prob[num_lf] <- 0
a <- rmultinom(1,1,prob)
num_lf <- which(a==1)
init[num_lf] <- init[num_lf]+1
if (init[num_lf]==number_sites) prob[num_lf] <- 0
}
{init[num_lf] <- init[num_lf]+1
   if (init[num_lf]==number_sites) prob[num_lf] <- 0
}
}
init
nbfull[j] <- sum(init==number_sites)
}

hist(nbfull)

for (n in 1:number_lf) {
dist[n+1] <- sum(nbfull==n)/nbsimul
}
dist[1] <- sum(nbfull==0)/nbsimul


return(dist)

}
#######################################################################
```

Figure 4.17. Simulation program developed with software R (version 3.1.1) to determine the fraction of saturated LF for specific FA_{bound}/LF molar ratio.

4.14.2 Determination of the energy contribution of saturated LF self-association

Knowing the concentration of LF that becomes saturated at each injection of the ITC analysis, the energy contribution of the self-association process was determined by adjusting the theoretical ITC profile constructed by superimposing the theoretical energy contributions (binding and self-associations steps) on the experimental binding isotherm. The theoretical energy contribution of the self-association step was calculated by multiplying the quantity of saturated LF per injection (moles of $LF_{saturated}$) by an enthalpy of self-association of saturated LF (cal mol^{-1} $LFs_{aturated}$) in order to best fit the experimental binding isotherm [Figure 4.14A, results].

To validate the model, the same algorithm was applied to the raw ITC data obtained at 20°C but at higher [LF] (0.02 mM). A binding enthalpy of – 6,750.4 ± 170.1 cal mol^{-1} of bound FA was calculated. As expected, this value was not statistically different from that determined for [LF] = 0.01 mM. The same enthalpy of self-association (98 kcal mol^{-1} of $LF_{saturated}$) was used for the two protein concentrations [Figure 4.14B, results].

4.15 Additional Data: Effect of FA on β-LG – LF complex coacervation

To verify the effect of FA on β-LG - LF complex coacervation, we prepared different mixtures at constant protein concentration and variable FA concentrations. The concentration of β-LG (native β-LG containing isoforms A and B) was fixed at 0.16 mM and the concentration of LF at 0.016 mM. The concentration of FA varied from 0 to 0.16 mM i.e. 10-fold excess compared to LF concentration. Three different mixing orders were tested: (1) β-LG + LF + FA; (2) β–LG + LF + FA and (3) LF + FA + β-LG. The supramolecular structures obtained in each mixture were observed by phase contrast microscopy.

Regardless the mixing order, the same trend was observed. As shown in Figure 4.18, the increase of the FA/LF molar ratio induced a gradual reduction of the size and the number of coacervates dispersed in the equilibrium solution (microspheres). Higher FA/LF molar ratios induced the transition between coacervation and aggregation regimes. The formation of amorphous aggregates were observed at FA/LF molar ratio around 10.

To better understand the organization of the β-LG - LF system in the presence of FA, it would be interesting to determine the partition of each molecule between the dense and dilute phases, as well as, the structures remaining in dilute phase to verify the predominance of FA-LF nanoparticles (~16 nm) or the β-LG-LF heterocomplexes (~12 nm).

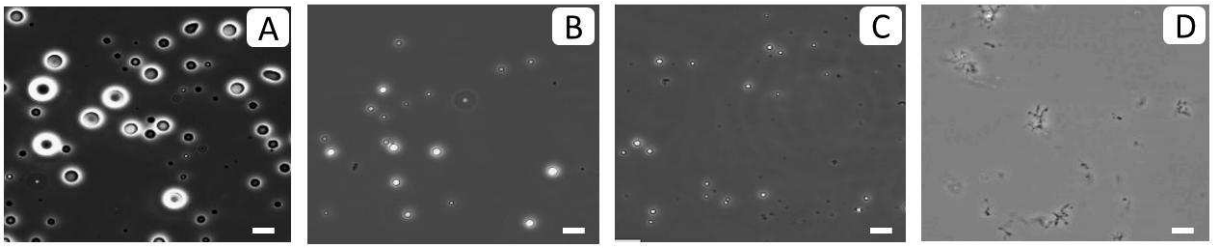

Figure 4.18. Optical microscopy images in phase contrast mode for mixtures containing 0.16 mM of β-LG, 0.016 mM of LF and different concentrations of FA according to mixing order 2. Different FA/LF molar ratios were tested: (A) 0, (B) 1, (C) 2 and (D) 10. Barre = 10 µm.

5 FINAL CONSIDERATIONS

5.1 General Discussion

5.1.1 Mechanism of β-LG-LF coacervation

Heteroprotein complex coacervation is rather recent research area. A priori, it is governed by the same principles reported for the complex coacervation of others polyions, even though it presents some specificities. As described by the classic models of complex coacervation [120-122], heteroprotein complex coacervation also seems to be divided into two main steps: (i) the first step leads to the formation of an elementary brick of coacervation. Its formation is governed by electrostatic interactions between oppositely charged proteins and an entropy gain linked to the release of counterions and water molecules. (ii) The second step leads to the formation of the coacervate phase by association of the previously formed elementary bricks through additional driving forces such as an increased contribution of non-electrostatic forces (hydrophobic...).

Because of the charge anisotropy and the relatively rigid structure of the globular proteins, it is not easy to predict the optimal conditions allowing their complex coacervation. Recently Du et al. [188] evidenced some structural differences between protein-polyelectrolyte, micelle-polyelectrolyte and protein-protein complex coacervates. These authors compared the proportion of structural water (non-freezing water) in different coacervates (BSA/PDADMAC (poly-dimethyldiallyammonium chloride), SDS (sodium dodecyl sulfate)/PDADMAC, β-LG /LF) and in solutions of the same free macromolecules at equivalent concentrations. The different conformation adopted by β-LG and LF into the coacervates greatly increased their hydration compared to the same proteins in solutions (absence of coacervation). In addition the proportion of structural water in heteroprotein complex coacervates was dramatically higher than in other coacervate systems, suggesting a lower entropic contribution linked to the release of water molecules during heteroprotein complex coacervation [188].

Before the beginning of this thesis project, the complex coacervation between apo α-LA-LYS was the best characterized heteroprotein complex coacervation system [15]. Apo α-LA and LYS are homologous, both are monomeric proteins and they are relatively small, presenting almost the same size (~14 kDa) but totally of opposite charge. At low ionic strength and neutral pH allowing the compensation of charge between these two proteins, coacervates presenting a well-defined and constant stoichiometry (equal to 1) are obtained. Apart some specific requirements such as the necessity to have α-LA under the apo-form (calcium-depleted) and a temperature higher than 30 °C, the apo α-LA-LYS system is simpler than the system studied in this thesis. Some other structural parameters were introduced by studying the β-LG-LF complex coacervation.

LF is a large glycoprotein of approximately 80 kDa formed by two homologous lobes presenting each an iron binding site. Thanks to these iron binding sites, LF appears under different forms: apo (iron-free); holo (iron-saturated) and with intermediate levels of bound iron. The commercial LF used during this work has an iron saturation level around 15 - 20% and was called native LF.

On the other hand, β-LG is about 4 times smaller than LF (~ 18.3 kDa) and is able to form non-covalent dimers in equilibrium with monomers in solution. This protein has several isoforms and the two main isoforms, β-LG A and β-LG B, differ only by the substitution of two AA. Anyway these AA substitutions are enough to make β-LG A slightly more hydrophobic and slightly more electronegative (pI=5.1) than the β-LG B (pI=5.2). The presence of these 2 variants allowed the investigation of the heteroprotein complex coacervation of LF with each purified variant and with the mixture of both variants.

The complex coacervation between globular proteins is definitely a universal process depending only on the optimization of the reactional conditions [53]. However, it is very susceptible to subtle variations. Despite β-LG A and β-LG B are able to interact with LF in

similar way in diluted conditions, in conditions allowing the coacervation to take place, the behavior of the 2 variants differed significantly. LF presents two binding sites at pH 5.5 for β-LG A and β-LG B one of high affinity (Ka_1 $4.5x10^7$ M^{-1}) and the other of lower affinity (Ka_2 $5x10^5$ M^{-1}). Both sites presenting a stoichiometry of one β-LG as deduced from ITC experiments (diluted conditions). Two binding sites with different affinities (site S of high affinity and site M of low affinity) were also deduced from simulation of the interaction between β-LG and LF by rigid docking. The stability of the complexes between LF and β-LG monomers or β-LG dimers was simulated to be of the same order. In fact, the simulation performed with β-LG dimers showed that only one β-LG molecule of the dimer was involved in the interaction with LF.

Even though in diluted conditions β-LG A and β-LG B bind to LF with similar association constant, the concentration domain of complex coacervation of LF - β-LG A was systematically found to be larger than that of LF- β-LG B. Interestingly, when the two β-LG isoforms were present in equimolar amount in solution (β-LG A + β-LG B), both isoforms were recovered in the coacervate at constant proportion. This was observed even in the zones where LF - β-LG B coacervates were not observed. This result support the assumption that the mechanism of coacervation is dependent on the interaction between LF molecules and β-LG dimers, as proposed by other authors [139]. These authors also suggested that the building blocks of β-LG-LF coacervation were pentamers formed by two β-LG dimers bound to one LF molecule. Although this model is partially consistent with our results - presence of two β-LG binding sites on LF and the β-LG/LF molar ratio of 4 quantified in the coacervate phase-, it could not explain the observed evolution of the β-LG/LF molar ratio from 4 to 8 as a function of total protein concentration. It should be noted, and this is not to be neglected, that

the two studies were not conducted in the same experimental conditions (protein concentrations and stoichiometry, ionic strength and pH mode).

Based on the hypothesis that the interaction between LF and β-LG dimer is essential for the coacervation, we simulated the stability of the various possible complexes formed between β-LG dimers and LF. The most stable complex was formed by the interaction of a β-LG dimer on the site S of LF (forming the trimer LF(β-LG_2)). Complexes involving a binding to the site M presented almost the same stability: (i) pentamer LF(β-LG_2)$_2$ formed by the interaction between a trimer and another β-LG dimer; (ii) hexamer LF_2(β-LG_2)$_2$ formed by the interaction of two trimers and (iii) octamer LF_2(β-LG_2)$_3$ formed by the interaction of a pentamer and a trimer. In the case of the two last complexes, a β-LG dimer could act as a bridge between 2 LF molecules. The less stable complex involved the interaction of two pentamers. Figure 5.1 summarizes the stability of the different β-LG - LF complexes according to docking simulation results. In the most stable complexes two LF and two β-LG_2 were never in close proximity.

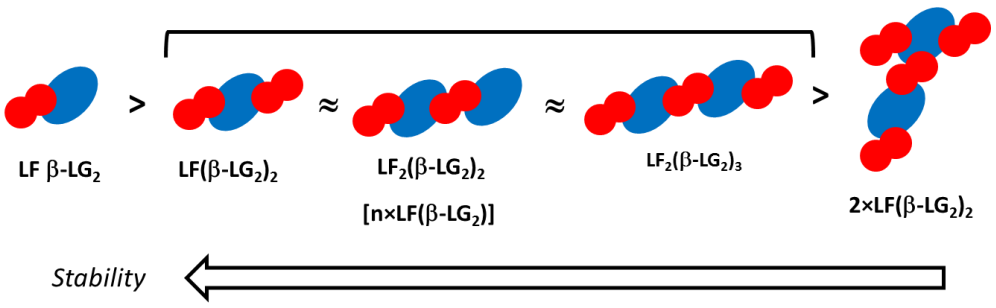

Figure 5.1. Relative stability of different β-LG_2 - LF complexes according to the docking simulations. Blue ellipse: lactoferrin; red circle: β-LG.

The ^{1}H NMR spectrum of the coacervate phase indicates the presence of different molecular and supramolecular entities. Their size was estimated from their rotation diffusion coefficients. Combining this result and docking simulation, the different β-LG - LF

complexes constituting the coacervate phase were deduced. The results suggest the coexistence of different complexes in co-existence in the coacervate phase instead of only one well-defined building block. Hence, our results complete those proposed by other authors for the same heteroprotein system [139, 141] as well as those reported for α-LA-LYZ coacervation [98, 131]. According to our results the coacervate phase could be formed by free β-LG (monomers/dimers), pentamers LF(β-LG_2)$_2$ and finally trimers LF(β-LG_2) assembled together to form large complexes (30-60 nm).

The proposed model gives an explanation of the evolution of the β-LG/LF molar ratio in the coacervate phase as a function of the β-LG/LF initial molar ratio. As described by Flanagan et al. [142], changing the initial molar ratio affects the protein heterocomplexes remaining in the lean phase (phase in equilibrium with the coacervate). In the same way, this variation may affect the proportion of the protein heterocomplexes in the coacervates, explaining the observed variability of the protein molar ratio. FRAP experiments support the existence of free and dynamic β-LG molecules in the coacervate phase.

From the simulation data, we will attempt to interpret the observed difference between β-LG A and β-LG B to form coacervates with LF. As both β-LG isoforms are mainly in monomeric state in the sample cell during the ITC titration, no difference could be detected on their binding ability. During the titration of LF by β-LG, saturation of site S then of site M occurred until the deduced β-LG/LF stoichiometry of 2. By increasing the concentration of β-LG, the proportion of β-LG dimer in the mixture increased. The interaction between LF and β-LG dimers being favored, allowing subsequent formation of coacervates. Based on the docking simulations of the binding between LF and β-LG monomer or dimer and on the ITC data, we suggest that LF interact with the β-LG domain opposite to that which carries the negative charge, the main discriminating factor between the two isoforms. Consequently, the formation of LF(β-LG)$_2$ and LF(β-LG_2)$_2$ species are not β-LG isoform dependent. Further, the presence

and the self-association of the trimers LF(β-LG_2) seem to be fundamental to the complex coacervation. In opposite to β-LG B, the more electronegative region on the interface of the β-LG A homodimer forming a trimer LF(β-LG_2) could favor throughout electrostatic attraction the binding of another LF molecule already involved in another trimer, as schematized in Figure 5.2. It could explain the higher "preference" of LF towards isoform A of β-LG. The limiting step would be therefore the association of trimers rather than the initial interactions. However, further experimental work is needed to determine the specific role of the AA substituted in β-LG on the coacervation process.

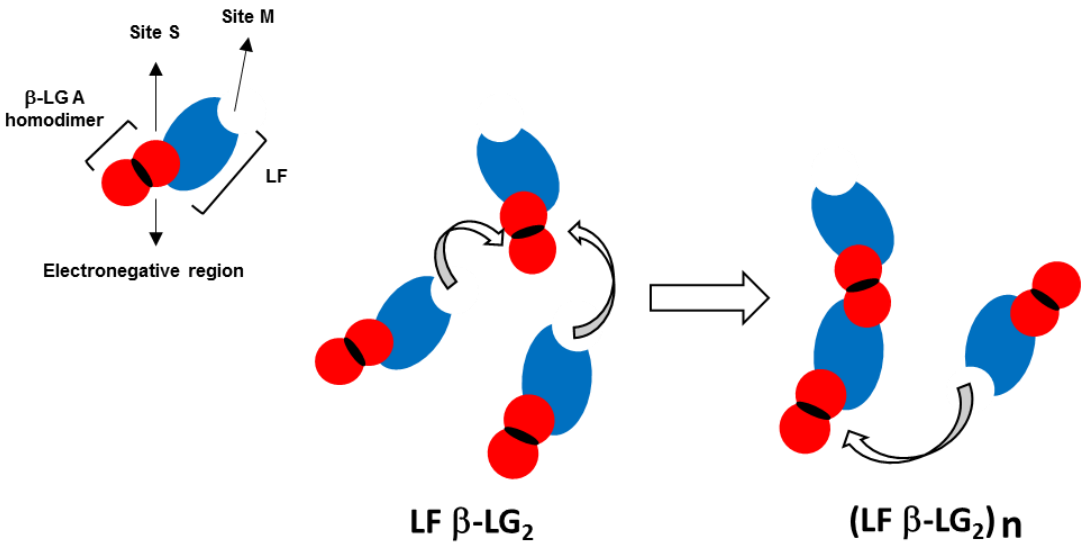

Figure 5.2. Hypothetic scheme of the self-assembly of trimers LF β-LG_2 formed by LF and β-LG A homodimers. Representation of the role of the electronegative region on the β-LG A homodimers interface promoting the self-assembly into coacervates.

5.1.2 Coacervation in the presence of small ligands

Among all putative applications of the complex coacervates, we studied their potential to be used as encapsulation devices. The potentiality of complex coacervation for encapsulation purpose was reported many years ago for other polyelectrolytes in particular protein-polysaccharide coacervates [189]. Determining the conditions giving rise to heteroprotein

complex coacervation and understanding the key parameters governing the interactions between the proteins are the first steps to optimize the formation of encapsulation devices.

One of our goals during this thesis was to prove the concept of the utilization of heteroprotein complex coacervates as encapsulation devices and to extract some relevant parameters that could affect the encapsulation process. How the bioactives interact with the proteins and how they are able to affect the proteins characteristics were identified as critical factors concerning the use of heteroprotein coacervates for encapsulation. The two small ligands studied (ANS and FA) did not interact with β-LG under the studied conditions, however, they interact with the LF. The interaction of both ANS and FA with LF induced a reduction of ζ-potential and an increase of Dh of the complexes with the increase of the ligand/LF molar ratio.

Unlike ANS-LF complexes that presented a continuous size growth when ANS/LF molar ratio increased, the FA-LF complexes formed well sized nanoparticles of around 16 nm presenting a well-defined stoichiometry (FA/LF = 10). The forces driving the formation of ANS-LF and FA-LF complexes were not exactly the same. Complex but different ITC profiles obtained by the titration of ANS or FA into LF (Figure 5.3) with and without 50 mM NaCl evidenced different interaction mechanisms. The formation and stabilization of FA-LF complexes seemed to be mainly driven by electrostatic, while for the ANS-LF complexes additional driving forces (hydrogen bonds and/or van der Waals interaction) were more pronounced.

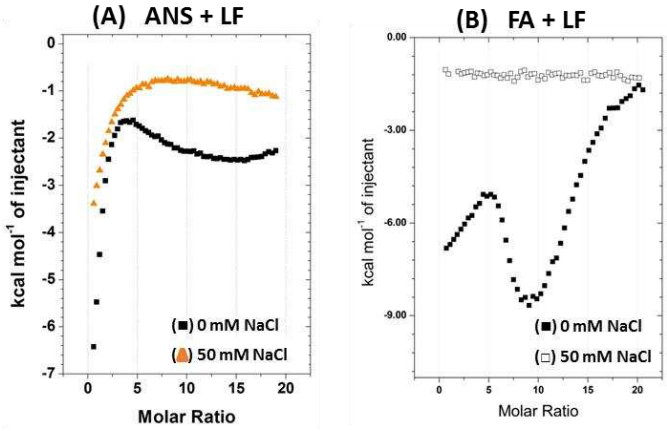

Figure 5.3. Binding isotherms of the titration of LF 0.05 mM with 4.25 mM ANS (A) and LF

0.01 mM with 1.0 mM FA (B). LF with (▲ and □) and without (■) 50 mM of NaCl.

LF self-association (aggregation) in the presence of small ligands resulting in size increase and ζ-potential decrease was able to modulate the β-LG - LF complex coacervation. A transition between the coacervation and aggregation regimes was observed. Potentially, LF self-association induced by the small ligands could affect the access of β-LG to its binding sites and/or the small ligands could compete with β-LG for the same binding site on LF. Competition between ANS and β-LG for the same binding site on LF could explain the quite small effect of the mixing order on the supramolecular structures formed and on the proportion of protein recovered in the coacervate phase.

The formation of β-LG – LF aggregates in the presence of small ligands indicates that even if β-LG and LF are able to interact, the equilibrium required to allow the coacervation could not be reached (formation of different elementary bricks and/or in different proportion). The transition between coacervation and aggregation regimes was also observed by the increase of the β-LG/LF initial molar ratio (phase boundaries diagrams) in the absence of small ligands. This information reinforces our assumption that the shift between coacervation and aggregation regimes is based on the change of the organization of the complexes formed by the proteins. Up to now, we do not know exactly why this transition, also reported for complex coacervation of other polyelectrolytes [114].

Our work provides preliminary elements for the use of heteroprotein complex coacervates for encapsulation of small ligands. The presence of small ligands in high concentrations affected the complex coacervation process, but intermediate concentrations do not seem to hinder the coacervation process. Relative stoichiometry between proteins and the molecule to be encapsulated, related to its physico-chemical properties, seems to be a crucial parameter to be further explored and optimized in the ongoing studies.

5.2 General Conclusion & Perspectives

At fundamental level, through a multiscale approach, we bring new elements on complex coacervation mechanisms between proteins, a relatively new research field. These elements can be explored to better understand the heteroprotein coacervation involving different proteins according to their structural and physico-chemical characteristics.

The use of whey heteroprotein complex coacervates as encapsulation devices represents a great opportunity for the dairy industry. Besides the possibility of development of functional products without the addition of external additives (clean label), the versatility of the coacervates represents an opportunity for diversifying the use of whey proteins and concomitantly to develop new products with further added value.

The aim of this thesis was to contribute to the elucidation of the complex coacervation mechanism between β-LG and LF and to show that these coacervates constitute a putative encapsulation device. The main results of this project are summarized in Table 5.1.

Table 5.1. Highlights of each chapter of this thesis

Experimental Chapters	Main Results
Chapter 1 Characterization of β-LG/LF complex coacervation	- β-LG and LF form coacervates at low ionic strength (< 20 mM), β-LG/LF molar ratio > 4 and pH between 5.4 and 6.0; - Compared to β-LG B, β-LG A is able to shift the coacervation equilibrium toward the formation of coacervates (optimal protein recovery, ~80%); - LF presents two binding sites for β-LG (monomer or dimer) with different affinities; - The interaction between LF and β-LG dimer is essential for the complex coacervation; - The β-LG/LF molar ratio in the coacervate phase varied from 4 to 8 as function of β-LG/LF bulk molar ratio; - Three different protein complexes co-exist and form the backbone of the coacervate phase: (i) β-LG (monomer/dimer); (ii) LF(β-LG_2)$_2$ and (iii) n(LF(β-LG_2)).
Chapter 2 Effect of the presence of small ligands on β-LG/LF complex coacervation	- β-LG does not interact with ANS or FA under the tested conditions; - ANS interacts with LF mainly by electrostatic interaction, but others (hydrophobic, hydrogen and/or van der Waals) are involved; - ANS is able to induce "infinite" aggregation of LF in the tested concentration range, reducing the ζ-potential of the complexes; - FA interacts with LF to form a critical complex with n = 10 FA/LF; - FA induces LF assembly into well sized nanoparticles (16 nm) presenting a slight positive ζ-potential; - The increase of the size and the reduction of ζ-potential of the ligand/LF complexes affect the β-LG-LF coacervation mechanism, reducing the protein recovery in the coacervates; - Critical ligand/LF molar ratio prevented the β-LG/LF coacervation, favoring the formation of aggregates; - The loading capacity of around 40 mg of ANS/g of LF on the coacervate phase was reached.

Through a multiscale approach we determined the optimal conditions of β-LG - LF complex coacervation and we propose a model to describe the coacervation mechanism from the molecular interaction between β-LG and LF to the formation of the coacervates. Further studies are needed to confirm the composition of β-LG - LF coacervates, their dynamics and their internal structure by combining a diversity of powerful technics: NMR, SAXS, SANS. Also, DSC preliminary experiments showed a significant change in the protein stability once in the coacervate phase. These results deserve to be deepened and extrapolated to the determination of the changes occurring in the secondary and tertiary structures for involved proteins. Likewise, we investigated the changes in protein characteristics (oligomerization state, surface properties) induced by small ligand binding and the impact they have on the complex coacervation. The self-association and the modification of the global charge of the proteins induced by small ligands binding were critical for the complex coacervation. With respect to protein concentration, high concentrations of small ligands abolished the complex coacervation. At intermediate concentrations, the complex coacervation in the presence of small ligands can be optimized taking into account the modifications induced on the proteins.

The encapsulation efficiency of β-LG – LF coacervates will be further explored in the thesis project conducted by A.L. CHAPEAU (started on November/2014) in the framework of the inter-regional program (*Bretagne & Pays de la Loire*) PROFIL (*Assemblages protéiques multifonctionnels pour l'innovation en industrie laitière*). The first year of the thesis project was dedicated to optimize the complex coacervation between β-LG and LF in the presence, among others, of FA. Based on the results obtained during the present thesis, the β-LG - LF complex coacervation was investigated at FA/LF molar ratios below those inducing LF self-association. By varying different physico-chemical conditions, both the coacervation yield and the loading capacity of the ligand were improved [190].

On the continuity of this line of research, the thesis project of A.L. CHAPEAU will focus on two important points: (i) the determination of the protection provided by the coacervates for the bioactive compounds and (ii) the stabilization of the coacervates as dispersed droplets of definite size.

Amoung others, one of the goal of the encapsulation is to protect sensitive bioactive compounds against adverse conditions (i.e. light, temperature, moisture or oxygen). In the case of the encapsulation of FA by the β-LG - LF coacervates, it would be interesting to determine the protective effect provided by the coacervates against FA photo-oxidation, in comparison to the protective effect provided by β-LG and LF solutions at equivalent concentration. The use of the complex coacervates as encapsulation devices would be justified if a gain in the protection effect is evidenced. It is expected that the coacervates should provide a better protection to FA, regardless the anti-oxidant effect of the proteins, as the formation of micrometric structures (coacervates) containing the FA would be able to generate a physical protection to the bioactive, preventing the access of light in the case of photo oxidation.

The complex coacervation corresponds to an equilibrium state in which a dense phase is dispersed into a diluted phase as micro-droplets. The droplets are usually close to charge neutrality and they naturally coalesce or fuse and sediment to form a continuous phase. For this reason the study of the stability of the coacervates as micro-droplets is an important step to develop systems that are able to withstand long storage period. Preliminary results show that the presence of the bioactive in the coacervates affects its stability. In the specific case of FA, it apparently makes the coacervates more stable against coalescence. However, the use of food grade crosslinking agents (for example transglutaminase) is a plausible option allowing a better control of the coacervate’s size and stability.

As already discussed in this manuscript, the protein recovery yield in the coacervates is, among several others, a key parameter considering industrial applications. Our results supported by published results highlight the importance of the protein conformation on the complex coacervation. Although it is known that the flexibility of the proteins favors heteroprotein complex coacervation, there is no detailed study describing the impact of induced conformational changes of the proteins (lactosylation, thermal denaturation, etc...). Some of our preliminary results suggest that slight conformational modifications of the protein structure constitute a potential mean to modulate heteroprotein complex coacervation. Figure 5.4 shows the phase boundaries of complex coacervation of LF with β-LG A from two different sources. One of the two β-LG A contained 30% of lactosylated molecules (Figure 5.4B), against native non lactosylated β-LG used in the present thesis (Figure 5.4A). The change of the coacervation domain due to the β-LG A lactosylation is flagrant. Similarly, the presence of denatured, aggregated fraction in the initial β-LG sample greatly interferes with its coacervation with LF [139]. Further studies are necessary to determine the proportion of protein recovery in the coacervate phase obtained with lactosylated β-LG and to identify the structural organization of the "lactosylated" coacervates.

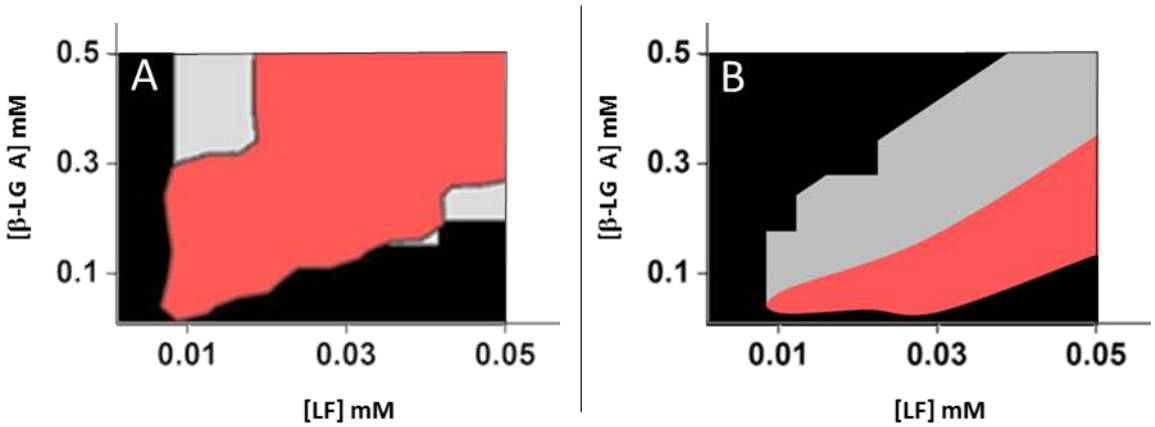

Figure 5.4. Phase boundaries of complex coacervation of LF with β-LG A at pH 5.5. (A) native non lactosylated sample; (B) lactosylated sample (lactosylation rate ≈ 30 %). Black

zone: domains without detectable supramolecular structure; Gray zone: aggregation domain; Salmon zone: coacervation domain.

Even for the application of the coacervates for the encapsulation purposes, the study of controlled protein conformational changes on the interaction of the proteins small ligands and their impact on the complex coacervation is of high interest. The interaction between proteins and bioactive compounds is dependent on the conformational state of the proteins [4] and may be a tool to increase the encapsulation efficiency of bioactives. Definitely, the complex coacervates of heteroproteins are promising encapsulation devices allowing the development of safe and durable food systems, as demanded by the consumers. However, despite the good results at laboratory scale, the up-scaling of laboratory results at pilot scale in this field remains a research challenge.

REFERENCES

1. Thompson, A., M.J. Boland, and H. Singh, *Milk proteins, from expression to food*. 1st ed. 2009, San Diego: Elsevier (Chapters 1, 3, 5 & 6). 568.
2. O'Mahony, J.A. and P.F. Fox, *Milk Proteins: Introduction and Historical Aspects*, in *Advanced Dairy Chemistry*, P.L.H. McSweeney and P.F. Fox, Editors. 2013, Springer US. p. 43-85.
3. Smithers, G.W., *Whey and whey proteins—From 'gutter-to-gold'.* International Dairy Journal, 2008. **18**(7): p. 695-704.
4. Tavares, G.M., et al., *Milk proteins as encapsulation devices and delivery vehicles: Applications and trends.* Trends in Food Science & Technology, 2014. **37**(1): p. 5-20.
5. BusinessWire. *Research and Markets: Food Encapsulation Market 2015-2020: Global Industry Analysis and Opportunity Assessment of the $5.46 Billion Market* 2015 [cited 2015; Available from: http://www.businesswire.com/news/home/20150605005251/en/#.VbXookbC_9I.
6. Tavares, G.M., et al., *Selective coacervation between lactoferrin and the two isoforms of β-lactoglobulin.* Food Hydrocolloids, 2015. **48**: p. 238-247.
7. Farrell, H.M., et al., *Casein micelle structure: What can be learned from milk synthesis and structural biology?* Current Opinion in Colloid & Interface Science, 2006. **11**(2-3): p. 135-147.
8. Livney, Y.D., *Milk proteins as vehicles for bioactives.* Current Opinion in Colloid & Interface Science, 2010. **15**(1-2): p. 73-83.
9. Walstra, P., J.T.M. Wouters, and T.J. Geurts, *Dairy Science and Technology*. 2nd ed. 2006, Boca Raton: CRC Press, (Chapters 2 & 3).
10. Farrell, H.M., Jr., et al., *Nomenclature of the proteins of cows' milk--sixth revision.* J Dairy Sci, 2004. **87**(6): p. 1641-74.
11. Qin, B.Y., et al., *Functional implications of structural differences between variants A and B of bovine beta-lactoglobulin.* Protein Sci., 1999. **8**(1): p. 75-83.
12. Yan, Y., et al., *pH-Dependent Aggregation and Disaggregation of Native beta-Lactoglobulin in Low Salt.* Langmuir, 2013. **29**(14): p. 4584-4593.

13. Qin, B.Y., et al., *Structural basis of the tanford transition of bovine beta-lactoglobulin.* Biochemistry, 1998. **37**(40): p. 14014-14023.

14. Croguennec, T., B.T. O'Kennedy, and R. Mehra, *Heat-induced denaturation/aggregation of beta-lactoglobulin A and B: kinetics of the first intermediates formed.* International Dairy Journal, 2004. **14**(5): p. 399-409.

15. Bouhallab, S. and T. Croguennec, *Spontaneous Assembly and Induced Aggregation of Food Proteins.* Adv. Polym. Sci., 2014. **256**: p. 67-101.

16. Ohtomo, H., K. Fujiwara, and M. Ikeguchi, *Important role of methionine 145 in dimerization of bovine beta-lactoglobulin.* J Biochem, 2012. **151**(3): p. 329-34.

17. Owusu Apenten, R.K. and D. Galani, *Thermodynamic parameters for beta-lactoglobulin dissociation over a broad temperature range at pH 2.6 and 7.0.* Thermochimica Acta, 2000. **359**(2): p. 181-188.

18. Brew, K., T.C. Vanaman, and R.L. Hill, *Comparison of the Amino Acid Sequence of Bovine α-Lactalbumin and Hens Egg White Lysozyme.* Journal of Biological Chemistry, 1967. **242**(16): p. 3747-3748.

19. Hiraoka, Y., et al., *Alpha-Lactalbumin - a Calcium Metalloprotein.* Biochemical and Biophysical Research Communications, 1980. **95**(3): p. 1098-1104.

20. Bernal, V. and P. Jelen, *Effect of Calcium-Binding on Thermal-Denaturation of Bovine Alpha-Lactalbumin.* Journal of Dairy Science, 1984. **67**(10): p. 2452-2454.

21. Xu, Y.S., et al., *Protein Purification by Polyelectrolyte Coacervation: Influence of Protein Charge Anisotropy on Selectivity.* Biomacromolecules, 2011. **12**(5): p. 1512-1522.

22. Celej, M.S., et al., *Ligand-induced thermostability in proteins: Thermodynamic analysis of ANS-albumin interaction.* Biochimica Et Biophysica Acta-Proteins and Proteomics, 2005. **1750**(2): p. 122-133.

23. Baker, E.N. and H.M. Baker, *A structural framework for understanding the multifunctional character of lactoferrin.* Biochimie, 2009. **91**(1): p. 3-10.

24. Mela, I., et al., *Charge reversal by salt-induced aggregation in aqueous lactoferrin solutions.* Colloids and Surfaces B: Biointerfaces, 2010. **78**(1): p. 53-60.

25. Persson, B.A., et al., *Molecular evidence of stereo-specific lactoferrin dimers in solution.* Biophysical Chemistry, 2010. **151**(3): p. 187-189.

26. Sawyer, L. and C. Holt, *The Secondary Structure of Milk-Proteins and Their Biological Function.* Journal of Dairy Science, 1993. **76**(10): p. 3062-3078.

27. Bokkhim, H., et al., *Physico-chemical properties of different forms of bovine lactoferrin.* Food Chem, 2013. **141**(3): p. 3007-13.

28. Garcia-Montoya, I.A., et al., *Lactoferrin a multiple bioactive protein: an overview.* Biochimica et Biophysica Acta, 2012. **1820**(3): p. 226-36.

29. Blanchard, E., P. Zhu, and P. Schuck, *Infant formula powders*, in *Handbook of food powders: process and properties*, B. Bhandari, et al., Editors. 2013, Woodhead Publishing: Cambridge. p. 465-483.

30. Matalanis, A. and D.J. McClements, *Hydrogel microspheres for encapsulation of lipophilic components: Optimization of fabrication & performance.* Food Hydrocolloids, 2013. **31**(1): p. 15-25.

31. Serrano-Cruz, M.R., et al., *Controlled release and antioxidant activity of Roselle (Hibiscus sabdariffa L.) extract encapsulated in mixtures of carboxymethyl cellulose, whey protein, and pectin.* Lwt-Food Science and Technology, 2013. **50**(2): p. 554-561.

32. Aberkane, L., et al., *Structuration mechanism of β-lactoglobulin – acacia gum assemblies in presence of quercetin.* Food Hydrocolloids, 2012. **29**(1): p. 9-20.

33. Zimet, P. and Y.D. Livney, *Beta-lactoglobulin and its nanocomplexes with pectin as vehicles for ω-3 polyunsaturated fatty acids.* Food Hydrocolloids, 2009. **23**(4): p. 1120-1126.

34. de Vos, P., et al., *Encapsulation for preservation of functionality and targeted delivery of bioactive food components.* International Dairy Journal, 2010. **20**(4): p. 292-302.

35. Augustin, M.A. and L. Sanguansri, *Encapsulation of Bioactives*, in *Food Materials Science - Principles and Pratice*, J.M. Aguilera and P.J. Lillforrd, Editors. 2008, Springer: New York. p. 577-601.

36. Gibbs, B.F., et al., *Encapsulation in the food industry: a review.* International Journal of Food Science and Nutrition, 1999. **50**(3): p. 213-24.

37. Velikov, K.P. and E. Pelan, *Colloidal delivery systems for micronutrients and nutraceuticals.* Soft Matter, 2008. **4**(10): p. 1964-1980.

38. Chen, L., G.E. Remondetto, and M. Subirade, *Food protein-based materials as nutraceutical delivery systems.* Trends in Food Science & Technology, 2006. **17**(5): p. 272-283.

39. Elzoghby, A.O., W.S. El-Fotoh, and N.A. Elgindy, *Casein-based formulations as promising controlled release drug delivery systems.* J Control Release, 2011. **153**(3): p. 206-16.

40. Gouin, S., *Microencapsulation: industrial appraisal of existing technologies and trends.* Trends in Food Science & Technology, 2004. **15**(7-8): p. 330-347.

41. Shahidi, F. and X.Q. Han, *Encapsulation of food ingredients.* Critical Reviews in Food Science and Nutrition, 1993. **33**(6): p. 501-47.

42. Heidebach, T., P. Forst, and U. Kulozik, *Transglutaminase-induced caseinate gelation for the microencapsulation of probiotic cells.* International Dairy Journal, 2009. **19**(2): p. 77-84.

43. Heidebach, T., P. Forst, and U. Kulozik, *Microencapsulation of probiotic cells by means of rennet-gelation of milk proteins.* Food Hydrocolloids, 2009. **23**(7): p. 1670-1677.

44. Betz, M. and U. Kulozik, *Whey protein gels for the entrapment of bioactive anthocyanins from bilberry extract.* International Dairy Journal, 2011. **21**(9): p. 703-710.

45. Martin, A.H. and G.A.H. de Jong, *Impact of protein pre-treatment conditions on the iron encapsulation efficiency of whey protein cold-set gel particles.* European Food Research and Technology, 2012. **234**(6): p. 995-1003.

46. Martin, A.H. and G.A.H. de Jong, *Enhancing the in vitro Fe(2+) bio-accessibility using ascorbate and cold-set whey protein gel particles.* Dairy Science & Technology, 2012. **92**(2): p. 133-149.

47. Alting, A.C., et al., *Physical and chemical interactions in cold gelation of food proteins.* Journal of Agricultural and Food Chemistry, 2002. **50**(16): p. 4682-9.

48. Viney, C., *Self-assembly as a route to fibrous materials: concepts, opportunities and challenges.* Current Opinion in Solid State & Materials Science, 2004. **8**(2): p. 95-101.

49. Bengoechea, C., I. Peinado, and D.J. McClements, *Formation of protein nanoparticles by controlled heat treatment of lactoferrin: Factors affecting particle characteristics.* Food Hydrocolloids, 2011. **25**(5): p. 1354-1360.

50. Giroux, H.J., J. Houde, and M. Britten, *Preparation of nanoparticles from denatured whey protein by pH-cycling treatment.* Food Hydrocolloids, 2010. **24**(4): p. 341-346.

51. Semo, E., et al., *Casein micelle as a natural nano-capsular vehicle for nutraceuticals.* Food Hydrocolloids, 2007. **21**(5-6): p. 936-942.

52. Esmaili, M., et al., *Beta casein-micelle as a nano vehicle for solubility enhancement of curcumin; food industry application.* Lwt-Food Science and Technology, 2011. **44**(10): p. 2166-2172.

53. Desfougeres, Y., et al., *Charge and size drive spontaneous self-assembly of oppositely charged globular proteins into microspheres.* J. Phys. Chem. B, 2010. **114**(12): p. 4138-44.

54. Ko, S. and S. Gunasekaran, *Preparation of sub-100-nm beta-lactoglobulin (BLG) nanoparticles.* Journal of Microencapsulation, 2006. **23**(8): p. 887-98.

55. Gunasekaran, S., S. Ko, and L. Xiao, *Use of whey proteins for encapsulation and controlled delivery applications.* Journal of Food Engineering, 2007. **83**(1): p. 31-40.

56. Gulseren, I., Y. Fang, and M. Corredig, *Whey protein nanoparticles prepared with desolvation with ethanol: Characterization, thermal stability and interfacial behavior.* Food Hydrocolloids, 2012. **29**(2): p. 258-264.

57. Gulseren, I., Y. Fang, and M. Corredig, *Zinc incorporation capacity of whey protein nanoparticles prepared with desolvation with ethanol.* Food Chem, 2012. **135**(2): p. 770-4.

58. López-Rubio, A. and J.M. Lagaron, *Whey protein capsules obtained through electrospraying for the encapsulation of bioactives.* Innovative Food Science & Emerging Technologies, 2012. **13**: p. 200-206.

59. López-Rubio, A., et al., *Electrospinning as a useful technique for the encapsulation of living bifidobacteria in food hydrocolloids.* Food Hydrocolloids, 2012. **28**(1): p. 159-167.

60. Torres-Giner, S. and J.M. Lagaron, *Zein-Based Ultrathin Fibers Containing Ceramic Nanofillers Obtained by Electrospinning. I. Morphology and Thermal Properties.* Journal of Applied Polymer Science, 2010. **118**(2): p. 778-789.

61. Doshi, J. and D.H. Reneker, *Electrospinning Process and Applications of Electrospun Fibers.* Journal of Electrostatics, 1995. **35**(2-3): p. 151-160.

62. Zorilla, R., et al., *Interaction of epigallocatechin-3-gallate with β-lactoglobulin: molecular characterization and biological implication.* Dairy Science & Technology, 2011. **91**(5): p. 629-644.

63. Loch, J.I., et al., *Binding of 18-carbon unsaturated fatty acids to bovine β-lactoglobulin—Structural and thermodynamic studies.* International Journal of Biological Macromolecules, 2013. **57**(0): p. 226-231.

64. Kontopidis, G., C. Holt, and L. Sawyer, *Beta-lactoglobulin: Binding properties, structure, and function.* Journal of Dairy Science, 2004. **87**(4): p. 785-796.

65. Sneharani, A.H., et al., *Interaction of Curcumin with beta-Lactoglobulin-Stability, Spectroscopic Analysis, and Molecular Modeling of the Complex.* Journal of Agricultural and Food Chemistry, 2010. **58**: p. 11130-11139.

66. Tavel, L., et al., *Interactions between aroma compounds and β-lactoglobulin in the heat-induced molten globule state.* Food Chemistry, 2010. **119**(4): p. 1550-1556.

67. Le Maux, S., et al., *Beta-Lactoglobulin as a molecular carrier of linoleate: characterization and effects on intestinal epithelial cells in vitro.* Journal of Agricultural and Food Chemistry, 2012. **60**(37): p. 9476-83.

68. Kuhn, J., et al., *Binding of 2-nonanone and milk proteins in aqueous model systems.* Journal of Agricultural and Food Chemistry, 2007. **55**(9): p. 3599-604.

69. Liang, L. and M. Subirade, *Beta-lactoglobulin/folic acid complexes: formation, characterization, and biological implication.* Journal of Physical Chemistry B, 2010. **114**(19): p. 6707-12.

70. Liang, L., H.A. Tajmir-Riahi, and M. Subirade, *Interaction of beta-lactoglobulin with resveratrol and its biological implications.* Biomacromolecules, 2008. **9**(1): p. 50-6.

71. Liang, L., V. Tremblay-Hébert, and M. Subirade, *Characterisation of the β-lactoglobulin/α-tocopherol complex and its impact on α-tocopherol stability.* Food Chemistry, 2011. **126**(3): p. 821-826.

72. Arts, M.J.T.J., et al., *Interactions between flavonoids and proteins: Effect on the total antioxidant capacity.* Journal of Agricultural and Food Chemistry, 2002. **50**(5): p. 1184-1187.

73. Mok, K.H., et al., *HAMLET, protein folding, and tumor cell death.* Biochemical and Biophysical Research Communications, 2007. **354**(1): p. 1-7.

74. Liskova, K., et al., *Effect of denaturation of alpha-lactalbumin on the formation of BAMLET (bovine alpha-lactalbumin made lethal to tumor cells).* Journal of Agricultural and Food Chemistry, 2010. **58**(7): p. 4421-7.

75. Liskova, K., et al., *Cytotoxic complexes of sodium oleate with beta-lactoglobulin.* European Journal of Lipid Science and Technology, 2011. **113**(10): p. 1207-1218.

76. Li, B., et al., *Preservation of (-)-epigallocatechin-3-gallate antioxidant properties loaded in heat treated beta-lactoglobulin nanoparticles.* Journal of Agricultural and Food Chemistry, 2012. **60**(13): p. 3477-84.

77. Shpigelman, A., G. Israeli, and Y.D. Livney, *Thermally-induced protein–polyphenol co-assemblies: beta lactoglobulin-based nanocomplexes as protective nanovehicles for EGCG.* Food Hydrocolloids, 2010. **24**(8): p. 735-743.

78. Shpigelman, A., Y. Cohen, and Y.D. Livney, *Thermally-induced β-lactoglobulin–EGCG nanovehicles: Loading, stability, sensory and digestive-release study.* Food Hydrocolloids, 2012. **29**(1): p. 57-67.

79. Relkin, P. and R. Shukat, *Food protein aggregates as vitamin-matrix carriers: impact of processing conditions.* Food Chem, 2012. **134**(4): p. 2141-8.

80. Giroux, H.J. and M. Britten, *Encapsulation of hydrophobic aroma in whey protein nanoparticles.* Journal of Microencapsulation, 2011. **28**(5): p. 337-43.

81. Fang, R., et al., *Design and characterization of protein-quercetin bioactive nanoparticles.* Journal of Nanobiotechnology, 2011. **9:19**: p. 1-14.

82. Fang, R., et al., *Bovine serum albumin nanoparticle promotes the stability of quercetin in simulated intestinal fluid.* Journal of Agricultural and Food Chemistry, 2011. **59**(11): p. 6292-8.

83. Betz, M., et al., *Preparation of novel whey protein-based aerogels as drug carriers for life science applications.* Journal of Supercritical Fluids, 2012. **72**: p. 111-119.

84. Remondetto, G.E., P. Paquin, and M. Subirade, *Cold gelation of beta-lactoglobulin in the presence of iron.* Journal of Food Science, 2002. **67**(2): p. 586-595.

85. Remondetto, G.E. and M. Subirade, *Molecular mechanisms of Fe2+induced beta-lactoglobulin cold gelation.* Biopolymers, 2003. **69**(4): p. 461-9.

86. Remondetto, G.E., E. Beyssac, and M. Subirade, *Iron availability from whey protein hydrogels: an in vitro study.* Journal of Agricultural and Food Chemistry, 2004. **52**(26): p. 8137-43.

87. Reid, A.A., et al., *Microentrapment of probiotic bacteria in a Ca2+-induced whey protein gel and effects on their viability in a dynamic gastro-intestinal model.* Journal of Microencapsulation, 2005. **22**(6): p. 603-619.

88. Hebrard, G., et al., *Use of whey protein beads as a new carrier system for recombinant yeasts in human digestive tract.* Journal of Biotechnology, 2006. **127**(1): p. 151-60.

89. Doherty, S.B., et al., *Development and characterisation of whey protein micro-beads as potential matrices for probiotic protection.* Food Hydrocolloids, 2011. **25**(6): p. 1604-1617.

90. Beaulieu, L., et al., *Elaboration and characterization of whey protein beads by an emulsification/cold gelation process: Application for the protection of retinol.* Biomacromolecules, 2002. **3**(2): p. 239-248.

91. Liang, L., et al., *In vitro release of α-tocopherol from emulsion-loaded β-lactoglobulin gels.* International Dairy Journal, 2010. **20**(3): p. 176-181.

92. Cornacchia, L. and Y.H. Roos, *Stability of beta-carotene in protein-stabilized oil-in-water delivery systems.* Journal of Agricultural and Food Chemistry, 2011. **59**(13): p. 7013-20.

93. Tippetts, M., et al., *Fortification of cheese with vitamin D3 using dairy protein emulsions as delivery systems.* Journal of Dairy Science, 2012. **95**(9): p. 4768-74.

94. Loveday, S.M., et al., *β-Lactoglobulin nanofibrils: Effect of temperature on fibril formation kinetics, fibril morphology and the rheological properties of fibril dispersions.* Food Hydrocolloids, 2012. **27**(1): p. 242-249.

95. Lara, C., et al., *General self-assembly mechanism converting hydrolyzed globular proteins into giant multistranded amyloid ribbons.* Biomacromolecules, 2011. **12**(5): p. 1868-75.

96. Domike, K.R., et al., *Investigating the inner structure of irregular beta-lactoglobulin spherulites.* European Physical Journal E, 2009. **29**(2): p. 173-182.

97. Graveland-Bikker, J.F. and C.G. de Kruif, *Unique milk protein based nanotubes: Food and nanotechnology meet.* Trends in Food Science & Technology, 2006. **17**(5): p. 196-203.

98. Nigen, M., et al., *Temperature affects the supramolecular structures resulting from alpha-lactalbumin-lysozyme interaction.* Biochemistry, 2007. **46**(5): p. 1248-55.

99. Nigen, M., T. Croguennec, and S. Bouhallab, *Formation and stability of alpha-lactalbumin-lysozyme spherical particles: Involvement of electrostatic forces.* Food Hydrocolloids, 2009. **23**(2): p. 510-518.

100. Arnaudov, L.N., et al., *Multiple steps during the formation of beta-lactoglobulin fibrils.* Biomacromolecules, 2003. **4**(6): p. 1614-22.

101. Goers, J., et al., *Conformational prerequisites for alpha-lactalbumin fibrillation.* Biochemistry, 2002. **41**(41): p. 12546-51.

102. Akkermans, C., et al., *Peptides are building blocks of heat-induced fibrillar protein aggregates of beta-lactoglobulin formed at pH 2.* Biomacromolecules, 2008. **9**(5): p. 1474-9.

103. Ipsen, R. and J. Otte, *Self-assembly of partially hydrolysed alpha-lactalbumin.* Biotechnology Advances, 2007. **25**(6): p. 602-5.

104. Loveday, S.M., et al., *Effect of calcium on the morphology and functionality of whey protein nanofibrils.* Biomacromolecules, 2011. **12**(10): p. 3780-8.

105. Krebs, M.R.H., K.R. Domike, and A.M. Donald, *Protein aggregation: more than just fibrils.* Biochemical Society Transactions, 2009. **37**: p. 682-686.

106. Graveland-Bikker, J.F., et al., *Influence of calcium on the self-assembly of partially hydrolyzed alpha-lactalbumin.* Langmuir, 2004. **20**(16): p. 6841-6.

107. Nigen, M., et al., *Dynamic and supramolecular organisation of alpha-lactalbumin/lysozyme microspheres: A microscopic study.* Biophys. Chem., 2010. **146**(1): p. 30-5.

108. IUPAC, *Compendium of Chemical Terminology*. 2nd ed. 1997: Blackwell Scientific Publications.

109. Bungenberg de Jong, H. and H. Kruyt, *Coacervation (partial miscibility in colloid systems).* Proc Koninklijke Nederlandse Akademie Wetenschappen, 1929. **32**: p. 849-856.

110. Miller, S.L., J.W. Schopf, and A. Lazcano, *Oparin's``Origin of Life'': Sixty Years Later.* Journal of molecular evolution, 1997. **44**(4): p. 351-353.

111. Oparin, A., *The orgin of life*. 1938: New York: The MacMillan Company.

112. Stewart, R.J., C.S. Wang, and H. Shao, *Complex coacervates as a foundation for synthetic underwater adhesives.* Advances in Colloid and Interface Science, 2011. **167**(1–2): p. 85-93.

113. Matus, M., *Artists Enlist Caddisfly Larvae to "Build" Jewelry From Gold, Gemstones*, in *Ecouterre*2012.

114. Burgess, D.J., *Practical Analysis of Complex Coacervate Systems.* J. Colloid Interface Sci., 1990. **140**(1): p. 227-238.

115. Kayitmazer, A.B., et al., *Protein-polyelectrolyte interactions.* Soft Matter, 2013. **9**(9): p. 2553-2583.

116. Voorn, M.J., *Complex coacervation. I. General theoretical considerations.* Recueil des Travaux Chimiques des Pays-Bas, 1956. **75**(3): p. 317-330.

117. Michaeli, I., J.T.G. Overbeek, and M.J. Voorn, *Phase separation of polyelectrolyte solutions.* Journal of Polymer Science, 1957. **23**(103): p. 443-450.

118. Sato, H. and A. Nakajima, *Complex coacervation in sulfated polyvinyl alcohol-aminoacetalyzed polyvinyl alcohol system.* Colloid and Polymer Science, 1974. **252**(11): p. 944-948.

119. Veis, A., E. Bodor, and S. Mussell, *Molecular weight fractionation and the self-suppression of complex coacervation.* Biopolymers, 1967. **5**(1): p. 37-59.

120. Tainaka, K.-i., *Study of complex coacervation in low concentration by virial expansion method. I. Salt free systems.* Journal of the Physical Society of Japan, 1979. **46**(6): p. 1899-1906.

121. Tainaka, K.-I., *Effect of counterions on complex coacervation.* Biopolymers, 1980. **19**(7): p. 1289-1298.

122. Veis, A., *A review of the early development of the thermodynamics of the complex coacervation phase separation.* Advances in Colloid and Interface Science, 2011. **167**(1–2): p. 2-11.

123. Kizilay, E., A.B. Kayitmazer, and P.L. Dubin, *Complexation and coacervation of polyelectrolytes with oppositely charged colloids.* Advances in Colloid and Interface Science, 2011. **167**(1-2): p. 24-37.

124. Matsudomi, N., Y. Yamamura, and K. Kobayashi, *Aggregation between Lysozyme and Heat-denatured Ovalbumin.* Agricultural and Biological Chemistry, 1987. **51**(7): p. 1811-1817.

125. Lampreave, F., et al., *Interaction of Bovine Lactoferrin with Other Proteins of Milk Whey.* International Journal of Biological Macromolecules, 1990. **12**(1): p. 2-5.

126. Howell, N.K., N.A. Yeboah, and D.F.V. Lewis, *Studies on the electrostatic interactions of lysozyme with alpha-lactalbumin and beta-lactoglobulin.* Int. J. Food Sci. Technol., 1995. **30**(6): p. 813-824.

127. Salvatore, D., et al., *Kinetics and Structure during Self-Assembly of Oppositely Charged Proteins in Aqueous Solution.* Biomacromolecules, 2011. **12**(5): p. 1920-1926.

128. Nigen, M., et al., *Apo alpha-lactalbumin and lysozyme are colocalized in their subsequently formed spherical supramolecular assembly.* FEBS J., 2007. **274**(23): p. 6085-93.

129. Aberkane, L., et al., *Thermodynamic characterization of acacia gum-beta-lactoglobulin complex coacervation.* Langmuir, 2010. **26**(15): p. 12523-33.

130. Nigen, M., et al., *Molecular interaction between apo or holo alpha-lactalbumin and lysozyme: formation of heterodimers as assessed by fluorescence measurements.* Biochim. Biophys. Acta, 2009. **1794**(4): p. 709-15.

131. Salvatore, D., et al., *Investigation at Residue Level of the Early Steps during the Assembly of Two Proteins into Supramolecular Objects.* Biomacromolecules, 2011. **12**(6): p. 2200-2210.

132. Anema, S.G. and C.G. de Kruif, *Co-acervates of lactoferrin and caseins.* Soft Matter, 2012. **8**(16): p. 4471-4478.

133. Anema, S.G. and C.G. de Kruif, *Coacervates of lysozyme and beta-casein.* J. Colloid Interface Sci., 2013. **398**: p. 255-61.

134. de Kruif, C.G., et al., *Coacervates of Lactotransferrin and beta- or kappa-Casein: Structure Determined Using SAXS.* Langmuir, 2013. **29**(33): p. 10483-10490.

135. Anema, S.G. and C.G. de Kruif, *Phase separation and composition of coacervates of lactoferrin and caseins.* Food Hydrocolloids, 2016.

136. Biesheuvel, P.M., et al., *Phase Behavior of Mixtures of Oppositely Charged Nanoparticles: Heterogeneous Poisson−Boltzmann Cell Model Applied to Lysozyme and Succinylated Lysozyme.* Langmuir, 2006. **22**(3): p. 1291-1300.

137. Tiwari, A., S. Bindal, and H.B. Bohidar, *Kinetics of Protein-Protein Complex Coacervation and Biphasic Release of Salbutamol Sulfate from Coacervate Matrix.* Biomacromolecules, 2009. **10**(1): p. 184-189.

138. Diarrassouba, F., et al., *Self-assembly of beta-lactoglobulin and egg white lysozyme as a potential carrier for nutraceuticals.* Food Chem, 2015. **173**(0): p. 203-9.

139. Yan, Y., et al., *Heteroprotein complex coacervation: bovine beta-lactoglobulin and lactoferrin.* Langmuir, 2013. **29**(50): p. 15614-23.

140. Anema, S.G. and C.G. de Kruif, *Complex coacervates of lactotransferrin and beta-lactoglobulin.* J. Colloid Interface Sci., 2014. **430**(0): p. 214-20.

141. Kizilay, E., et al., *Structure of Bovine beta-Lactoglobulin/Lactoferrin Coacervates.* Soft Matter, 2014.

142. Flanagan, S., et al., *Complex Equilibria, Speciation, and Heteroprotein Coacervation of Lactoferrin and β-lactoglobulin.* Langmuir, 2015.

143. Stradner, A., F. Cardinaux, and P. Schurtenberger, *A small-angle scattering study on equilibrium clusters in lysozyme solutions.* J. Phys. Chem. B, 2006. **110**(42): p. 21222-31.

144. Mercadante, D., et al., *Bovine beta-lactoglobulin is dimeric under imitative physiological conditions: dissociation equilibrium and rate constants over the pH range of 2.5-7.5.* Biophys. J., 2012. **103**(2): p. 303-12.

145. Manderson, G.A., L.K. Creamer, and M.J. Hardman, *Effect of heat treatment on the circular dichroism spectra of bovine beta-lactoglobulin A, B, and C.* J. Agric. Food Chem., 1999. **47**(11): p. 4557-4567.

146. Bouhallab, S., et al., *Copper-catalyzed formation of disulfide-linked dimer of bovine beta-lactoglobulin.* Lait, 2004. **84**(6): p. 517-525.

147. Boye, J.I., C.Y. Ma, and A. Ismail, *Thermal stability of beta-lactoglobulins A and B: effect of SDS, urea, cysteine and N-ethylmaleimide.* J. Dairy Res., 2004. **71**(2): p. 207-215.

148. Loch, J.I., et al., *The differences in binding 12-carbon aliphatic ligands by bovine beta-lactoglobulin isoform A and B studied by isothermal titration calorimetry and X-ray crystallography.* J. Mol. Recognit., 2013. **26**(8): p. 357-67.

149. Chen, K.M., et al., *Electrostatic Selectivity in Protein-Nanoparticle Interactions.* Biomacromolecules, 2011. **12**(7): p. 2552-2561.

150. Kurut, A., et al., *Anisotropic Interactions in Protein Mixtures,: Self Assembly and Phase Behavior in Aqueous Solution.* J. Phys. Chem. Lett., 2012. **3**(6): p. 731-734.

151. Sperber, B.L., et al., *Overall charge and local charge density of pectin determines the enthalpic and entropic contributions to complexation with beta-lactoglobulin.* Biomacromolecules, 2010. **11**(12): p. 3578-83.

152. Girard, M., S.L. Turgeon, and S.F. Gauthier, *Thermodynamic parameters of beta-lactoglobulin-pectin complexes assessed by isothermal titration calorimetry.* J. Agric. Food Chem., 2003. **51**(15): p. 4450-4455.

153. Olsson, M.H.M., et al., *PROPKA3: Consistent Treatment of Internal and Surface Residues in Empirical pKa Predictions.* J. Chem. Theory Comput., 2011. **7**(2): p. 525-537.

154. Schmitt, C., et al., *Complex coacervation between β-lactoglobulin and acacia gum in aqueous medium.* Food Hydrocolloids, 1999. **13**(6): p. 483-496.

155. Weinbreck, F., R.H. Tromp, and C.G. de Kruif, *Composition and structure of whey protein/gum arabic coacervates.* Biomacromolecules, 2004. **5**(4): p. 1437-45.

156. Anema, S.G. and C.G. de Kruif, *Protein Composition of Different Sized Casein Micelles in Milk after the Binding of Lactoferrin or Lysozyme.* Journal of Agricultural and Food Chemistry, 2013. **61**(29): p. 7142-7149.

157. Jimenez-Garcia, B., C. Pons, and J. Fernandez-Recio, *pyDockWEB: a web server for rigid-body protein-protein docking using electrostatics and desolvation scoring.* Bioinformatics, 2013. **29**(13): p. 1698-9.

158. Hammond, G.R.V., et al., *Reversible binding and rapid diffusion of proteins in complex with inositol lipids serves to coordinate free movement with spatial information.* The Journal of Cell Biology, 2009. **184**(2): p. 297-308.

159. Sprague, B.L. and J.G. McNally, *FRAP analysis of binding: proper and fitting.* Trends in Cell Biology, 2005. **15**(2): p. 84-91.

160. Silva, J.V.C., et al., *Transport phenomena in a model cheese: The influence of the charge and shape of solutes on diffusion.* Journal of Dairy Science, 2013. **96**(10): p. 6186-6198.

161. Boulat, B. and G. Bodenhausen, *Measurement of proton relaxation rates in proteins.* Journal of Biomolecular NMR, 1993. **3**(3): p. 335-348.

162. Ando, T. and J. Skolnick, *Crowding and hydrodynamic interactions likely dominate in vivo macromolecular motion.* Proceedings of the National Academy of Sciences, 2010. **107**(43): p. 18457-18462.

163. Haug, I.J., et al., *Electrostatic effects on beta-lactoglobulin transitions during heat denaturation as studied by differential scanning calorimetry.* Food Hydrocolloids, 2009. **23**(8): p. 2287-2293.

164. Bokkhim, H., et al., *Interactions between different forms of bovine lactoferrin and sodium alginate affect the properties of their mixtures.* Food Hydrocolloids, 2015. **48**(0): p. 38-46.

165. van de Weert, M., M.B. Andersen, and S. Frokjaer, *Complex coacervation of lysozyme and heparin: complex characterization and protein stability.* Pharm Res, 2004. **21**(12): p. 2354-9.

166. Waldron, T.T. and K.P. Murphy, *Stabilization of proteins by ligand binding: application to drug screening and determination of unfolding energetics.* Biochemistry, 2003. **42**(17): p. 5058-64.

167. Yang, W., et al., *Molecular interaction between (−)-epigallocatechin-3-gallate and bovine lactoferrin using multi-spectroscopic method and isothermal titration calorimetry.* Food Research International, 2014. **64**(0): p. 141-149.

168. Jha, N.S. and N. Kishore, *Thermodynamic studies on the interaction of folic acid with bovine serum albumin.* J. Chem. Thermodyn., 2011. **43**(5): p. 814-821.

169. Lakowicz, J.R., *Principles of Fluorescence Spesctroscopy*. 2006: Springer.

170. Semisotnov, G.V., et al., *Study of the "molten globule" intermediate state in protein folding by a hydrophobic fluorescent probe.* Biopolymers, 1991. **31**(1): p. 119-128.

171. Matulis, D. and R. Lovrien, *1-Anilino-8-naphthalene sulfonate anion-protein binding depends primarily on ion pair formation.* Biophys J, 1998. **74**(1): p. 422-9.

172. D'Alfonso, L., M. Collini, and G. Baldini, *Evidence of heterogeneous 1-anilinonaphthalene-8-sulfonate binding to β-lactoglobulin from fluorescence spectroscopy.* Biochimica et Biophysica Acta (BBA) - Protein Structure and Molecular Enzymology, 1999. **1432**(2): p. 194-202.

173. Weber, G. and L.B. Young, *Fragmentation of Bovine Serum Albumin by Pepsin. I. The Origin of the Acid Expansion of the Albumin Molecule.* J Biol Chem, 1964. **239**: p. 1415-23.

174. Augustin, M.A. and L. Sanguansri, *Challenges in developing delivery systems for food additives, nutraceuticals and dietary supplements*, in *Encapsulation Technologies and Delivery Systems for Food Ingredients and Nutraceuticals*, N. Garci and J. McClements, Editors. 2012, Woodhead Publ Food S. p. 19-48.

175. Shpigelman, A., et al., *β-Lactoglobulin–naringenin complexes: Nano-vehicles for the delivery of a hydrophobic nutraceutical.* Food Hydrocolloids, 2014. **40**(0): p. 214-224.

176. Le Maux, S., et al., *Bovine beta-lactoglobulin/fatty acid complexes: binding, structural, and biological properties.* Dairy Science & Technology, 2014. **94**: p. 409-426.

177. Zhang, J., et al., *A study of multi-ligand beta-lactoglobulin complex formation.* Food Chemistry, 2014. **165**(0): p. 256-61.

178. Eichholzer, M., O. Tonz, and R. Zimmermann, *Folic acid: a public-health challenge.* Lancet, 2006. **367**(9519): p. 1352-61.

179. Younis, I.R., et al., *Influence of pH on the dissolution of folic acid supplements.* Int. J. Pharm., 2009. **367**(1-2): p. 97-102.

180. Budavari, S., et al., *The Merck Index, an encyclopedia of chemical drug, and biologicals*. 11th ed. 1989: Merck & CO., Inc.

181. Scatchard, G., *The Attractions of Proteins for Small Molecules and Ions.* Ann. N. Y. Acad. Sci., 1949. **51**(4): p. 660-672.

182. Lin, L.N., et al., *Calorimetric studies of the binding of ferric ions to ovotransferrin and interactions between binding sites.* Biochemistry, 1991. **30**(50): p. 11660-11669.

183. Liang, L., et al., *Protective effect of ligand-binding proteins against folic acid loss due to photodecomposition.* Food Chemistry, 2013. **141**(2): p. 754-61.

184. Zhang, J., et al., *The folic acid/β-casein complex: Characteristics and physicochemical implications.* Food Research International, 2014. **57**(0): p. 162-167.

185. Bouchemal, K., et al., *A comprehensive study on the inclusion mechanism of benzophenone into supramolecular nanoassemblies prepared using two water-soluble associative polymers.* Journal of Thermal Analysis and Calorimetry, 2009. **98**(1): p. 57-64.

186. Canon, F., et al., *Aggregation of the salivary proline-rich protein IB5 in the presence of the tannin EgCG.* Langmuir, 2013. **29**(6): p. 1926-37.

187. Jobstl, E., et al., *Molecular model for astringency produced by polyphenol/protein interactions.* Biomacromolecules, 2004. **5**(3): p. 942-9.

188. Du, X., et al., *Nonfreezing Water Structuration in Heteroprotein Coacervates.* Langmuir, 2015.

189. de Kruif, C.G., F. Weinbreck, and R. de Vries, *Complex coacervation of proteins and anionic polysaccharides.* Current Opinion in Colloid & Interface Science, 2004. **9**(5): p. 340-349.

190. Chapeau, A.-L., et al. *Spontaneous co-assembly of proteins for encapsulation of a hydrophilic vitamin*. in *23th International Conference on Bioencapsulation*. 2015. Delft, Netherlands.